STRUCTURES AND EXCHANGE REACTIONS OF SILYL AND GERMYL GROUP V DERIVATIVES.

by

James Dunlop Murdoch

Thesis presented for the degree of

Doctor of Philosophy

University of Edinburgh July, 1972.

ACKNOWLEDGEMENTS

I am grateful to many people who have helped me in the work described, but in particular, to my supervisors, Professor E.A.V. Ebsworth and Dr. S. Cradock, for their continual help and advice.

I also thank Dr. B.E. Mann (Leeds University) for his help with n.m.r., Dr. S. Cradock for recording photoelectron spectra, Professor D.W.J. Cruickshank and Dr. B. Beagley (Manchester University) for provision of experimental facilities for electron diffraction, and Dr. D.W.H. Rankin for his patient guidance through all my computing, electron diffraction, and spin decoupling experiments.

My thanks are also due to the University of Edinburgh for providing laboratory facilities, and the Science Research Council for a maintenance grant.

I am very grateful to my typist, Mrs. E. Courtney, who has worked quickly, accurately and cheerfully. Finally, I would like to thank my wife for her help and support in the production of this thesis.

SUMMARY

Section I of the thesis describes structural investigations of silyl and germyl pseudohalides. The molecular structures of silyl isoselenocyanate, germyl isocyanate, germyl azide and digermyl carbodiimide have been determined by electron diffraction, and shrinkage corrections to the angles found are discussed.

The photoelectron spectra of methyl, silyl, germyl and trimethyl silyl azides, isocyanates and isothiocyanates have been recorded. The ionisation potentials and band contours have been explained by the existence of π-bonding in the silyl and germyl compounds.

The infrared spectra of silyl isocyanate and isothiocyanate, and germyl isocyanate have been studied using ^{15}N and ^{2}H substitution. Proton magnetic resonance spectra of silyl and germyl isocyanates and isothiocyanates containing 90% ^{15}N, and germyl and silyl cyanides containing 60% ^{13}C were recorded. The signs of all coupling constants in the silyl compounds were related to $J(^{29}SiH)$. The spectra showed that normal-cyanates and thiocyanates, and isocyanides could only be present in concentrations of less than one percent of, and were not involved in fast exchange with, the predominant isomers.

Section II of the thesis describes preparative and spectroscopic studies of silyl and germyl phosphine complexes. The complexes were of general formula $L_xMo(CO)_{6-x}$. Complexes of trigermyl phosphine (for $x = 1,2,3$), trisilyl phosphine (for $x = 1$), mono-silyl phosphine (for $x = 2$) and mono-germyl phosphine

(for x = 2) were prepared. Also complexes of formula L $PH_3Mo(CO)_4$ were prepared for L = mono-silyl phosphine and mono-germyl phosphine. The mono-germyl phosphine complexes were both prepared by exchange reactions.

No evidence was found that the phosphines used were weaker donors than phosphine itself.

CONTENTS

S E C T I O N I

CHAPTER 1

THE MOLECULAR STRUCTURES OF SILYL AND GERMYL PSEUDOHALIDES

"A foul and pestilent congregation of vapours"

- Hamlet, Act II, Sc.II.

1.1 Introduction

The name "pseudohalide" was originally given to this group of compounds to emphasise their very close resemblance in physical and chemical properties to the halides. They are structurally and electronically very similar in that the groups all contain unsaturation and also at least one atom with a formal lone pair of electrons. At first the term was used to include only the groups which were anions derived from the dimeric pseudohalogen parents but now other species are included for which no pseudohalogen parent exists. They are included because of their great similarity to the rest of the groups previously included.

The molecular structures of a great many pseudohalides have been investigated using a variety of spectroscopic and diffraction techniques. Very rarely, however, has definitive structural information been produced by the application of any of these techniques but much more often by a combination of several. Thus a general discussion of the structural information and an assessment of its importance and validity must precede an analysis of the results in this thesis.

There are two reasons for the interest in the structures of pseudohalides. In the case of all the pseudohalides included in this study except azides, the pseudohalide moiety possesses two potential donor sites and hence the radical attached to the moiety may be attached to either of these. Thus one or more

structural isomer may exist in each case. The other interest in the structure of the pseudohalides is in the angle between the bonds at the donor atom. In some cases this is found to be far from that expected on simple criteria and thus information from as large a number of compounds as possible is helpful in determining the factors involved.

The following discussion of the present structural information available on these compounds will be restricted to these two main points of interest.

1.2 Donor Site

(a) Cyanides

For methyl cyanide both the normal-cyanide and iso-cyanide isomers are stable and thus spectroscopic information may be obtained on both forms. Chemical evidence for the existence of either isomer in the silicon and germanium analogues may be discounted as such evidence can always be explained by an equilibrium between the two forms or by isomerisation taking place immediately prior to reaction.

Infra-red evidence was not easy to obtain at first and a crystalline sample of trimethyl silyl cyanide had to be used to obtain sufficiently sharp bands to detect isotopic shifts in vibrational frequency on partial ^{13}C and ^{15}N substitution. The information obtained favoured the normal-cyanide structure[1] but was not accepted as conclusive[2] as the bands could have been overtones

or combination bands.

A vapour phase study of trimethyl silyl and triethyl silyl cyanides[3] showed two bands in the carbon-nitrogen stretching region. The strong one was assigned to the normal-cyanide and the much weaker one to the iso-cyanide. The n-cyanide band was demonstrated to decrease in intensity with increasing temperature while the iso-cyanide band increased reversibly. A temperature dependent equilibrium between the two isomers was thus postulated. The ^{15}N and ^{13}C shifts of the two bands agreed with calculated shifts assuming the assignments to the normal-cyanide and iso-cyanide.

Detailed infrared study was also carried out on silyl cyanide[4] using ^{13}C, ^{15}N, ^{2}H substitution. All the observed bands could be satisfactorily assigned on the basis of a linear normal-cyanide structure and the isotopic shifts were in good agreement with this assignment. A similar study of germyl cyanide[5], comparing calculated shifts for the two possible isomers with the observed shifts led to the same conclusion.

Further support for the normal cyanide structure for silyl cyanide was obtained from the chemical shift of the protons in the magnetic resonance spectrum[6]. It is very close to that measured for silyl acetylene and very different from the value in compounds in which the silyl group is directly bound to nitrogen. The chemical shifts of silyl protons are very sensitive to the β -atom but not to atoms further away. A very similar series

of spectra were also obtained for the series $Me_x Si H_{3-x} CN$,[6] and the magnitudes of ^2J (^{13}CH) and ^1J ($^{29}Si H$) and the chemical shift of the silyl protons were found to vary in the same way as in the series where the cyanide group was replaced by iodide, chloride, and a methyl group. Thus it was likely that the same atom was attached to silicon in each case.

The broadening of the absorption in silyl cyanide has been shown, however, to be consistent with quadrupole relaxation of ^{14}N only.[6] These nuclear magnetic resonance measurements, however, do not rule out the possibility of the presence of small amounts of the isocyanide form. In fact, a more recent study[7] using 60% of ^{13}C in the cyanide group reported the absence of coupling between this nucleus and the protons. This supports the infra-red evidence for an equilibrium between the two isomers in this case.

b) Cyanates, thiocyanates and selenocyanates

No covalent normal-cyanates are known to exist and methyl cyanate is found to have the iso-structure from infrared[8,9] and electron diffraction[10,11] evidence.

The infrared spectrum of the silyl compound was consistent with an isocyanate structure[12] although a weak band was observed 123 $cm.^{-1}$ above the very strong asymmetric (N-C-O) stretch. This was assigned to a combination of this band with the lowest vibrational bending mode which could not be observed within the

range of the instrumentation used. The chemical shift of the protons in the nuclear magnetic resonance spectrum[12] was found to be very similar to that of similar compounds in which the silyl group is bound directly to nitrogen. Further evidence for an isocyanate structure was obtained from the microwave spectrum[13] and electron diffraction.[14] None of the techniques used, however, rule out the possibility of the existence of both isomers with the normal-cyanate present to a very much lesser extent.

The evidence available on the germyl analogue is very similar but has been interpreted in a different way. Both the infrared[15,16] and proton magnetic resonance spectra[17] favour an isocyanate structure but a weak band in the infrared spectrum 102 cm.$^{-1}$ above the asymmetric (N-C-O) stretch is assigned to a small amount of the normal-cyanate form.[16] It was not assigned as a combination band because of the absence of the corresponding difference band. No information was obtained on whether the two isomers were in equilibrium.

In the case of the thiocyanates both methyl compounds are stable and hence their spectra could be used for comparison with the other thiocyanates.

The infrared,[18] proton magnetic resonance,[19] and microwave spectra[20] of the silyl compound show that it exists at least mainly in the iso-form. This is supported by electron diffraction data.[14] Similarly, vibrational and magnetic resonance spectra[21]

obtained for the germyl analogue also favour the iso-thiocyanate structure. However, in both the silyl and germyl cases the infrared spectra are extremely complex in the region in which the band of germyl thiocyanate, assigned to the normal thiocyanate form, was observed. This complexity is caused by fermi resonance between the asymmetric (N-C-S) stretch and the first overtone of the corresponding symmetric stretching vibration, because of the near-coincidence of these absorptions.

The infrared and proton magnetic resonance spectra of silyl selenocyanate[22] were again found to be in good agreement with those expected from the iso-form but a high resolution study of the infrared spectrum has not yet been attempted.

(c) Cyanamides

In this case the donor atom must obviously be nitrogen but both substituent groups may be attached to one nitrogen or they may be attached to different nitrogen atoms.

The infrared spectrum of the methyl compound shows it to have a cyanamide structure.[23] The vibrational spectra of the silyl[24,25] and germyl[25,26] compounds are very similar and quite different from that of the methyl compound, and were interpreted in terms of a carbodiimide structure. Their proton magnetic resonance spectra[24,26] were also consistent with this interpretation.

(d) Summary

It can be seen that there are often considerable structural differences between the silyl and germyl pseudohalides and their methyl analogues. These differences can only be explained in terms of the intramolecular forces involved. The work described in Chapter 3 is an attempt to compare the bonding found in these molecules. Some assessment can, however, be made from a comparative study of the geometrical structure of the series of molecules. The experimental evidence from which information has been derived and the interpretation of this evidence is now presented.

1.3 Geometrical Structure

(a) Azides

Information on the angle formed by the bonds at the donor nitrogen atom of the azide moiety has been derived from vibrational and microwave spectroscopy, and from electron diffraction studies. The results available from these studies are shown in table 1.1, which also gives similar information for the other pseudohalides studied.

The vibrational spectra of silyl azide[27] are in agreement with a C_{3v} model for the molecule (linear skeleton) but no rotational detail was observed on any of the infrared bands. It was assumed, therefore, that the molecule is non-linear and of C_s symmetry, but that the angle at nitrogen is not wide enough to

-Y	Substituent (X)						*
	H	CH_3	SiH_3	SiF_3	$SiMe_3$	GeH_3	
-NCO	-	140[11]	152[14]	161[73]	150[35]	141	E
	128[53]	140[32]	180[13]	-	-	-	M
-NCS	-	141[11]	163[14]	-	154[35]	-	E
	135[53]	147[76]	180[20]	-	-	-	M
-NCSe	-	-	160	-	-	-	E
	-	-	-	-	-	-	M
-NNN	-	117[11]	-	-	120[77]	123	E
	114[53]	-	$<$ 180[28]	-	-	-	M

* E denotes measurement by electron diffraction.

M " " " microwave spectroscopy.

TABLE 1.1 - Angles at nitrogen in pseudohalides (XY).

allow resolution of the a′ and a″ components of the asymmetric vibrations. The absence of rotational detail also implies a high energy barrier to free rotation of the silyl group about the silicon-nitrogen bond. These conclusions were confirmed by a μwave study[28] which showed the molecule to be an asymmetric top.

The infrared[29] and raman[30] evidence available for germyl azide is very similar except that one too many polarised absorptions appear in the raman spectrum for the molecule to possess C_{3v} symmetry. Irregular fine structure was observed on one of the vibrational absorptions in the infrared spectrum which could be due to internal rotation, since (GeN) > (SiN) > (CN). The molecule was, therefore, assumed to be bent at nitrogen although no microwave study is yet available.

(b) Isocyanates

The vibrational spectra of silyl and germyl isocyanate[12,15,16] are consistent with the molecules possessing C_{3v} symmetry. Rotational fine structure with a three-fold intensity pattern (strong, weak, weak) is reported on all the asymmetric vibrational bands. It was assumed, therefore, that both these molecules have a linear heavy-atom skeleton.

The infrared spectrum of methyl isocyanate[31] is also consistent with C_{3v} molecular symmetry and shows rotational structure. Since the molecule is known to be an asymmetric top

from its microwave spectrum[32] the fine structure was attributed to internal rotation of the methyl group about its local C_3 axis (the (CN) bond).

The separation between the PR branches of the parallel bands in the infrared spectrum of germyl isocyanate[15,16] gave an angle at the nitrogen atom of approximately 170°. A preliminary microwave study[33] of the molecule, however, showed the angle to be about 154°.

A microwave study of silyl isocyanate[13] did confirm that the molecule is a symmetric top in its ground state, but unusual features in the spectrum were explained in terms of a very low-lying excited state. This corresponded to a vibrational frequency of less than 50 $cm.^{-1}$ if the assumptions used for small amplitude vibrations are valid.

A recent electron-diffraction study[14] of the same species has given an angle at the nitrogen atom of 152°. In order for this result to be consistent with the molecules' linearity as shown by microwave the molecule must have a skeletal bending vibration corresponding to a frequency of about 69 $cm.^{-1}$. This supports the explanation proposed for the microwave spectrum and is also consistent with assignments made in the infrared spectrum to combinations involving this skeletal bending vibration.

The infrared spectrum of trimethyl silyl isocyanate[34] is also consistent with a linear skeleton of the heavy atoms. Microwave data is not available but an electron diffraction study[35]

found an angle at nitrogen of 150°. This angle was defined by the peaks in the radial distribution curve corresponding to the non-bonded distances r(Si..O) and r(Si..C). Since no smearing of these peaks was observed the authors concluded that the molecule was non-linear.

(c) Isothiocyanates

Information available on the structure of the isothiocyanates is very similar to that previously discussed for the isocyanates. The conclusions drawn from this evidence are also very similar.

The silyl species was shown to be linear from its microwave spectrum[20] but again the spectrum is complicated by a low-lying excited state corresponding to a vibrational frequency rather greater than in the isocyanate. An electron diffraction study[14] of the molecule found an angle of 164° at the nitrogen atom and thus predicted a vibrational frequency of about 113 $cm.^{-1}$ for the skeletal deformation.

Microwave data is not available for germyl isothiocyanate but in this case the molecule was shown to be non-linear by the observation of two components (a' and a'') of the rocking deformation of the germyl group in the infrared spectrum.[21] The separation of the PR branches of the "parallel bands" in this spectrum suggest an angle of about 156° at nitrogen.

Again infrared evidence on the trimethyl silyl species

favours a linear skeleton but an electron diffraction study[35] showed an angle of 154° at the nitrogen atom. This was taken to imply a non-linear skeleton for the molecule, as shrinkage was not taken into account because of the absence of smearing on the peaks due to r(Si. .S) and r(Si..C).

(d) Summary

It is apparent that there are differences in geometrical structure between the germyl and silyl pseudohalides although these differences may not be as great as those between the species and their methyl analogues. The contrast between the silyl and methyl pseudohalides is best shown by the linearity of the skeletons of the silyl species'. Similar comparisons can be made in molecules containing carbon or silicon bound to an atom of group 6 (table 1.2).

The position of the germyl pseudohalides is less clear-cut. The spectroscopic evidence on these molecules often does not give definitive information on whether they resemble the silyl or methyl species more closely.

Structural evidence is thus presented in this work in an attempt to make this decision easier. Electron diffraction studies of germyl isocyanate and azide are reported (Chapter 2.2 and 2.4) together with infrared spectra in which the checking of assignments has been assisted by isotopic labelling (Chapter 4). The proton magnetic resonance spectra of the isotopically

M X Y	C H	Si H	Si F	Ge H	*
O	112[78]	144[82]	156[74]	126[85]	E
	112[79]	-	-	-	M
S	-	97[83]	-	99[85]	E
	99[80]	-	-	-	M
Se	-	97[84]	-	95[86]	E
	97[81]	-	-	-	M

* E denotes measurement by electron diffraction.

M " " " microwave spectroscopy.

TABLE 1.2 - The Angle ($\hat{MYM}$) in the Molecules $(MX_3)_2Y$.

substituted species' were recorded (Chapter 4) to investigate exchange between the possible isomers.

Photoelectron spectra of trimethyl silyl, silyl, germyl, and methyl pseudohalides were also recorded (Chapter 3) to determine any differences in bonding in these series' which could be used to interpret the structural data.

The aim of the work reported in Section I of this thesis was, therefore, to obtain as much information as possible on the molecular structures of silyl and germyl pseudohalides, and to correlate this information to give some idea of the differences in bonding between analogous carbon, silicon, and germanium compounds.

CHAPTER 2

MOLECULAR STRUCTURES OF PSEUDOHALIDES BY ELECTRON DIFFRACTION TECHNIQUES

2.1 General

The molecules studied by this method were:
germyl isocyanate, germyl azide, silyl isoselenocyanate, and digermyl carbodiimide.

The determination of the molecular structures of these species required different techniques and they will, therefore, be described in separate sections. The general experimental work was, however, very similar and thus will be described here.

The electron diffraction patterns obtained for each species were recorded photographically using the Balzers' KD.62 gas diffraction apparatus at the University of Manchester Institute of Science and Technology.[36] Three plates were exposed for each sample at nozzle-to-plate distances of 250, 500, and 1000 mms. The intensity information on the plates was converted to digital form using a fully-automated Joyce-Loebl microdensitometer at the Royal Observatory, Edinburgh. Reduction of the data and least squares refinements were performed on an IBM 360/50 computer at the Edinburgh Regional Computing Centre.

The programs used were very similar to those previously described by G.M. Sheldrick et al.[37] and are in four stages.

The first stage combines the corrected traces and subtracts a calculated atomic scattering curve. A cubic curve (found by least-squares fitting) is then subtracted to level the data across the plate.

The second stage allows subtraction of a background curve to account for incoherent atomic and other extraneous scattering. The best curve was found, in each case, by comparison of data from all three plates.

The third stage is the least squares refinement program based on that of Hedberg.[38] The complex scattering factors of Cox and Bonham[39] are used. The errors quoted at this stage were increased to allow for systematic errors such as the measurement of the wavelength associated with the electron beam (estimated error usually $\pm$ 0.00003 A°). This program also calculates two 'R-factors':-

$$R_G = \left(\frac{\bar{U}WU}{\bar{I}WI} \right)^{\frac{1}{2}}$$

and $$R_D = \left(\frac{\sum w_{jj} U_j^2}{\sum w_{jj} I_j^2} \right)^{\frac{1}{2}}$$

where I = vector of intensities, U = vector of residuals,

W = weight matrix with elements w_{jk}.

The final stage of the programs calculates and plots the radial distribution curves (P(r) and P(r)/r) by fourier inversion of the intensity curves. The distances calculated in the refinement stage correspond to the centres of gravity of the peaks in the P(r)/r curve.[40] No shrinkage corrections were applied in the programs.

The wavelength associated with the electron beam used to

produce the diffraction patterns remained constant for all the species studied. It was measured from the pattern given by a sample of powdered Thallous Chloride and was found to be 0.05659 ($\pm$ 0.00003) A°.

2.2 Germyl Isocyanate

The injection temperature of the sample used to obtain the diffraction pattern was maintained at 60°C. Sufficient flow of gaseous sample to photograph this pattern was possible with the bulk of the sample at room temperature.

The molecular intensity curves, final weighted difference curves, and weighting functions are shown in figure 2.1 and table 2.1.

Two sets of refinements (A and B) were carried out since best refinement of the model was achieved with less weight on the 250 mm. data than on the 500 and 1000 mm. data. The second set (figure 2.2 and table 2.2) are included to show that the results obtained by inclusion of the 250 mm. data with full weight were not significantly different from those with this data weighted down.

Only two assumptions were made about the structure of the molecule and these were incorporated in the model which was refined to fit the experimental data. These were that the (NCO) moiety is linear in its equilibrium position and that the germyl group has local C_3 symmetry although the rotation axis

Figure 2.1 - Intensity and difference curves for germyl isocyanate (Refinement A)

(a) 250 mm. data

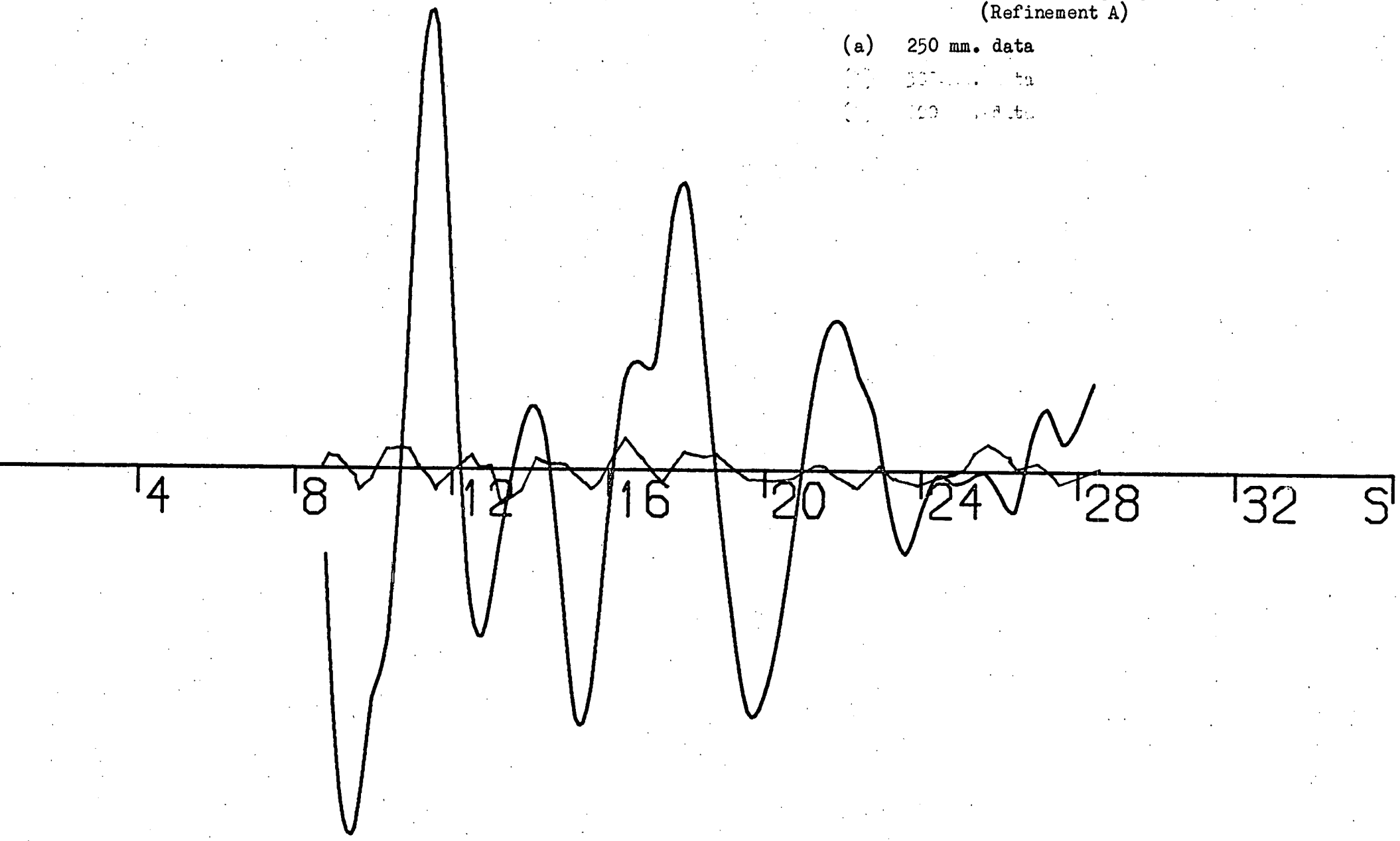

Figure 2.1 - Intensity and difference curves for germyl isocyanate (Refinement A)

(a) [illegible]

(b) 500 mm. data

(c) [illegible] mm. data

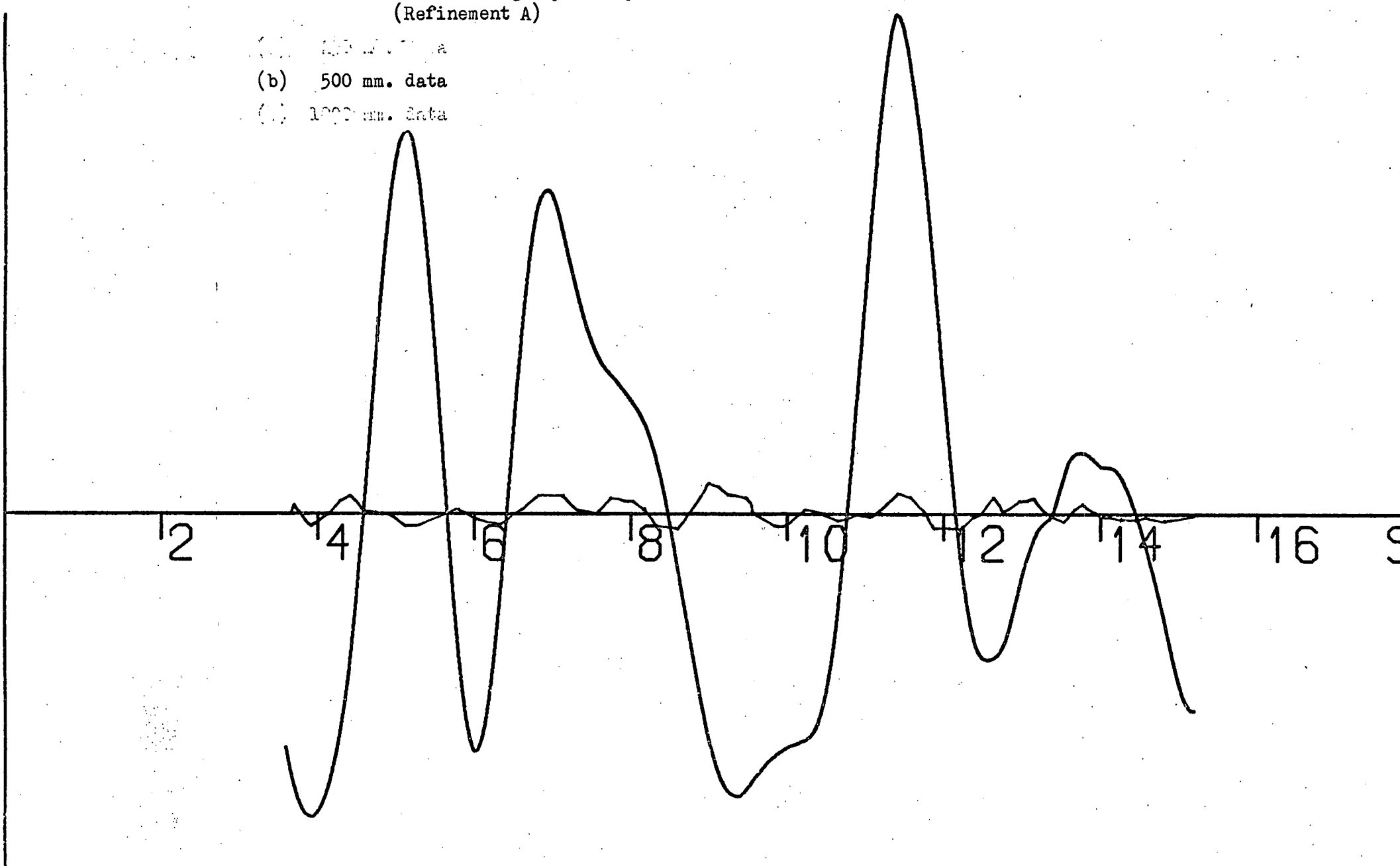

Figure 2.1 - Intensity and difference curves for germyl isocyanate (Refinement A)

(a) 250 mm. data

(b) 500 mm. data

(c) 1000 mm. data

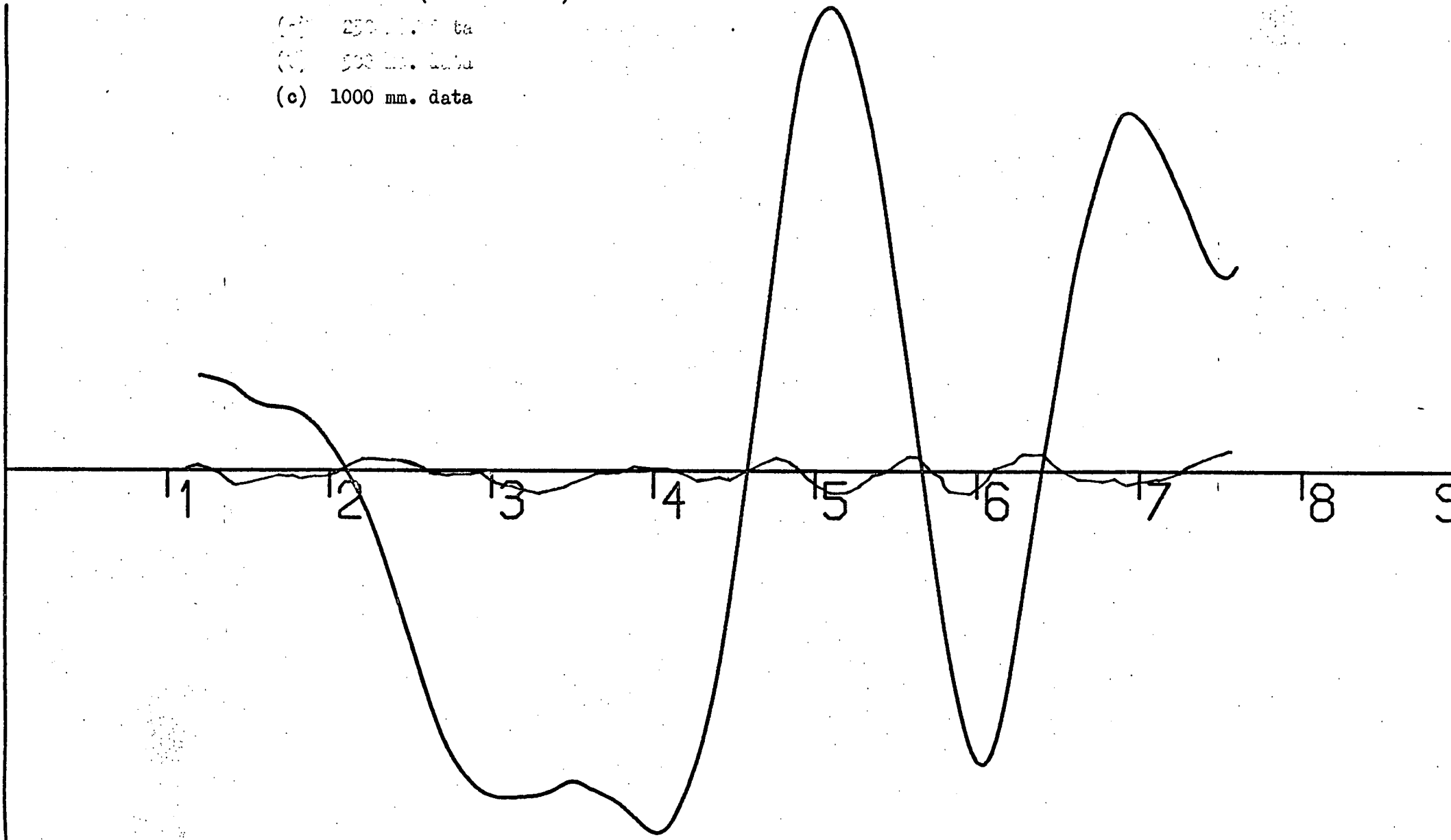

HEIGHT	DEL S	S MIN	S1	S2	S MAX	P/H	SCALE FACTOR	WAVELENGTH
250.0710	0.400	8.800	12.000	23.000	28.400	0.3502	0.801 ± 0.027	0.05659
500.0908	0.200	3.600	4.500	13.000	15.200	0.4179	0.762 ± 0.013	0.05659
1000.0950	0.100	1.200	2.200	6.400	7.600	0.4773	0.757 ± 0.017	0.05659

TABLE 2.1 WEIGHTING FUNCTIONS, CORRELATION PARAMETERS AND SCALE FACTORS (Refinement A)

HEIGHT	DEL S	S MIN	S1	S2	S MAX	P/H	SCALE FACTOR	WAVELENGTH
250.0710	0.400	8.800	12.000	23.000	28.400	0.3367	0.812 ± 0.033	0.05659
500.0908	0.200	3.600	4.500	13.000	15.200	0.4655	0.769 ± 0.020	0.05659
1000.0950	0.100	1.200	2.200	6.400	7.600	0.4871	0.757 ± 0.028	0.05659

TABLE 2.2 WEIGHTING FUNCTIONS, CORRELATION PARAMETERS AND SCALE FACTORS (Refinement B)

Figure 2.2 - Intensity and difference curves at 250 mm. for germyl isocyanate (Refinement B)

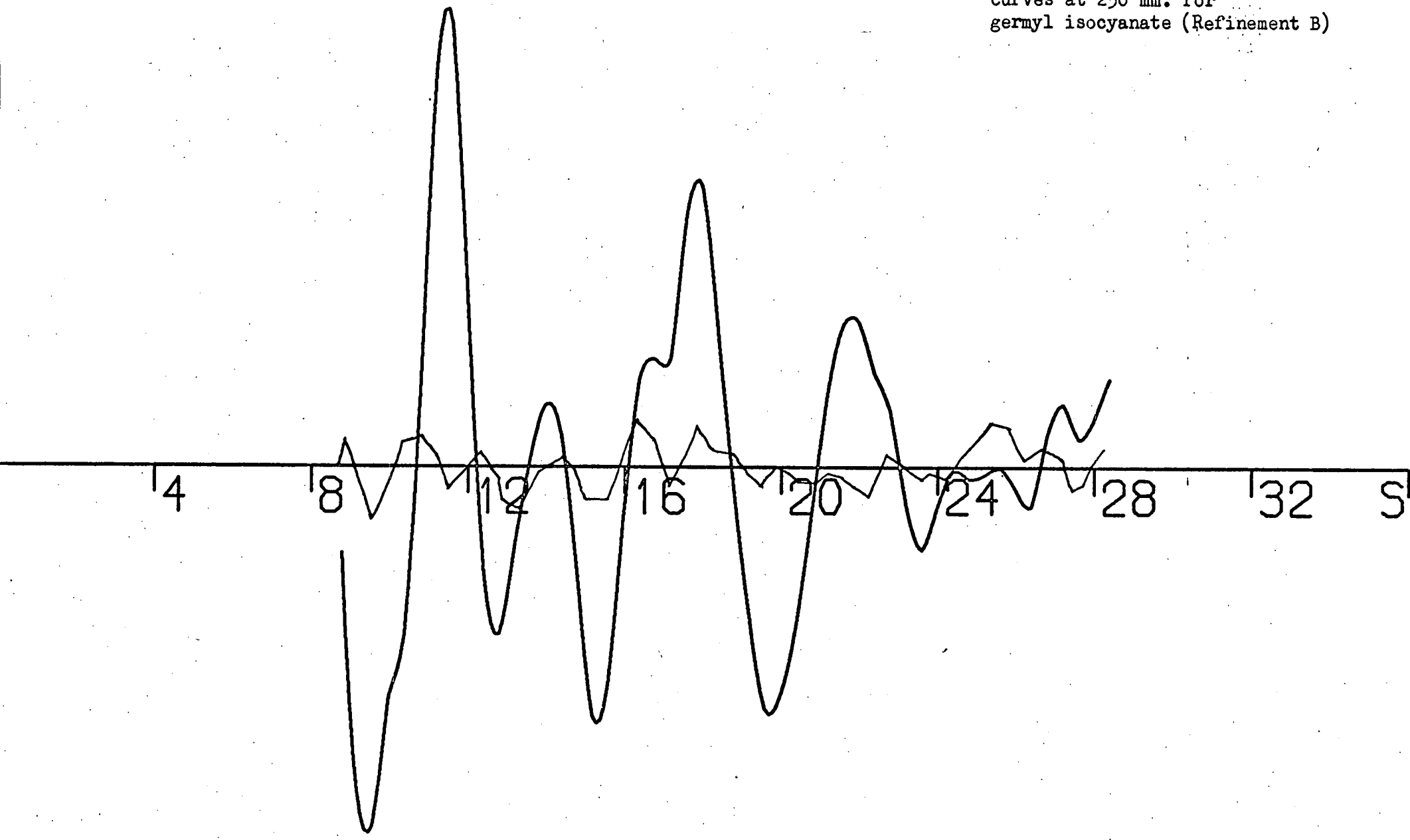

was not constrained to coincide with the (GeN) bond.

With these constraints eight parameters were required to define the relative positions of all the atoms in the molecule. The ones chosen were the equilibrium bond lengths (Ge H), (Ge N), (NC), and (CO), the bond angles (H $\hat{\text{Ge}}$ N) and (Ge $\hat{\text{N}}$C), the angle of twist of the germyl group relative to the (NC) bond, and the angle between the C_3 axis of the germyl group and the (Ge-N) bond.

All four bonded distances, the amplitudes of all of these except the (CO) bond, and the (Ge $\hat{\text{N}}$C) angle refined together independently.

The (Ge-H) and (Ge-N) peaks in the radial distribution curve (figure 2.3) are well separated but the peaks due to the (NC) and (CO) bonded distances are very close and overlap. Useful information on these distances was, however, obtained using the peak at 2.364 A° due to the (NO) distance. Careful refinement with few other parameters varying yielded a satisfactory ratio between the amplitudes of the (NC) and (CO) distances. With this ratio fixed the amplitude of the (CO) distance also refined satisfactorily with the other parameters.

Two other well-defined peaks in the radial distribution curve at 3.962 and 2.858 A° are due to the (Ge..C) and (Ge..O) non-bonded distances. Their amplitudes also refined satisfactorily.

No amplitudes of non-bonded distances to the hydrogen atoms would refine but some information was obtained from the

FIGURE 2.3(a)

Radial distribution curve for
germyl isocyanate (Refinement A)

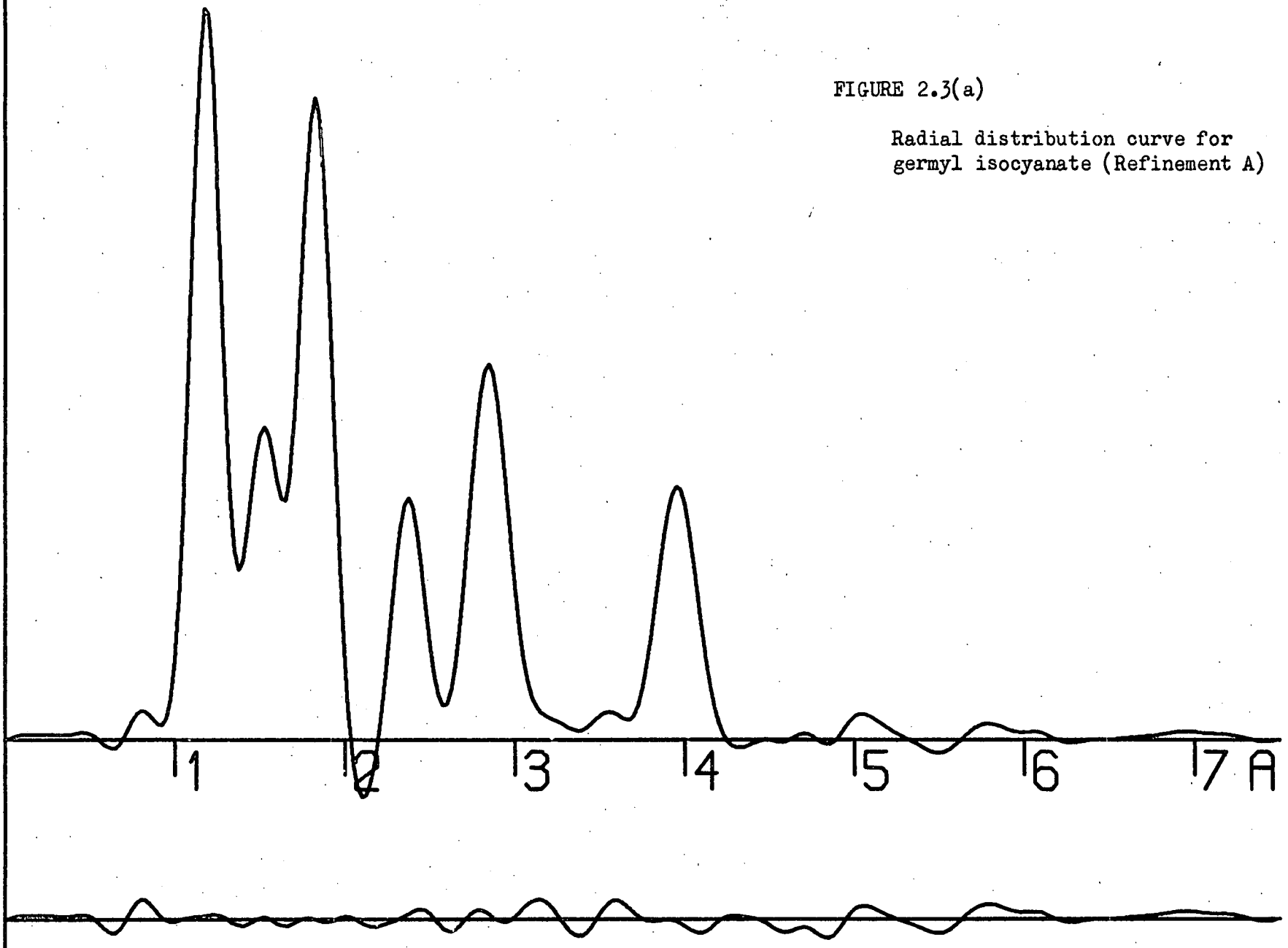

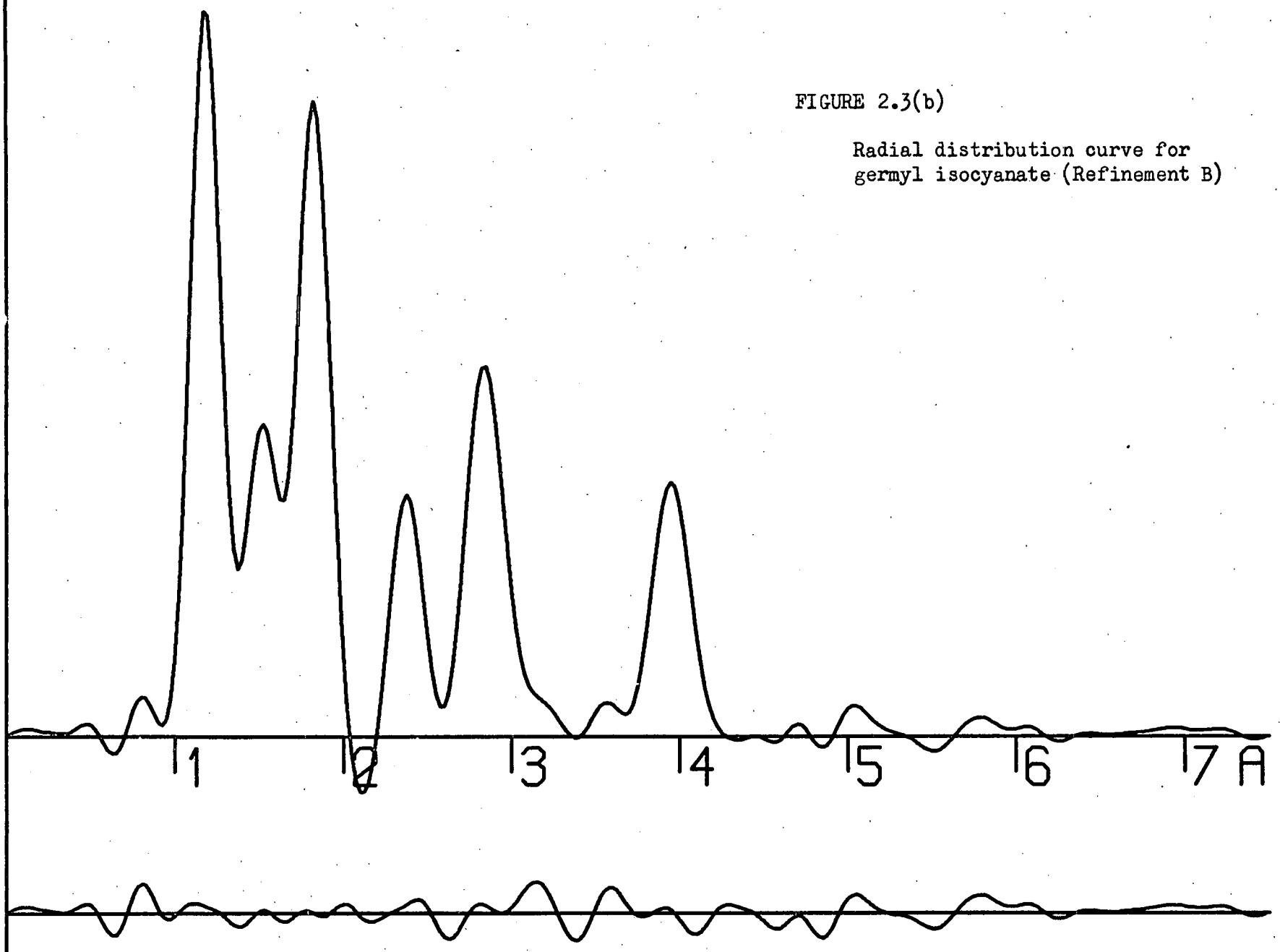

FIGURE 2.3(b)

Radial distribution curve for germyl isocyanate (Refinement B)

peaks due to these distances. Their amplitudes were fixed at reasonable values by comparison with similar molecules and refinements were carried out with the twist angle fixed at angles in the range 0° to 60°. A graph of these results showing the final R-factor obtained by refinement at the fixed twist angle is shown in figure 2.4. The 90% confidence level[41] is marked on this graph. The curve shows a minimum at 32° and when the twist angle was then set to 32° it refined within a region close to this value. It was therefore fixed at 32° for subsequent investigation of the positions of the hydrogen atoms.

This was attempted by a similar refinement with the angle of tilt (between the C_3 axis and the (GeN) bond) fixed at values in the range - 4.0 to +4.0°. A graph of the final R-factors obtained for each angle of tilt is shown in figure 2.5. The 95% confidence level[41] is marked on this curve. The minimum R-factor was obtained for a tilt angle of 0° and when set to this value it changed very little on refinement. It was therefore fixed at 0°.

The final molecular parameters and least squares correlation matrices for the two sets of refinements differing only in the weights given to the 250 mm. data set are shown in tables 2.3 to 2.6.

The final R-factors obtained in the two cases were:

Figure 2.4 - Variation of R- factor with twist angle in germyl isocyanate.

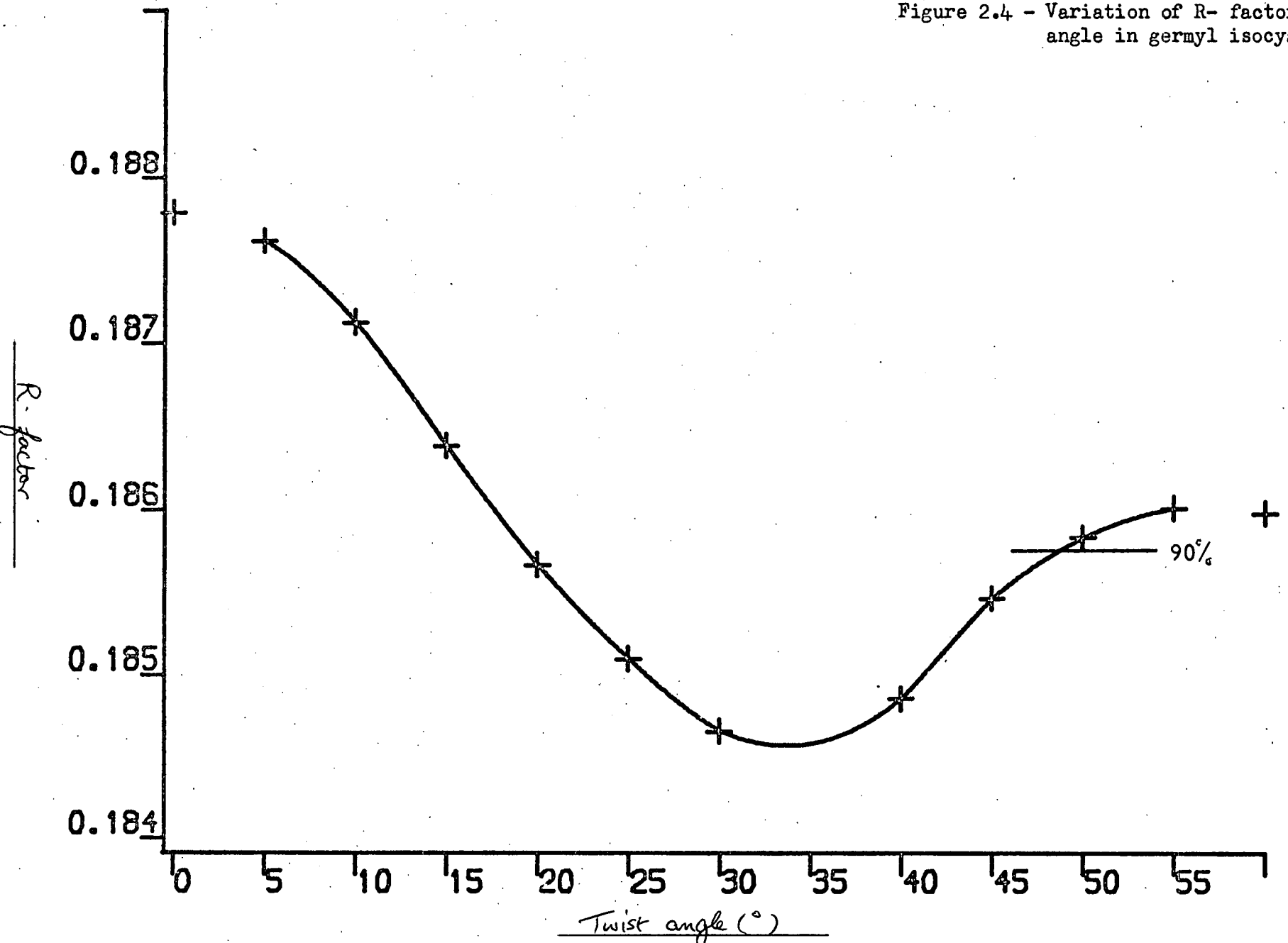

Figure 2.5 - Variation of R- factor with tilt angle in germyl isocyanate.

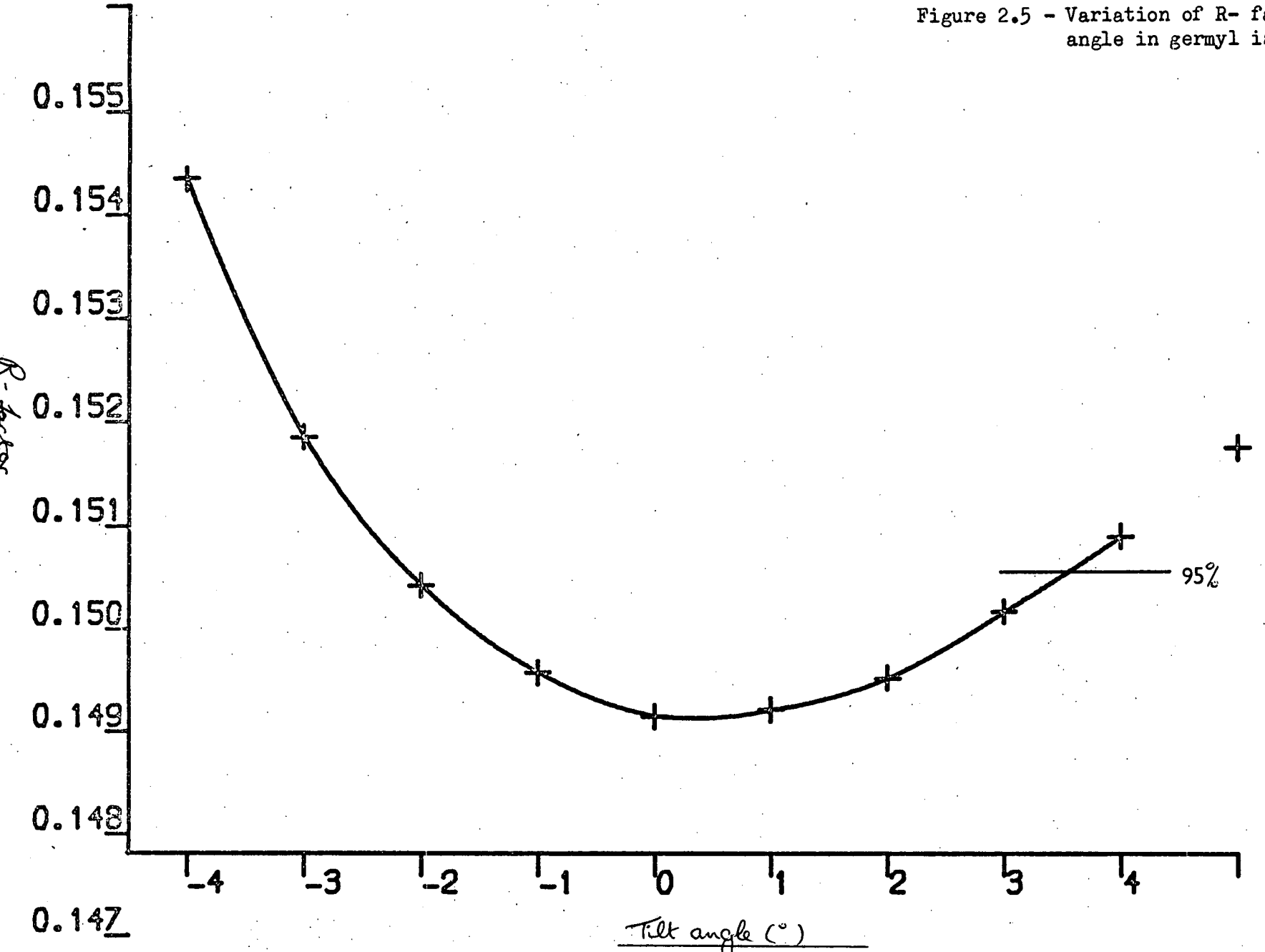

(A) Independent Distances

		Distance	Amplitude
R 1	(Ge - H)	1.532 ± 0.006	0.050 ± 0.010
R 2	(Ge - N)	1.831 ± 0.004	0.046 ± 0.006
R 3	(N - C)	1.190 ± 0.007	0.039 ± 0.006
R 4	(C - O)	1.182 ± 0.007	0.042 (Tied to U 3)

(B) Dependent Distances

D 1	(H... H)	2.493 ± 0.010	0.120 (Fixed)
D 2	(Ge... O)	3.961 ± 0.009	0.099 ± 0.006
D 3	(Ge... C)	2.858 ± 0.009	0.074 ± 0.006
D 4	(C... H)	3.902 ± 0.012	0.140 (Fixed)
D 5	(C... H)	3.393 ± 0.007	0.140 (Fixed)
D 6	(C... H)	3.671 ± 0.009	0.140 (Fixed)
D 7	(O... H)	5.050 ± 0.019	0.180 (Fixed)
D 8	(O... H)	4.258 ± 0.009	0.180 (Fixed)
D 9	(O... H)	4.695 ± 0.009	0.180 (Fixed)
D10	(N... O)	2.364 ± 0.007	0.045 ± 0.012
D11	(N... H)	2.760 ± 0.007	0.120 (Fixed)
D12	(N... H)	2.760 ± 0.009	0.120 (Fixed)
D13	(N... H)	2.760 ± 0.009	0.120 (Fixed)

(C) Independent Angles

∠1(H - Ge - N)	110.0 (Fixed)
∠2(Ge - N - C)	141.3 ± 0.2
∠3(Twist)	32.0 (Fixed)
∠4(Tilt)	0.0 (Fixed)

(D) Dependent Angles

∠5(H - Ge - H)	108.9 ± 0.2

TABLE 2.3 - Molecular Parameters for Germyl Isocyanate (refinement A).

R 1	R 2	R 3	R 4	<2	U 1	U 2	U 3	U 6	U 7	U14	K 1	K 2	K 3
1000	551	-27	327	-424	-2	-54	91	-32	69	-156	-7	-125	31
	1000	-211	398	-449	48	26	56	34	154	-129	28	56	105
		1000	-763	-566	-60	10	-79	97	-58	144	28	23	-53
			1000	73	-4	24	72	-92	34	-181	-26	-32	9
				1000	64	-44	10	-71	-76	33	-37	-48	0
					1000	383	237	29	36	15	282	-79	87
						1000	423	265	227	-27	562	453	113
							1000	251	297	118	601	427	115
								1000	193	110	343	430	153
									1000	-77	370	431	181
										1000	198	150	-64
											1000	469	142
												1000	79
													1000

TABLE 2.4 LEAST SQUARES CORRELATION MATRIX MULTIPLIED BY 1000 (Refinement A)

(A) Independent Distances

		Distance	Amplitude
R1	(Ge - H)	1.531 ± 0.007	0.049 ± 0.012
R2	(Ge - N)	1.830 ± 0.004	0.047 ± 0.006
R3	(N - C)	1.184 ± 0.008	0.040 ± 0.006
R4	(C - O)	1.190 ± 0.008	0.042 (tied to U 3)

(B) Some Dependent Distances

D2	3.962 ± 0.010	0.101 ± 0.007
D3	2.851 ± 0.011	0.077 ± 0.007
D10	2.367 ± 0.007	0.047 ± 0.012

(C) Independent Angles

∠ 1	(H - Ge - N)	110.0	(Fixed)
∠ 2	(Ge - N - C)	141.1 ± 0.3	
∠ 3	(Twist)	32.0	(Fixed)
∠ 4	(Tilt)	0.0	(Fixed)

TABLE 2.5 - Molecular Parameters for Germyl Isocyanate (refinement B).

R 1	R 2	R 3	R 4	<2	U 1	U 2	U 3	U 6	U 7	U14	K 1	K 2	K 3
1000	364	-120	182	-136	72	-312	-48	-103	-28	-90	-156	-215	-6
	1000	-291	318	-282	347	-123	-146	-37	5	-19	-83	-66	68
		1000	-803	-547	-165	98	164	99	-1	61	76	74	-13
			1000	137	70	-29	-107	-65	22	-35	-9	-21	-7
				1000	30	-63	-83	-69	-52	-45	-68	-71	-16
					1000	11	-111	-25	18	18	33	-159	57
						1000	549	369	371	226	725	498	84
							1000	360	403	292	731	440	75
								1000	255	194	461	416	124
									1000	151	534	406	126
										1000	395	234	4
											1000	510	107
												1000	39
													1000

TABLE 2.6 LEAST SQUARES CORRELATION MATRIX MULTIPLIED BY 1000 (Refinement B)

R_G = 0.125 and R_D = 0.069

for a weight of 0.3 to the 250 mm. data (refinement A),

and

R_G = 0.160 and R_D = 0.092

for full weight to the 250 mm. data (refinement B).

2.3 Digermyl Carbodiimide

The sample temperature and injection temperature used in this case were both 60°C. and plates were exposed at the usual three camera distances. The 1000 mm. plate however was too light to trace, and the 250 mm. data contained extraneous scattering. Therefore, the structure determination was performed with only the 500 mm. plate.

Figure 2.6 and table 2.7 show the molecular intensity curve, final weighted difference curve, and weighting functions used.

Three assumptions were made about the molecular structure and imposed as constraints in the refinement of the model. The (NCN) chain was assumed to be linear and the(C_3)axis of the germyl groups to be colinear with the (GeN) bond. The conformation of the hydrogens of the germyl groups was taken to be staggered with respect to the (NCN) skeleton.

Because of the symmetry of the molecule only six parameters were then required to define the relative positions of the atoms.

Figure 2.6 - Intensity and difference curves for digermyl carbodiimide.

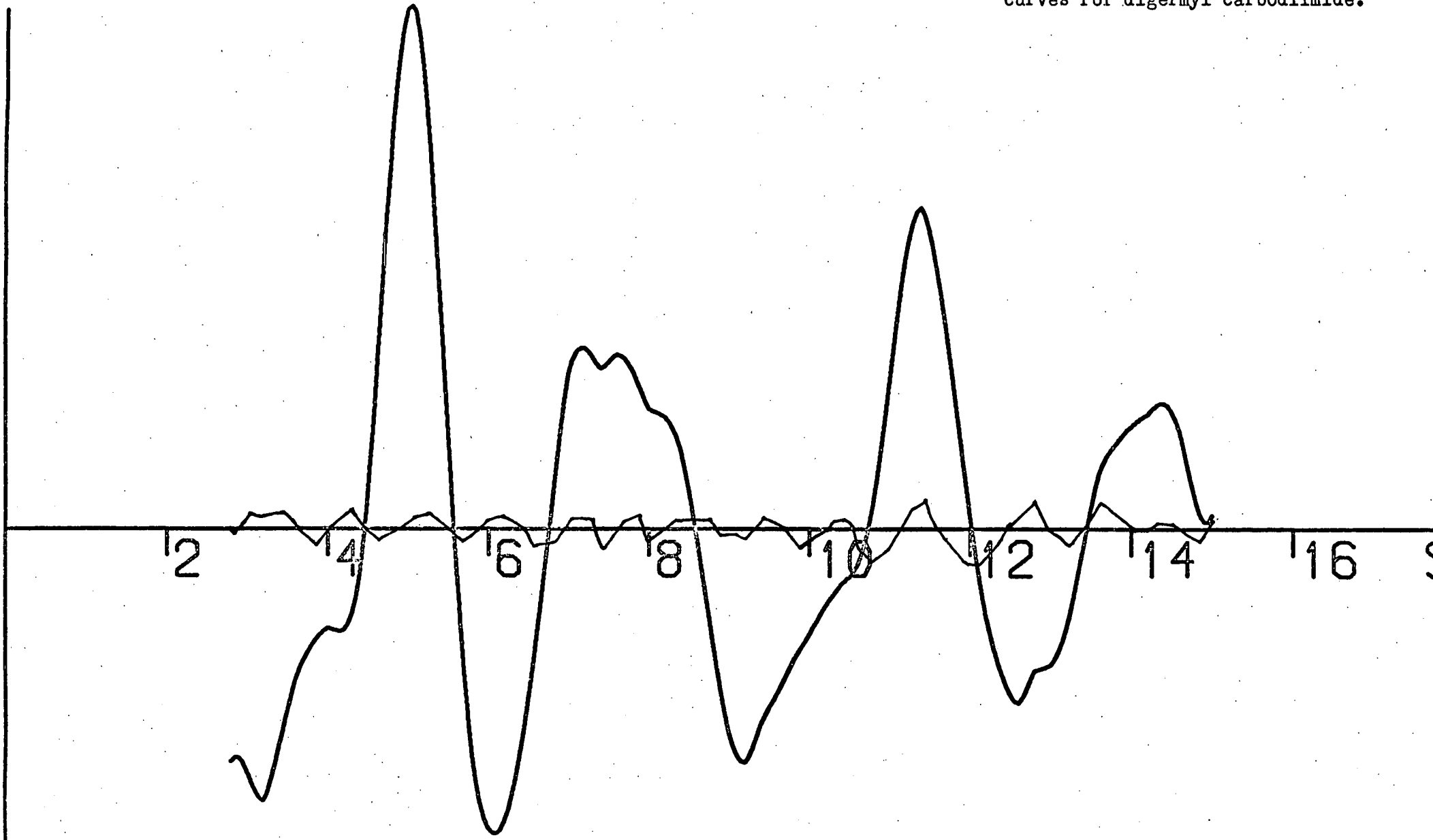

HEIGHT	DEL S	S MIN	S1	S2	S MAX	P/H	SCALE FACTOR	WAVELENGTH
500.0908	0.200	2.800	4.000	13.500	15.000	0.3036	0.679 ± 0.014	0.05659

TABLE 2.7 WEIGHTING FUNCTIONS, CORRELATION PARAMETERS AND SCALE FACTORS

Those chosen were the equilibrium bond lengths (GeH), (GeN) and (NC), the angles (HĜeN) and (GeN̂C), and the dihedral angle between the two (GeN) bonds - (Ge(N̂CN̂)Ge).

The absence of good 250 mm. data meant that no information could be obtained on the amplitudes of vibration of bonded distances. These amplitudes are small compared with those of longer interatomic distances and therefore, since information on an amplitude is derived from the damping of the sine wave corresponding to the interatomic distance involved, the scattering information at larger 'S' is required from the 250 mm. plate.

The amplitudes of vibration of the three bonded distances had to be fixed therefore to reasonable values by comparison with germyl isocyanate. The (GeH) bond length could not be refined satisfactorily at first and was also set to a reasonable value. The angle (HĜeN) was fixed to tetrahedral.

The dihedral angle (Ge(N̂CN̂)Ge) was initially fixed at 70° by comparison with the difluorophosphine compound[48] and the two bonded distances refined together with the angle (GeN̂C). After these refinements it was possible to refine the amplitude of (Ge...Ge) visually from the plot of the radial distribution curve - figure 2.7, although at this stage the agreement with the difference curve was not reflected significantly in the R-factor obtained. However, the amplitude (Ge..Ge) would then refine together with the amplitudes (Ge..C) and (Ge..N) if the dihedral angle remained fixed.

FIGURE 2.7

Radial distribution curve for digermyl carbodiimide

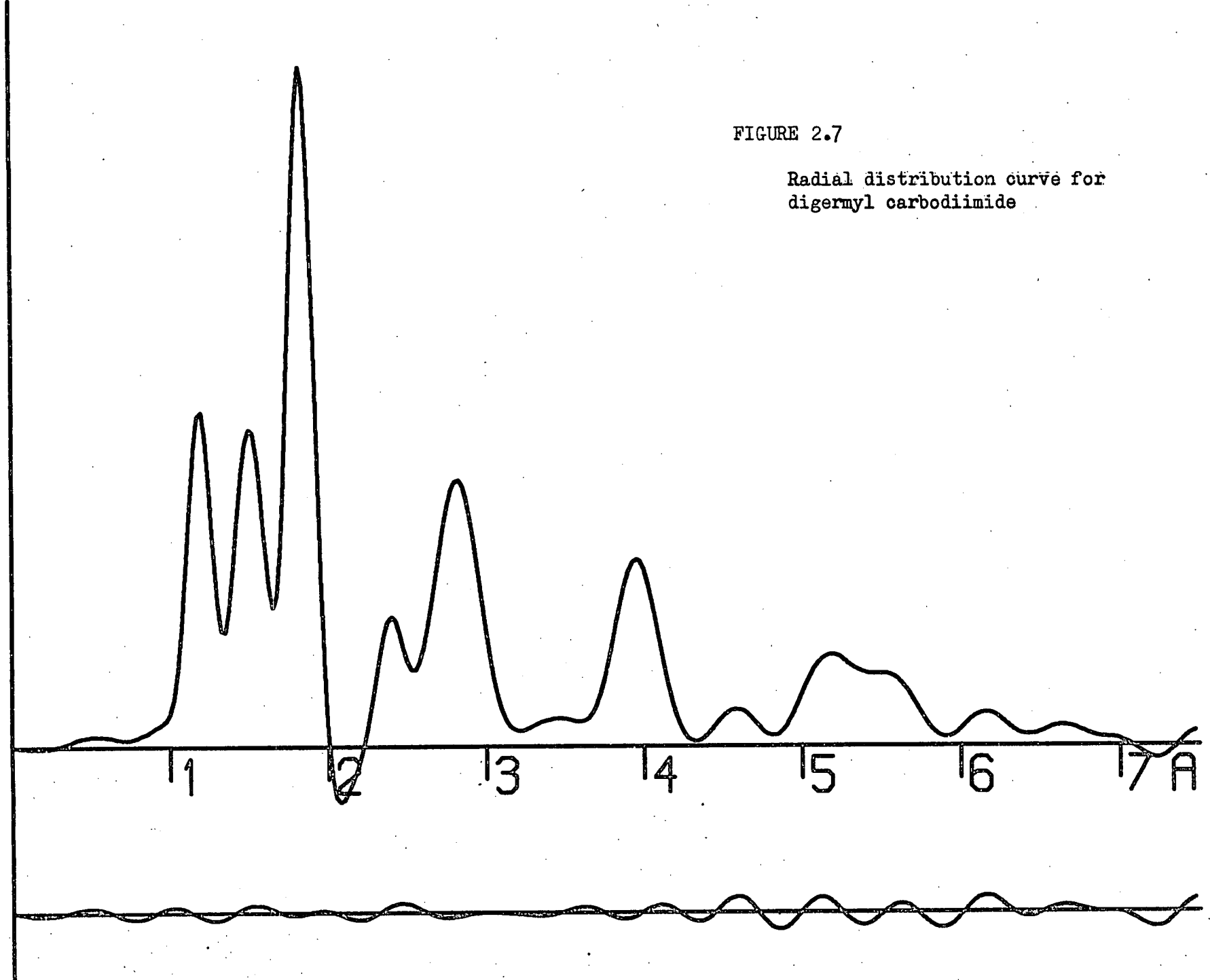

Allowing these refinements to continue the dihedral angle was fixed at values in the range 40 to 100° and a very definite minimum in the final R-factor was obtained for a dihedral angle of 75°. These results are plotted in figure 2.8. The 95% and 99.5% confidence levels[41] are marked on this graph. Figure 2.9 also shows the variation in the final amplitude (Ge..Ge) with the dihedral angle obtained in these refinements.

The dihedral angle was then set at 75° and allowed to refine with all the other parameters. The final angle found was 75.1° and the amplitude (Ge..Ge) was very close to that previously found to correspond with this dihedral angle.

The final molecular parameters and the least squares correlation matrix obtained from the refinements are shown in tables 2.8 and 2.9.

The final R-factors were:

$R_G = 0.118$ and $R_D = 0.090$

2.4 Germyl Azide

A sufficient flow of sample to photograph its diffraction pattern was obtained with the bulk of the sample cooled to 0°C. using an injection temperature of 60°C. Two series of three plates were exposed at the same three camera heights but one series when traced showed a considerable amount of random scattering. The second series was very much better but the data on the 500 mm. plate was not in good agreement with that from

Figure 2.8 - Variation of R- factor with the dihedral angle in digermyl carbodiimide.

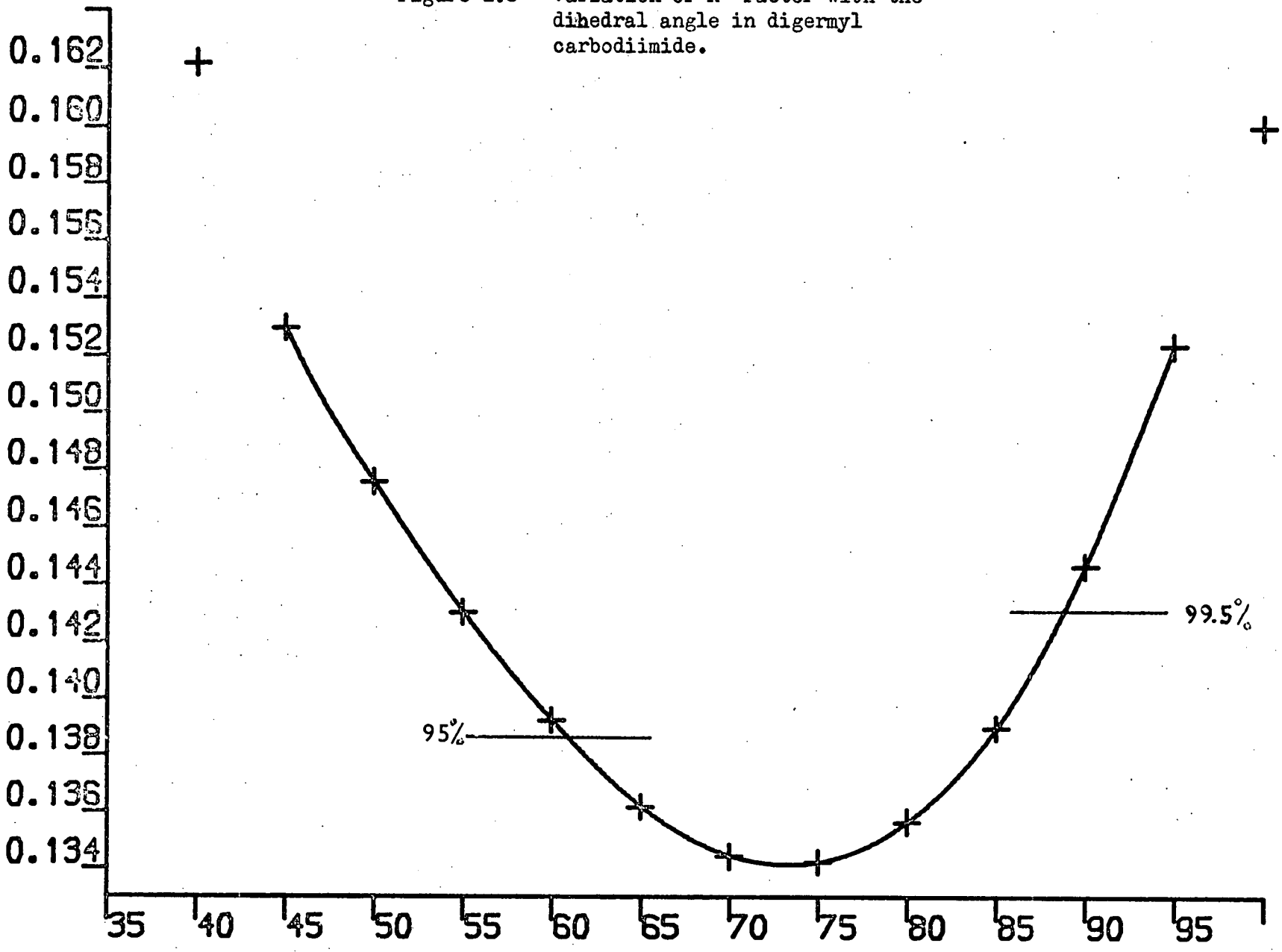

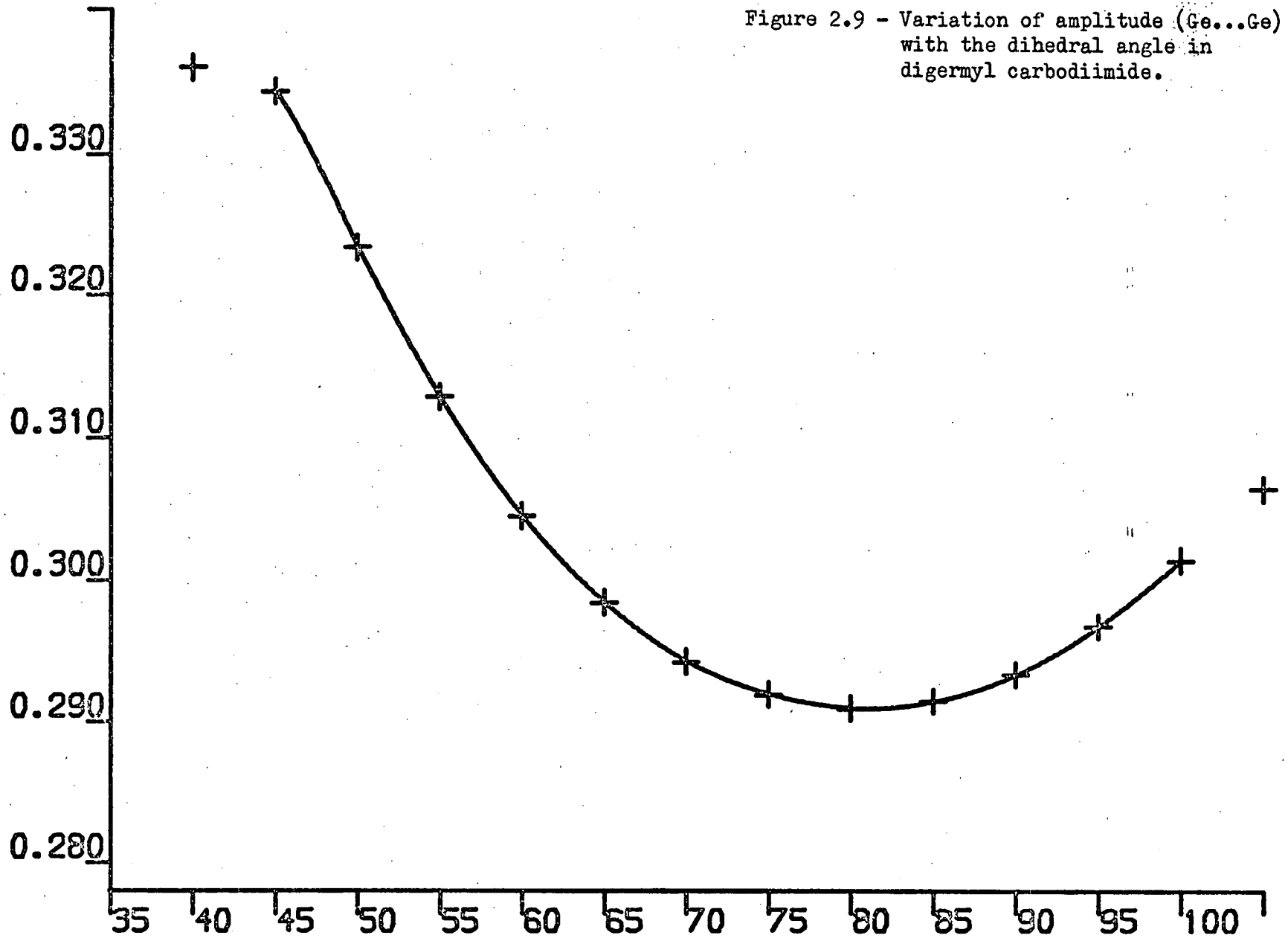

Figure 2.9 - Variation of amplitude (Ge...Ge) with the dihedral angle in digermyl carbodiimide.

(A) Independent Distances

		Distance	Amplitude
R 1	(Ge - H)	1.505 ± 0.010	0.050 (Fixed)
R 2	(Ge - N)	1.813 ± 0.005	0.035 (Fixed)
R 3	(C - N)	1.184 ± 0.009	0.040 (Fixed)

(B) Dependent Distances

D 1	(H... H)	2.456 ± 0.024	0.120 (Fixed)
D 2	(H... N)	2.714 ± 0.013	0.120 (Fixed)
D 3	(H... C)	3.423 ± 0.022	0.160 (Fixed)
D 4	(H... C)	3.883 ± 0.022	0.160 (Fixed)
D 5	(H... N)	4.341 ± 0.030	0.190 (Fixed)
D 6	(H... N)	5.058 ± 0.031	0.190 (Fixed)
D 7	(Ge... H)	6.488 ± 0.033	0.300 (Fixed)
D 8	(Ge... H)	5.782 ± 0.024	0.300 (Fixed)
D 9	(Ge... H)	5.261 ± 0.022	0.300 (Fixed)
D10	(Ge... C)	2.807 ± 0.015	0.121 ± 0.010
D11	(Ge... N)	3.906 ± 0.027	0.119 ± 0.010
D12	(Ge...Ge)	5.270 ± 0.030	0.291 ± 0.024
D13	(N... N)	2.367 ± 0.027	0.043 (Fixed)
D14	(H... H)	7.724 ± 0.045	0.320 (Fixed)
D15	(H... H)	6.602 ± 0.036	0.320 (Fixed)
D16	(H... H)	4.883 ± 0.007	0.320 (Fixed)
D17	(H... H)	5.675 ± 0.024	0.320 (Fixed)
D18	(H... H)	6.616 ± 0.024	0.320 (Fixed)
D19	(H... H)	6.790 ± 0.034	0.320 (Fixed)

(C) Independent Angles

∠1	(H - Ge-~~O~~-N)	109.5 (Fixed)
∠2	(Ge-N - C)	138.0 ± 0.5
*∠3	(Dihedral)	75.1 (Fixed)

(D) Dependent Angles

∠4	(H - Ge- H)	109.5 ± 0.1

* A dihedral angle of zero refers to the cis-configuration.

TABLE 2.8 - Molecular Parameters for Digermyl Carbodiimide.

HEIGHT	DEL S	S MIN	S1	S2	S MAX	P/H	SCALE FACTOR	WAVELENGTH
249.8810	0.400	6.800	8.400	24.000	28.400	0.0917	1.392 ± 0.050	0.05659
999.9048	0.100	1.200	2.250	6.000	7.700	0.4852	0.723 ± 0.054	0.05659

TABLE 2.10 WEIGHTING FUNCTIONS, CORRELATION PARAMETERS AND SCALE FACTORS FOR GERMYL AZIDE

R 1	R 2	R 3	⟨2	U13	U14	U15	K 1
1000	689	716	-753	-300	-66	-27	-307
	1000	414	-595	-73	21	17	-6
		1000	-895	-474	-97	-42	-416
			1000	383	56	29	309
				1000	170	91	551
					1000	71	331
						1000	183
							1000

TABLE 2.9 LEAST SQUARES CORRELATION MATRIX MULTIPLIED BY 1000

the 250 and 1000 mm. data. These two plates were therefore used for the final structure determination having checked that their data was consistent with the previous "noisy" series of plates.

The molecular intensity curves, final weighted difference curves, and weighting functions are shown in figure 2.10 and table 2.10.

The model refined to agree with the experimental data was identical to that used for germyl isocyanate except that the pseudohalide moiety (-NNN) was not constrained to a linear equilibrium configuration.

Nine parameters were therefore required to define the atomic positions - the equilibrium bond lengths of (GeH), (GeN), (N_1N_2), and (N_2N_3), the bond angles (HGeN), $(Ge\hat{N}_1N_2)$, the twist angle of the germyl group relative to the (N_1N_2) bond, the tilt angle between the C_3 axis of the germyl group and the (GeN) bond, and the non-linearity of the azide moiety $(N_1\hat{N}_2N_3)$.*

All four bonded distances in the molecule refined satisfactorily together with the angle $(Ge\hat{N}_1N_2)$,) despite the overlapping

---

* See figure 2.12 for the numbering of the nitrogen atoms of the azide moiety.

Figure 2.10 - Intensity and difference curves for germyl azide.

(a) 250 mm. data

(b) [illegible]

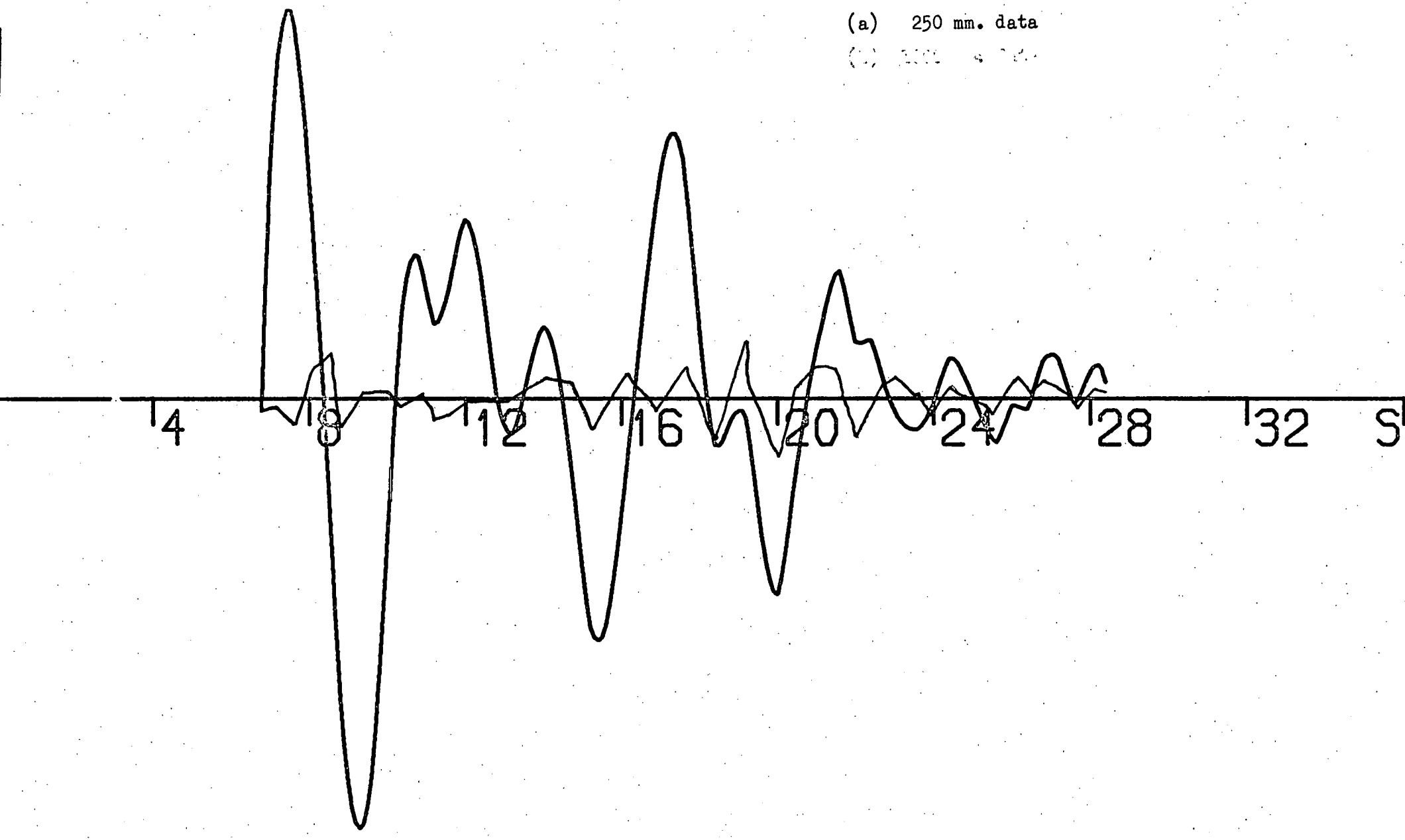

Figure 2.10 - Intensity and difference curves for germyl azide.

(b) 1000 mm. data

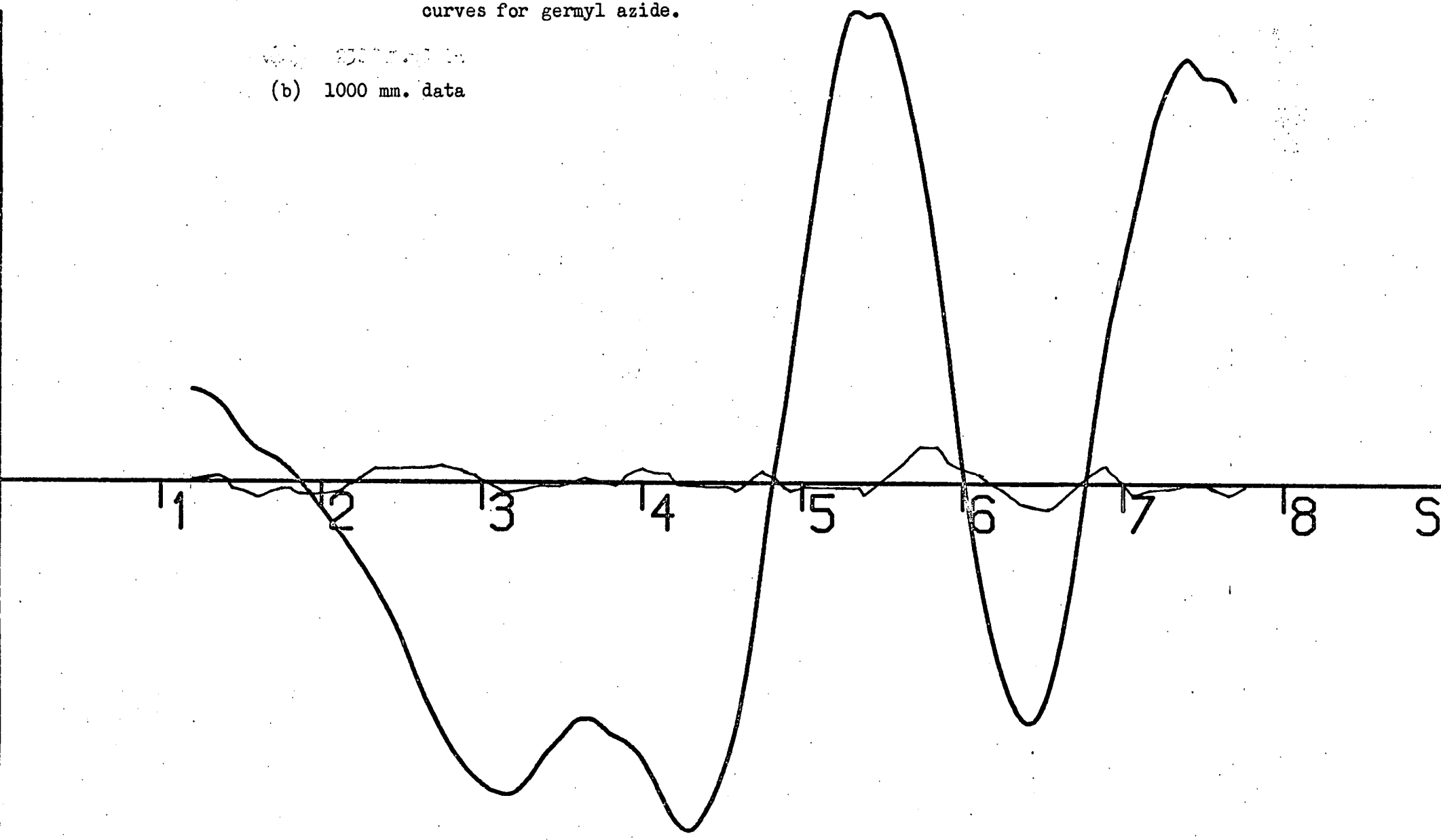

of the two peaks due to the two nitrogen/nitrogen distances in the radial distribution curve (figure 2.11). The vibrational amplitudes of the bonded distances all had to be fixed, however, except that of the (GeN) bond. They were all fixed at reasonable magnitudes by comparison with similar molecules. The tilt angle, the angle ($\hat{HGeN}$), all amplitudes involving hydrogen atoms, and the amplitude of the non-bonded ($N_1..N_3$) distance were similarly fixed. The bond angle within the pseudohalide moiety ($N_1\hat{N}_2N_3$) did refine, however, with the other parameters to very close to linear and the group was therefore constrained to linearity for further refinements.

The amplitudes of the other germanium-nitrogen distances - (Ge..N_2) and (Ge..N_3), also refined.

An attempt was also made to refine the phase parameter for the scattering produced by the (Ge-H) bonded distance. This parameter is defined in the data by the magnitude of the "S cut-off" - the point at which the envelope of the intensity curve produced by that molecular distance crosses the S axis of the intensity curve. In the case of germanium and hydrogen the S cut-off lies neither in the S region normally observed (using camera heights of 250 mm. and over), nor well outside this region. Its intermediate magnitude has an effect on the intensity curve which cannot be predicted without accurate knowledge of the phase parameter. It is not possible, however, to distinguish, in the observed S range, between the effects of the beating pattern defined by the phase parameter, and the exponential envelope of

FIGURE 2.11

Radial distribution curve for germyl azide

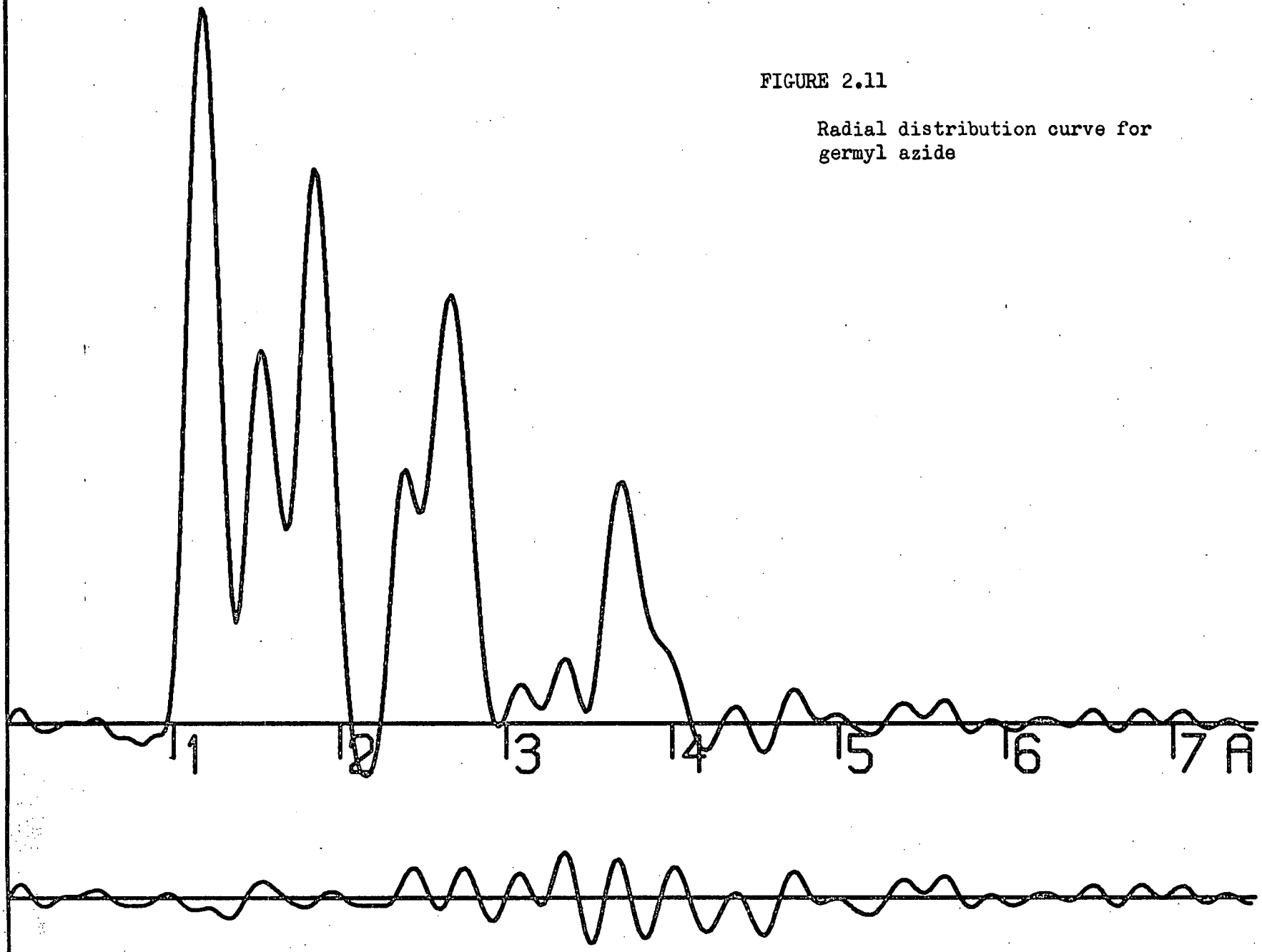

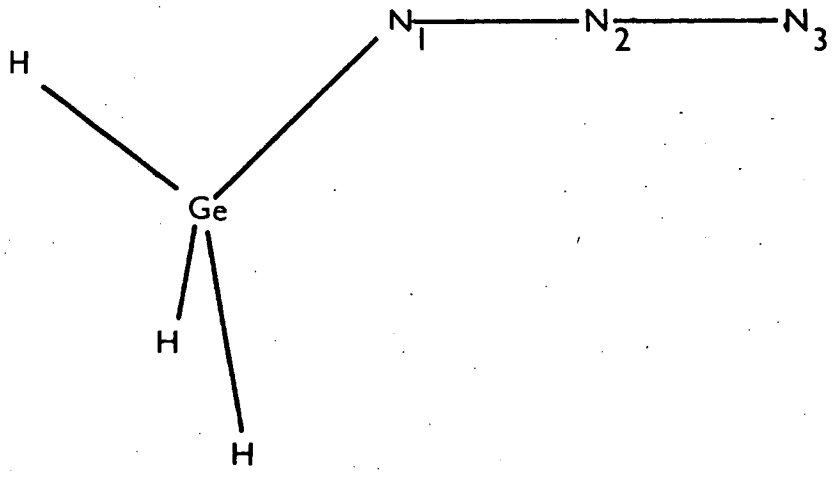

Figure 2.12 - Numbering of nitrogen atoms in germyl azide.

the intensity curve produced by the vibrational amplitudes of the molecule. As a result it is normal to accept the phase parameter derived from the separate germanium and hydrogen scattering factors and to refine the vibrational amplitudes of the molecule in the usual way.

This attempt to refine the phase parameter for (Ge-H) decreased the R-factor but only by adversely affecting the vibrational amplitudes. The R-factor decreased as the S cut - off decreased, but the amplitudes also decreased to magnitudes far smaller than those found in similar molecules. Refinement was also attempted with the vibrational amplitudes fixed but it then had very little effect on either the phase parameter or the R-factor.

A graph of the variation of the final R-factor with the twist angle from 0° to 60° is shown in figure 2.13 with the 99.5% confidence level[41] marked on it. The twist angle was then set at 18° and refined within the range 18 to 19°. There was, however, a high correlation between the twist angle and the amplitude (Ge...N_3).

The final parameters obtained for the molecule, and the least squares corrleation matrix are shown in tables 2.11 and 2.12. The final R-factors obtained from the two plates were:

$R_G = 0.178$ and $R_D = 0.130$.

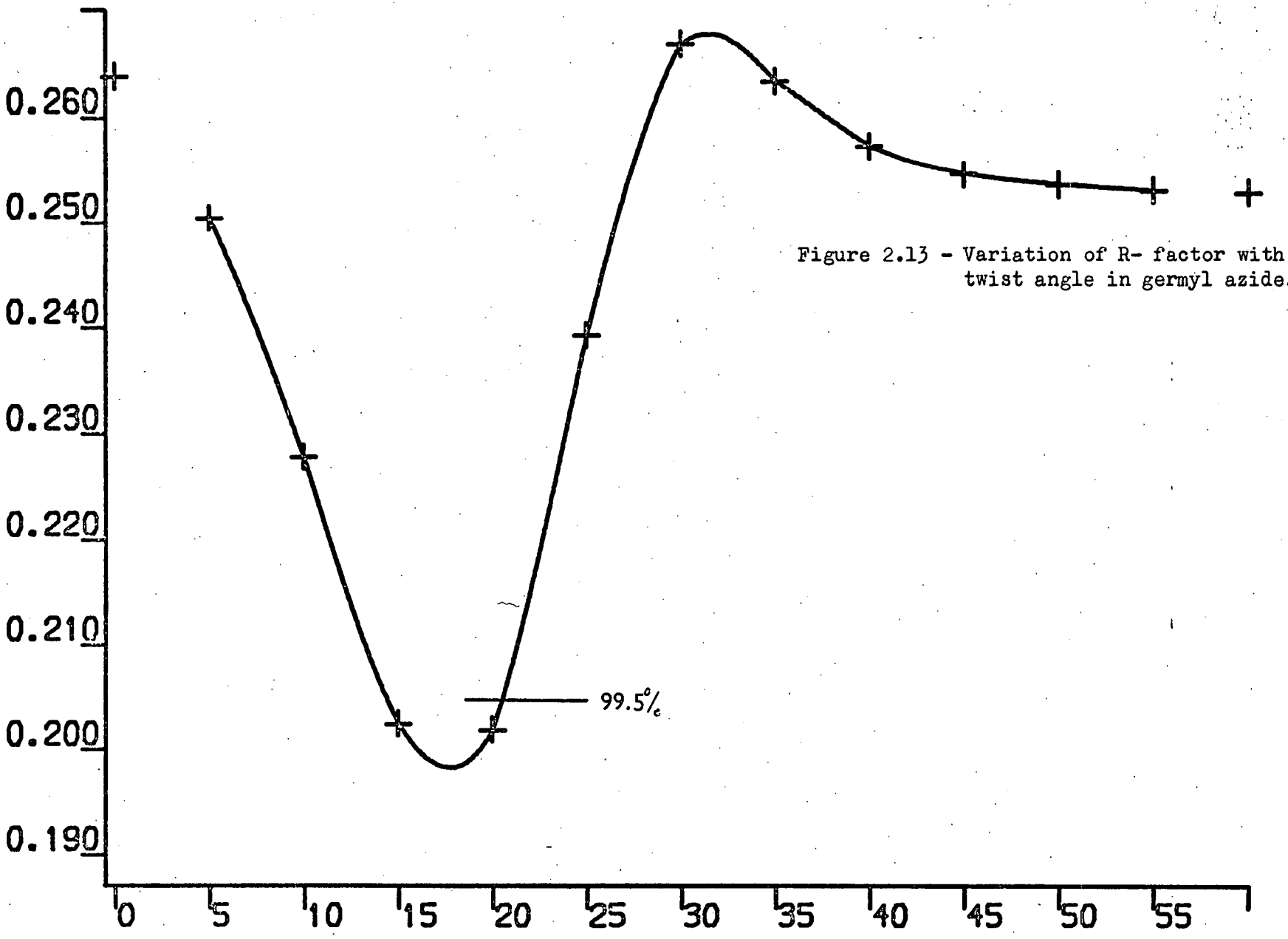

Figure 2.13 - Variation of R- factor with twist angle in germyl azide.

		Distance	Amplitude
(A) Independent Distances			
R 1	(Ge - H)	1.537 ± 0.007	0.040 (Fixed)
R 2	(Ge - N)	1.855 ± 0.004	0.081 ± 0.006
R 3	(N - N)	1.134 ± 0.004	0.035 (Fixed)
R 4	(N - N)	1.245 ± 0.004	0.034 (Fixed)
(B) Dependent Distances			
D 1	(H... H)	2.517 ± 0.013	0.120 (Fixed)
D 2	(Ge... N)	3.725 ± 0.022	0.134 ± 0.011
D 3	(Ge... N)	2.651 ± 0.012	0.095 ± 0.006
D 4	(H... N)	3.804 ± 0.013	0.170 (Fixed)
D 5	(H... N)	3.128 ± 0.012	0.170 (Fixed)
D 6	(H... N)	3.369 ± 0.012	0.170 (Fixed)
D 7	(H... N)	4.992 ± 0.018	0.200 (Fixed)
D 8	(H... N)	3.884 ± 0.018	0.200 (Fixed)
D 9	(H... N)	4.285 ± 0.012	0.200 (Fixed)
D10	(N... N)	2.370 ± 0.012	0.041 (Fixed)
D11	(H... N)	2.767 ± 0.009	0.130 (Fixed)
D12	(H... N)	2.767 ± 0.009	0.130 (Fixed)
D13	(H... N)	2.767 ± 0.009	0.130 (Fixed)
(C) Independent Angles			
∠ 1	(H-Ge-N)	109.0 (Fixed)	
∠ 2	(Ge-N-N)	123.2 ± 0.4	
∠ 3	(Twist)	19.1 ± 0.6	
∠ 4	(Tilt)	0.0 (Fixed)	
∠ 5	(N-N-N)	180.0 (Fixed)	
∠ 6	(Dihedral)	0.0 (Fixed)	
(D) Dependent Angles			
∠ 7	(H-Ge-H)	109.9 ± 0.02	

TABLE 2.11 - Molecular Parameters for Germyl Azide.

R 1	R 2	R 3	R 4	< 2	< 3	U 2	U 6	U 7	K 1	K 2
1000	485	181	-192	-287	147	-603	-157	-294	-527	49
	1000	41	-112	-356	-3	-250	-36	-19	-233	107
		1000	-76	-92	-175	-239	-97	-162	-336	-36
			1000	329	-406	484	140	291	621	-25
				1000	-742	276	58	288	362	-12
					1000	-256	-98	-392	-320	-44
						1000	223	420	791	-11
							1000	202	256	99
								1000	510	77
									1000	0
										1000

TABLE 2.12 - Least Squares Correlation Matrix Multiplied by 1000.

2.5 Silyl Isoselenocyanate

A suitable flow of sample was obtained with an injection temperature of 60°C. and the bulk of the sample at room temperature. Plates exposed at the usual three camera heights were used to refine the molecular structure but the R-factor was improved by decreasing the weight given to the 250 mm. plate in the total intensity data. The full weight was given to each of the other plates but only 50% to the 250 mm. plate in the final refinements.

Figure 2.14 and table 2.13 show the molecular intensity curves, final weighted difference curves, and weighting functions used.

The model used to refine the structure was identical to that used for germyl isocyanate (see section 2.2). The parameters used to define the relative atomic positions were the bonded distances (SiH), (SiN), (NC) and (CSe), the bond angles ($\hat{HSiN}$) and ($\hat{SiNC}$), the angle of twist of the silyl group relative to the (NC) bond, and the tilt angle between the C_3 axis of the silyl group and the (SiN) bond. The tilt angle was, however, fixed at 0°.

The (SiH) distance was also fixed - by comparison with similar molecules. All vibrational amplitudes of the bonded distances had to be fixed because of the poor 250 mm. data (See section 2.3).

Two major peaks in the radial distribution curve (figure 2.15)

Figure 2.14 - Intensity and difference curves for silyl isoselenocyanate.

(a) 250 mm. data

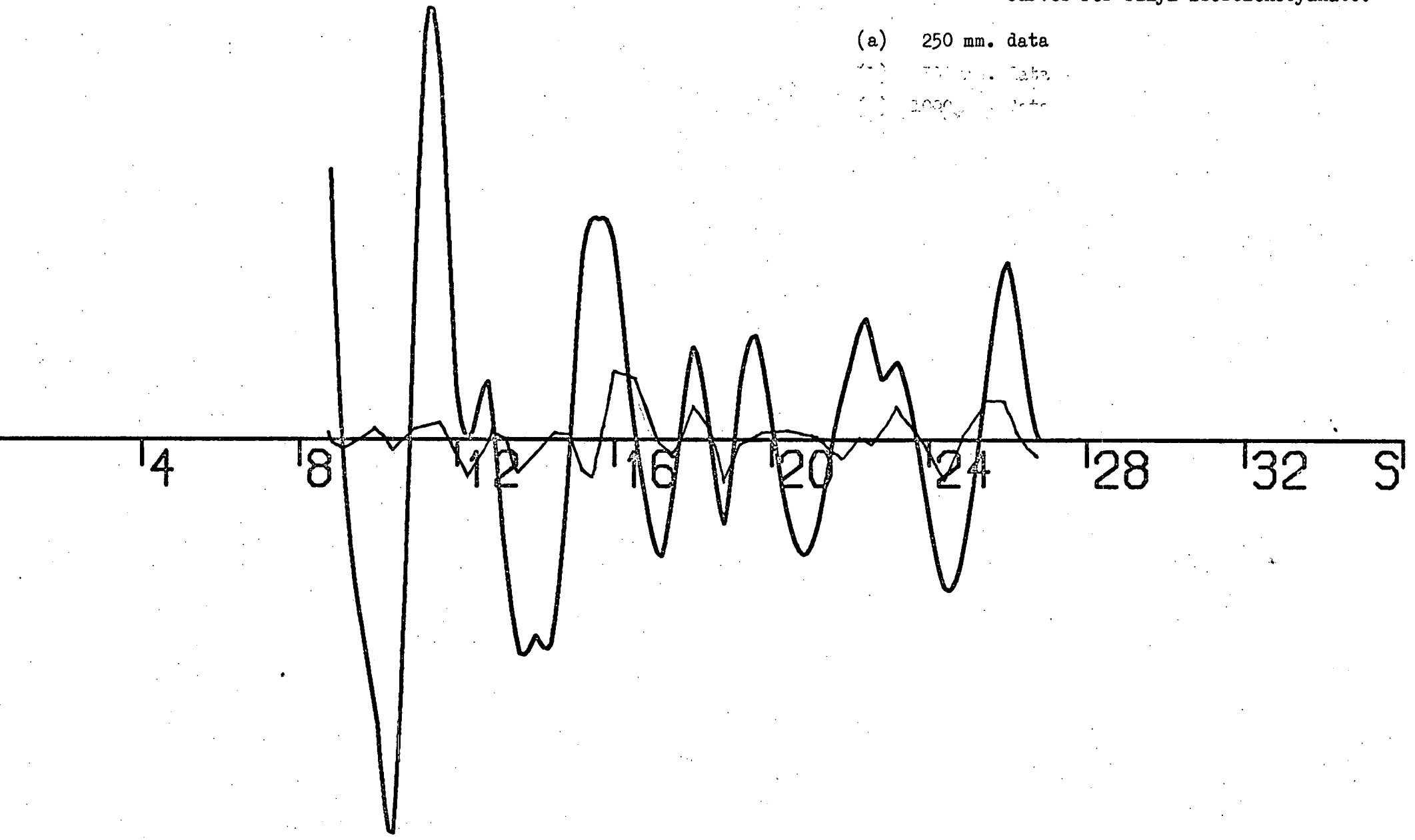

Figure 2.14 - Intensity and difference curves for silyl isoselenocyanate.

(a) 250 mm. data

(b) 500 mm. data

(c) 1000 mm. data

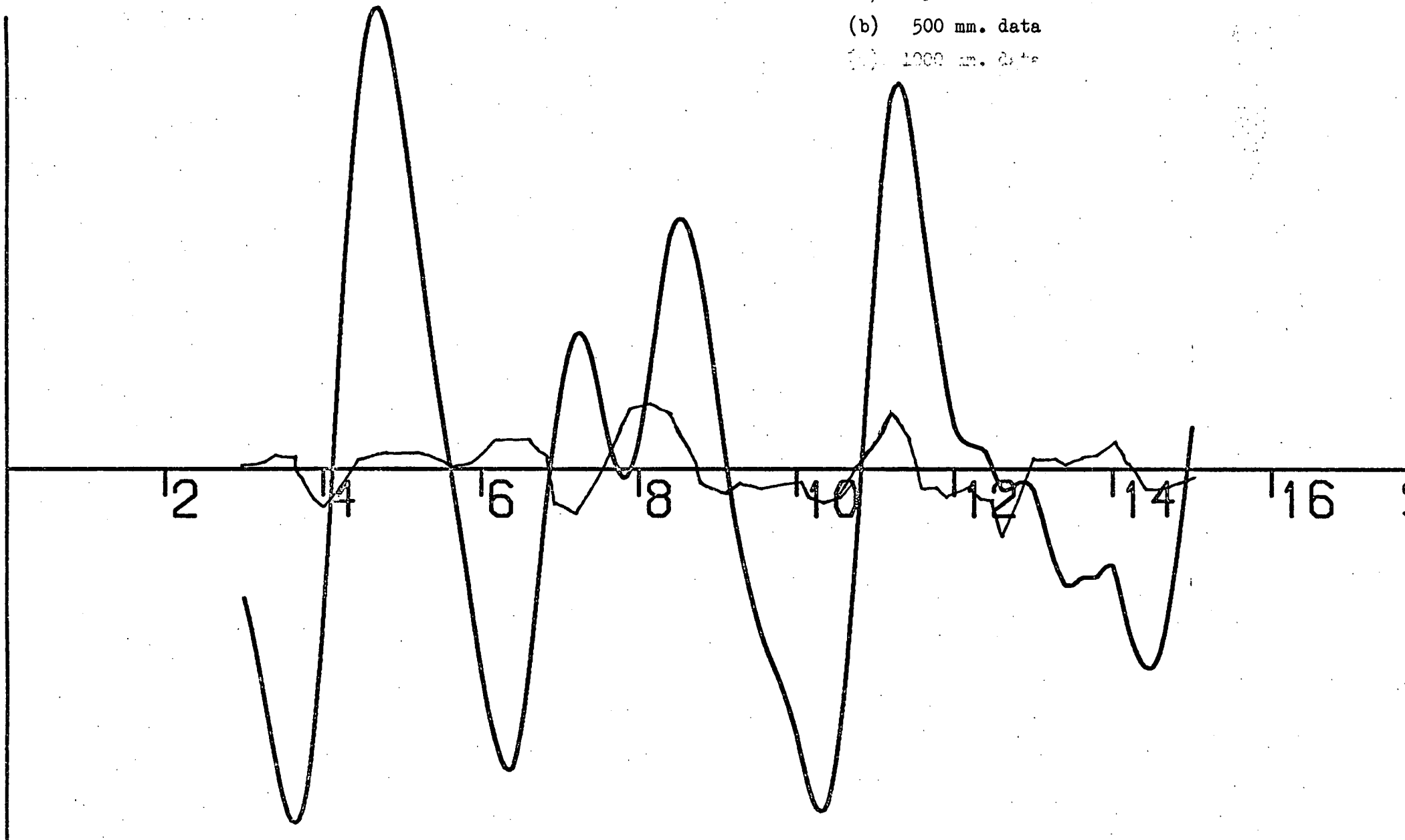

Figure 2.14 - Intensity and difference curves for silyl isoselenocyanate.

(c) 1000 mm. data

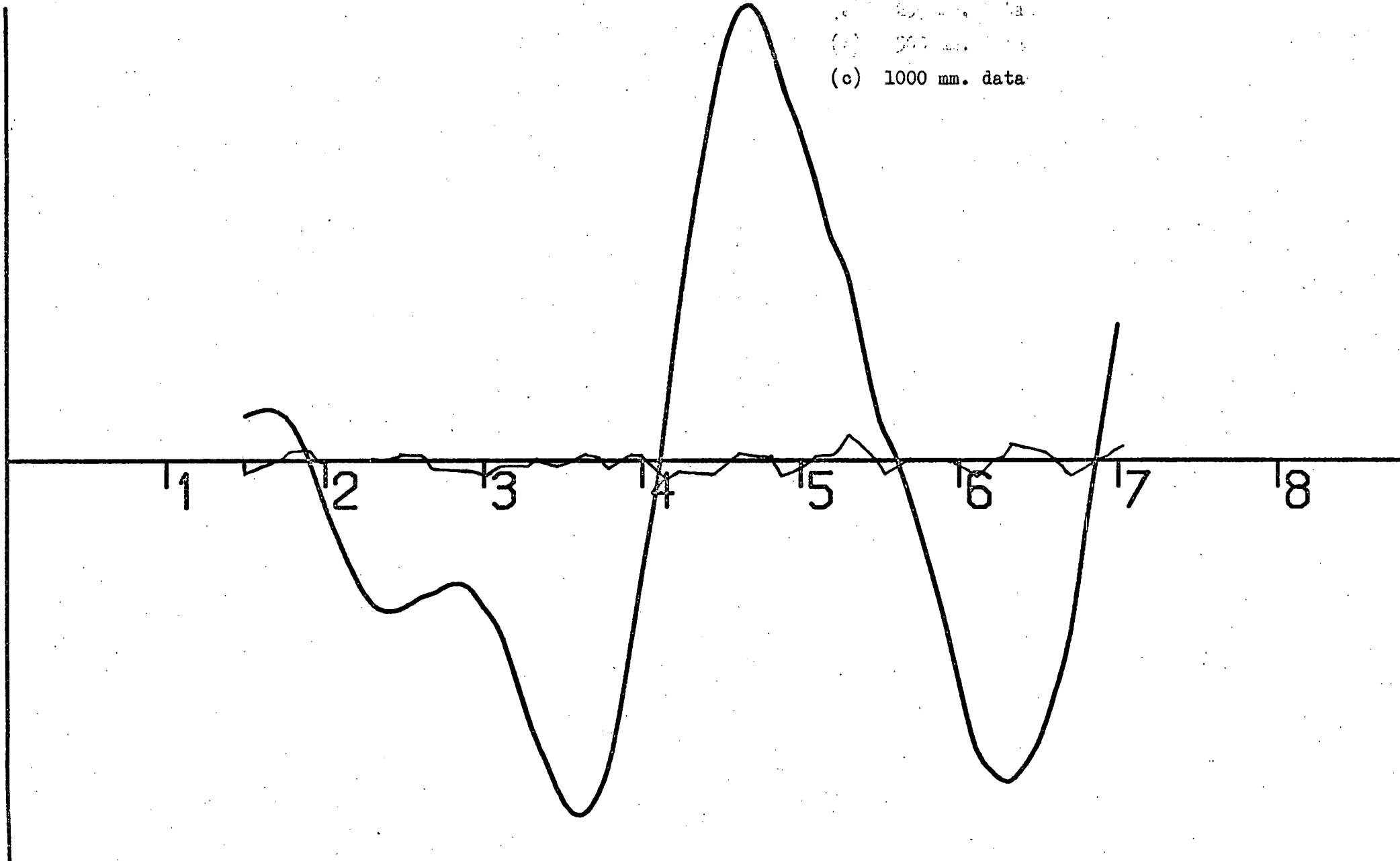

HEIGHT	DEL S	S MIN	S1	S2	S MAX	P/H	SCALE FACTOR	WAVELENGTH
250.0710	0.400	8.800	11.000	23.000	26.800	0.2924	0.646 ± 0.029	0.05659
500.0908	0.200	3.000	4.000	13.000	15.000	0.4798	1.020 ± 0.022	**0.05659**
1000.0950	0.100	1.500	2.000	6.500	7.000	0.3895	0.588 ± 0.017	0.05659

TABLE 2.13 WEIGHTING FUNCTIONS, CORRELATION PARAMETERS AND SCALE FACTORS

FIGURE 2.15

Radial distribution curve for silyl isoselenocyanate

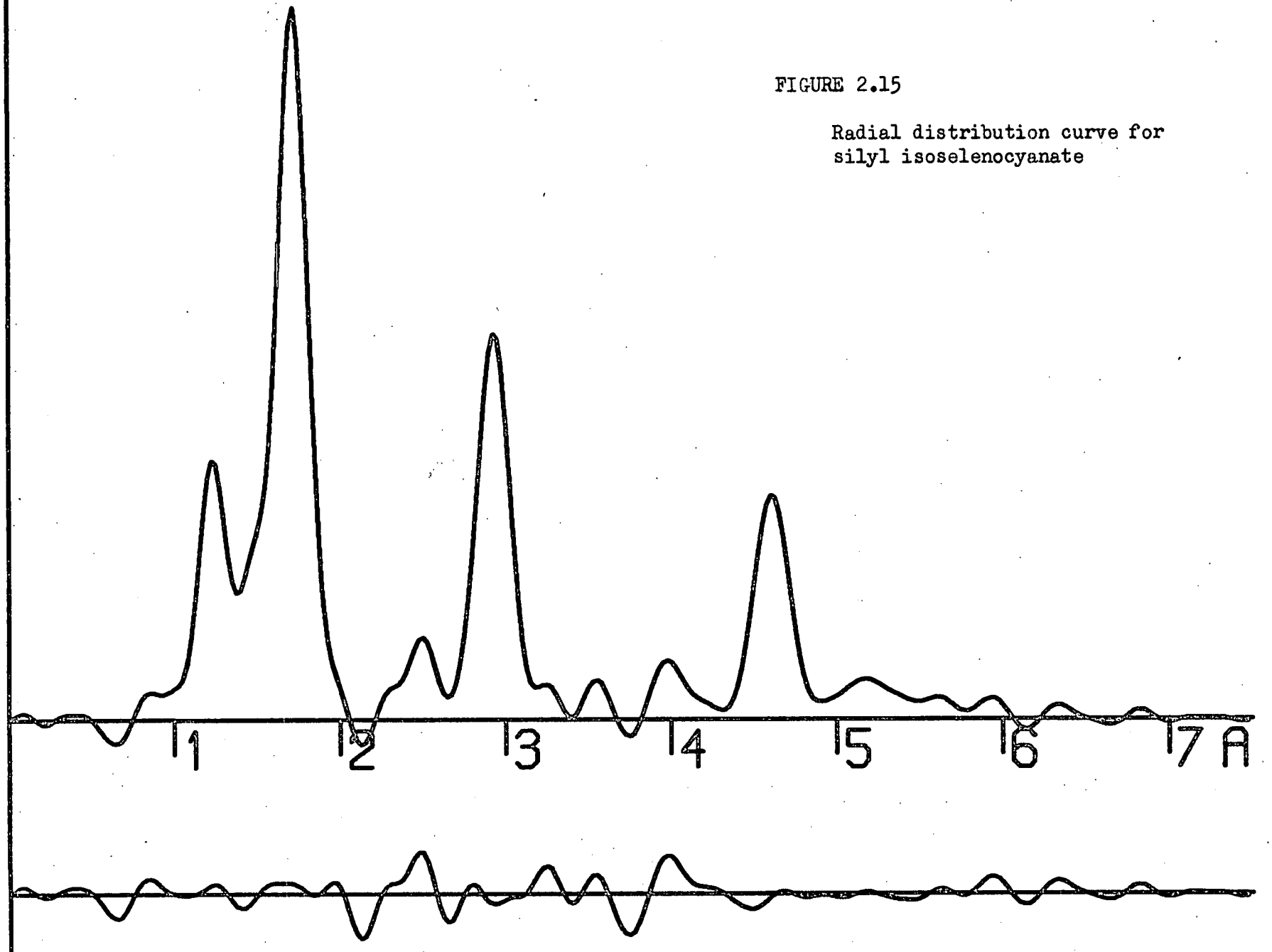

- due to (CSe) and (SiN), overlap. This caused considerable difficulty in the refinements. These two distances would not at first refine together using the available intensity data. The distance (CSe) was, therefore, fixed at a magnitude slightly larger than in the molecules COSe[42] and CSSe[43]. (1.709 A° in both). The (CS) distance in COS[44], CSSe[43], and CS_2[45] is 1.56 A° and in -NCS is also 1.56 A°.[46] The (CO) distance in COS,[44] CO_2[47]; and COSe[42] is 1.16 A° while in -NCO[46] is 1.17 A°. The amplitude of (CSe) was also fixed in agreement with the series -NCO[46], -NCS[46], -NCSe.

After refinement of the other parameters - the bonded distances (SiN) and (CN), the amplitudes of (Si..Se) and (Se..N), and the angle (SiNC), the bond length (CSe) was released and refined satisfactorily together with the other parameters close to its magnitude when previously fixed. The amplitude (Si..C) also refined satisfactorily if the 250 mm. data was fully weighted but had to be fixed to its refined value when the weight was reduced to 50%.

Tables 2.14 and 2.15 show the effect on the final R-factor of variation of the twist angle in the regions 0 to 60°, and 0 to 20°. The first set of data shows a minimum R-factor for a twist angle of about 10° and the more accurate data gives a minimum at about 7°. The twist angle was, therefore, fixed at 7° for the final refinement.

The final molecular parameters and the least squares

Angle	R-factor
0	0.1856
5	o.1841
10	0.1828
15	0.1848
20	0.1855
25	0.1866
30	0.1863
35	0.1872
40	0.1888
45	0.1899
50	0.1909
55	0.1915
60	0.1921

TABLE 2.14 - Variation of R-factor with twist angle for silyl isoselenocyanate.

Angle	R-factor
0	0.1856
2	0.1844
4	0.1838
6	0.1830
8	0.1832
10	0.1842
12	0.1860
14	0.1848
16	0.1857
18	0.1858
20	0.1848

TABLE 2.15 - Variation of R-factor with twist angle for silyl isoselenocyanate.

correlation matrix are shown in tables 2.16 and 2.17.

The final R-factors obtained were:

$$R_G = 0.184 \text{ and } R_D = 0.128$$

for weights on the three data sets of 0.5, 1.0, and 1.0.

2.6 Discussion

The parameters obtained in the electron-diffraction structure determinations described above are discussed, together with spectroscopic results obtained using isotopically substituted pseudohalides, in Chapter 5.

(A) Independent Distances

		Distance	Amplitude
R 1	(Si - H)	1.485 (Fixed)	0.080 (Fixed
R 2	(Si - N)	1.703 ± 0.024	0.050 (Fixed)
R 3	(N - C)	1.215 ± 0.013	0.035 (Fixed)
R 4	(Se - C)	1.716 ± 0.018	0.045 (Fixed)

(B) Dependent Distances

D 1	(H... H)	2.417 ± 0.012	0.120 (Fixed)
D 2	(Si... Se)	4.554 ± 0.028	0.096 ± 0.005
D 3	(Si... C)	2.871 ± 0.040	0.056 ± 0.029
D 4	(C... H)	3.812 ± 0.037	0.140 (Fixed)
D 5	(C... H)	3.550 ± 0.033	0.120 (Fixed)
D 6	(C... H)	3.585 ± 0.033	0.140 (Fixed)
D 7	(Se... H)	5.508 ± 0.033	0.180 (Fixed)
D 8	(Se... H)	5.068 ± 0.028	0.180 (Fixed)
D 9	(Se... H)	5.129 ± 0.022	0.180 (Fixed)
D10	(Se... N)	2.952 ± 0.015	0.044 ± 0.015
D11	(N... H)	2.617 ± 0.027	0.120 (Fixed)
D12	(N... H)	2.617 ± 0.022	0.120 (Fixed)
D13	(N... H)	2.617 ± 0.022	0.120 (Fixed)

(C) Independent Angles

∠1	(H-Si-N)	110.0 (Fixed)
∠2	(Si-N-C)	159.0 ± 0.6
∠3	(Twist)	7.0 (Fixed)
∠4	(Tilt)	0.0 (Fixed)

(D) Dependent Angles

∠5	(H-Si-H)	109.0 ± 0.5

TABLE 2.16 - Molecular Parameters for Silyl Isoseleno-cyanate.

R 2	R 3	R 4	< 2	U 6	U 7	U14	K 1	K 2	K 3
1000	479	-927	-525	-136	602	-57	-239	-204	-314
	1000	-480	-834	-83	33	231	-153	-84	-245
		1000	361	147	-543	19	249	245	372
			1000	57	-245	-11	126	29	147
				1000	-40	75	184	342	131
					1000	-612	-72	-73	-116
						1000	138	128	10
							1000	44	185
								1000	188
									1000

TABLE 2.17 - Least Squares Correlation Matrix Multiplied by 1000.

CHAPTER 3

THE PHOTO-ELECTRON SPECTRA OF GROUP FOUR PSEUDOHALIDES

3.1 Introduction

The photo-ionisation of molecules by a source of known energy, followed by an analysis of the kinetic energy of the electrons released, gives a direct measure of ionisation potentials. The bands observed in photo-electron spectra, therefore, correspond to excitation of an electron from particular orbitals in the molecule. For small molecules the observed bands can be assigned to ionisation from specific molecular orbitals if, as is usual, Koopmans' theorem[49] is accepted. For larger molecules, however, assignment of the observed bands to excitation from specific molecular orbitals is usually only possible for the first ionisation potential, which corresponds to the highest occupied level. Further assignments can sometimes be made in these molecules by comparison within an extensive series of very similar molecules.

The approach used in making assignments in this study of the group four pseudohalides was one of comparison of the silyl, germyl, and trimethyl silyl species with their methyl analogues and also with their corresponding hydrides. The degree of complexity of these molecules precluded the use of molecular orbital calculations directly for the assignment of the observed bands.

The hydrides were used as the basis for comparison as their spectra could be satisfactorily assigned by comparison with the linear species - carbon dioxide, carbonyl sulphide, and

nitrous oxide.[50]

3.2 Molecular Orbitals

The 'σ' molecular orbitals of carbon dioxide are formed from combinations of the 2s and $2p_z$ atomic orbitals of oxygen and the 2s and $2p_z$ orbitals of carbon, where the 'z' axis is taken to be coincident with the molecular symmetry axis. Molecular orbitals of 'π' symmetry are produced by combinations of the $2p_x$ and $2p_y$ orbitals of both carbon and oxygen. An energy diagram of the molecular orbitals produced from these combinations is shown in figure 3.1. The occupied levels may thus be described in order of increasing energy as - 1σ, 2σ, 3σ, 4σ, 1π, 2π. Photoelectron spectroscopy has been used to determine the energies of these orbitals[50] and has shown that the order is as given above. Similar sets of energy levels may be derived for carbonyl sulphide and nitrous oxide, although since the point group is $C_{\infty v}$ rather than $D_{\infty h}$ the orbitals may no longer be labelled 'u' and 'g'.

The order of the levels in nitrous oxide,[49] however, is not the same, as the 1π level is of lower energy than the 4σ level giving the order - 1σ, 2σ, 3σ, 1π, 4σ, 2π.

The energy levels used in this discussion of the pesudohalides are shown in figure 3.2. For pseudohalide molecules with a linear skeleton the pattern of levels of the pseudohalide group is identical to that used for carbonyl sulphide and nitrous

Figure 3.1 - M.O. energy diagram for carbon dioxide
(bonding and non-bonding levels only)

Order of levels in increasing energy is

$1\sigma_g$, $2\sigma_g$, $3\sigma_u$, $4\sigma_u$, $1\pi_g$, $2\pi_u$

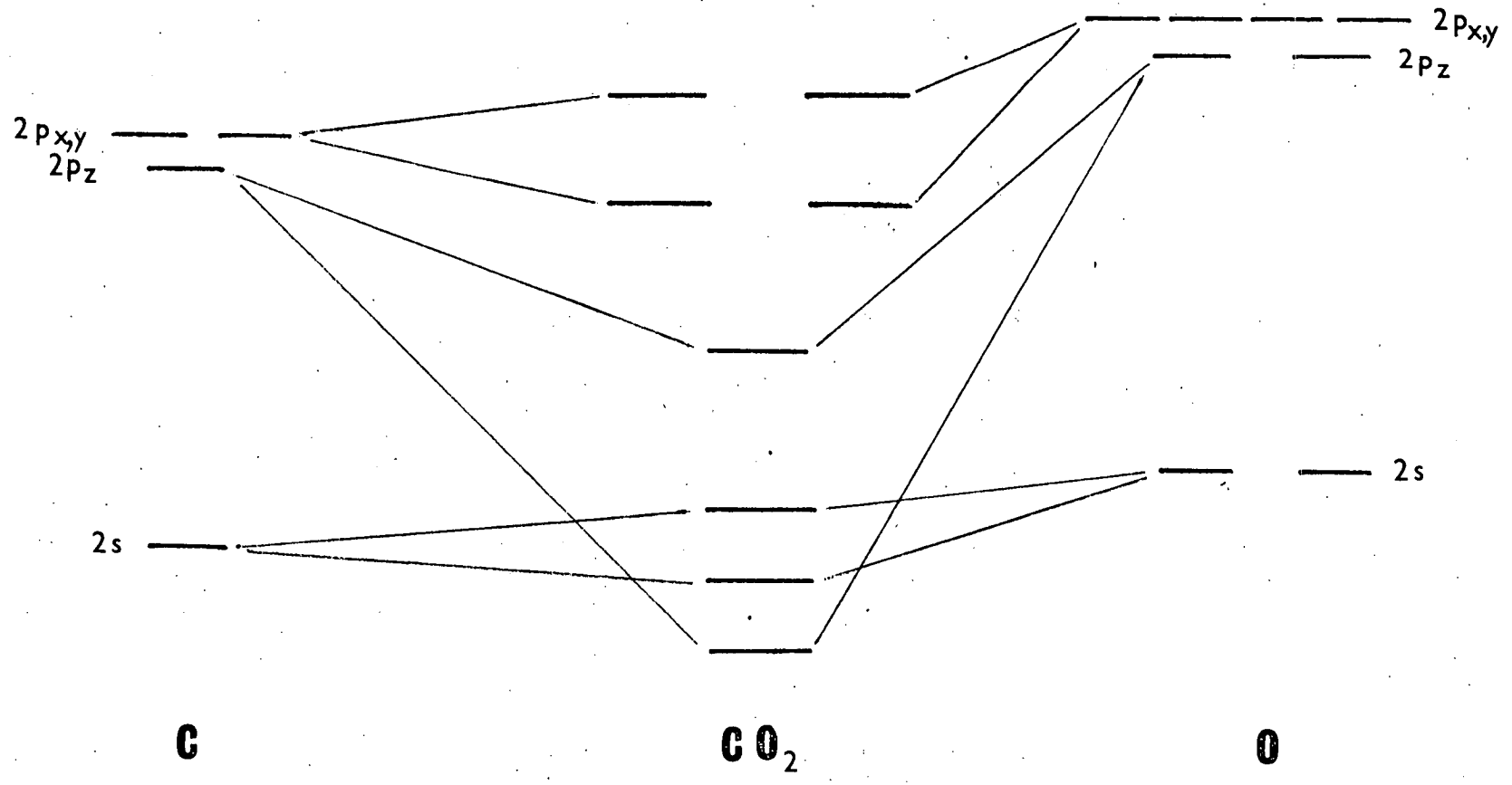

Figure 3.2 - M.O. energy diagram for pseudohalides.

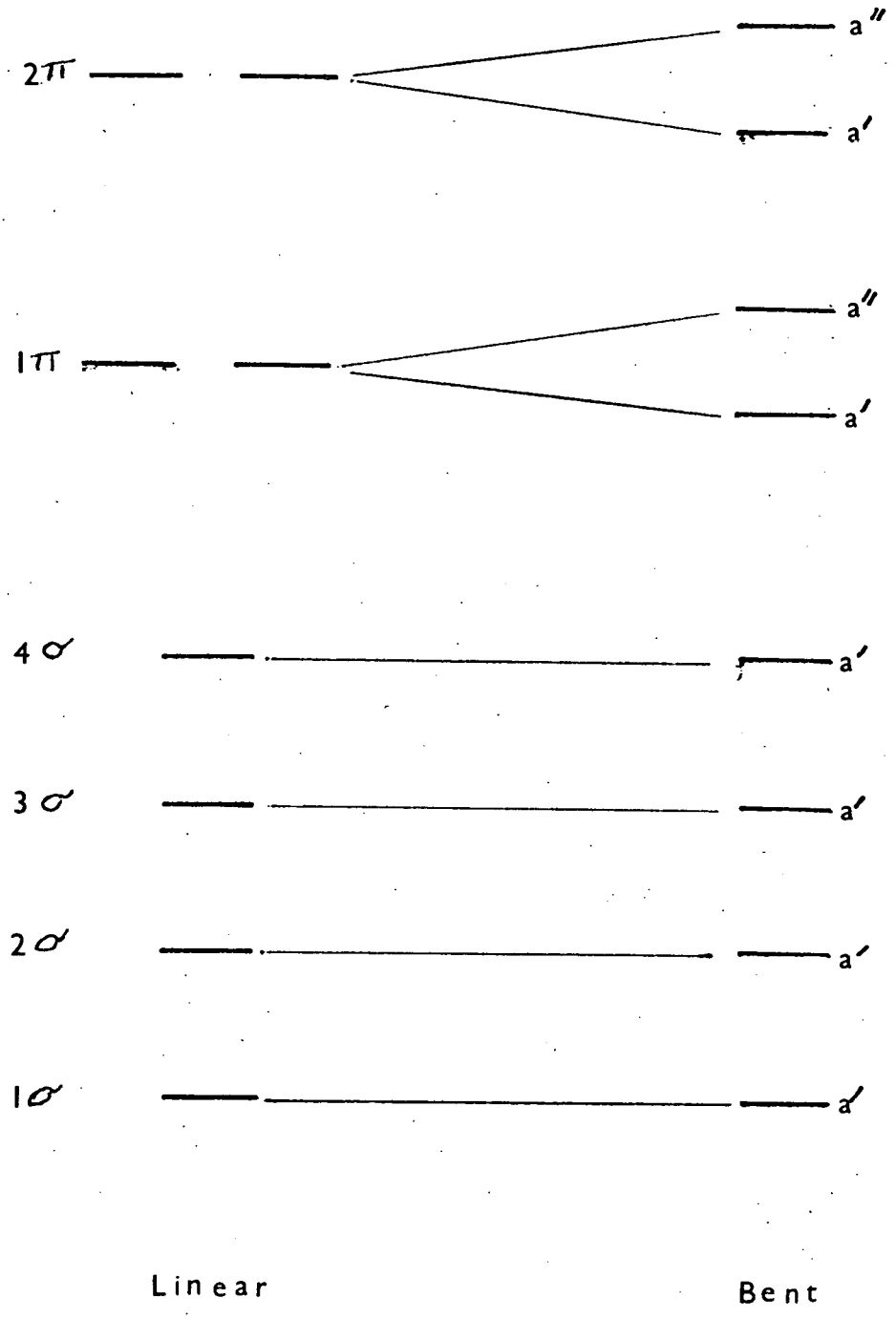

oxide. When the skeleton is bent, however, the point group is C_s rather than C_{∞} and as a consequence the π levels are split into those which are symmetric with respect to the plane of symmetry (a') and those which are antisymmetric (a"). The σ levels thus become a', as shown in figure 3.2.

The relative energies of the 'π' and 'σ' sets need not remain fixed in a series of compounds, and it seems that in the azides, as in nitrous oxide,[49] the 1π levels are lower in energy than the 4σ level.

Consideration of the energy levels discussed so far was sufficient for the hydrides but for the species MH_3Q, where Q represents the pseudohalide group, we must also consider the (MH) levels. These are well separated, as in the parent hydrides MH_4[51] into sets derived from the (np) orbitals of M, denoted by Mp, and from the (ns) orbitals of M, denoted by Ms. In a bent molecule of C_s symmetry, Ms is of symmetry class a', and Mp has two components Mp(a') and Mp(a"). In a linear species, of course, Ms is of σ symmetry and Mp of π symmetry.

Some of the orbitals discussed will lie below - 21.2 eV (the exciting energy) and will not give rise to observable bands in the spectra. In general, 1σ, 2σ, and Ms (for M = carbon) are likely to be of low energy. When M is silicon or germanium Ms may be expected to give rise to very weak bands in the region of 15 to 19 eV as in the MH_4 spectra.[51] The following discussion is thus in terms of the 3σ, 4σ, 1π, 2π, and Mp levels only.

Mixing between 'MH_3' and 'pseudohalide' levels of the same symmetry will take place and thus the assignment of a band to one or other of these is not always possible.

3.3 Photoelectron spectra

The spectra of the 15 pseudohalides of general formula RQ (where R = H, CH_3, SiH_3, GeH_3, Me_3Si and Q = NCO, NCS, N_3) are summarised in table 3.1, in which are given the ionisation potentials of all the observed bands.

The spectra of HQ are given by Eland[52] and the spectra obtained for MH_3Q are shown in figures 3.3 to 3.5. Three distinct types of band were identified in the spectra. One had the strongest feature corresponding to the adiabatic transition, in which no change of vibrational quanta occurred. These bands were derived from ionisation by loss of an electron from a non-bonding orbital. They are denoted by N in table 3.1. The rest of the bands were derived from excitation of bonding (or antibonding) electrons and had a broad outline. Some of these bands showed a progression in one vibrational frequency as fine structure and these are denoted by P in table 3.1.

3.4 Assignment of bands to molecular energy levels.

In order to assign the bands observed in the spectra of the hydrides (HQ) the vertical ionisation potentials[50] for CO_2, COS, and N_2O were used. As can be seen in table 3.2

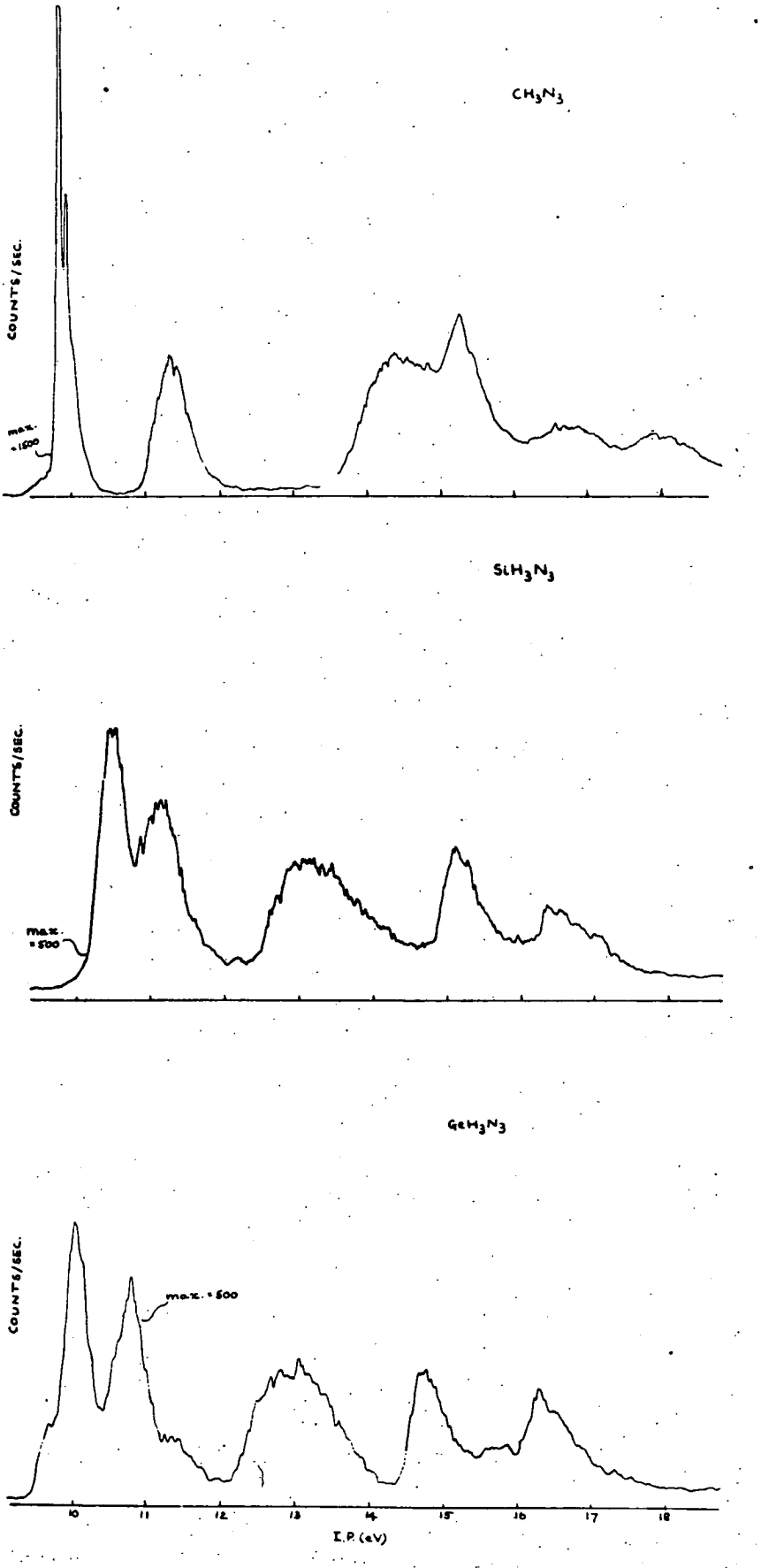

Figure 3.3 - Photoelectron spectra of MH_3N_3.

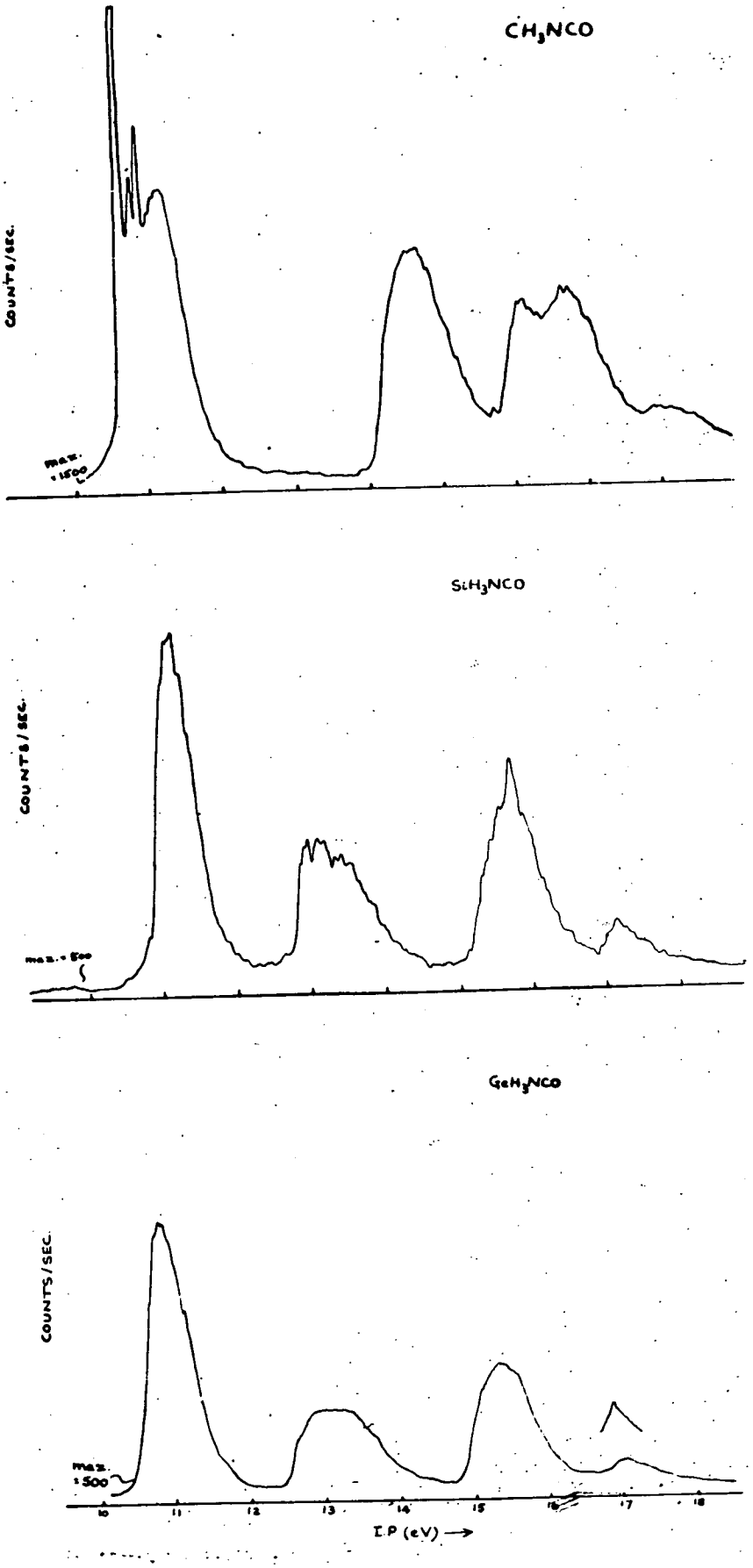

Figure 3.4 - Photoelectron spectra of MH_3NCO.

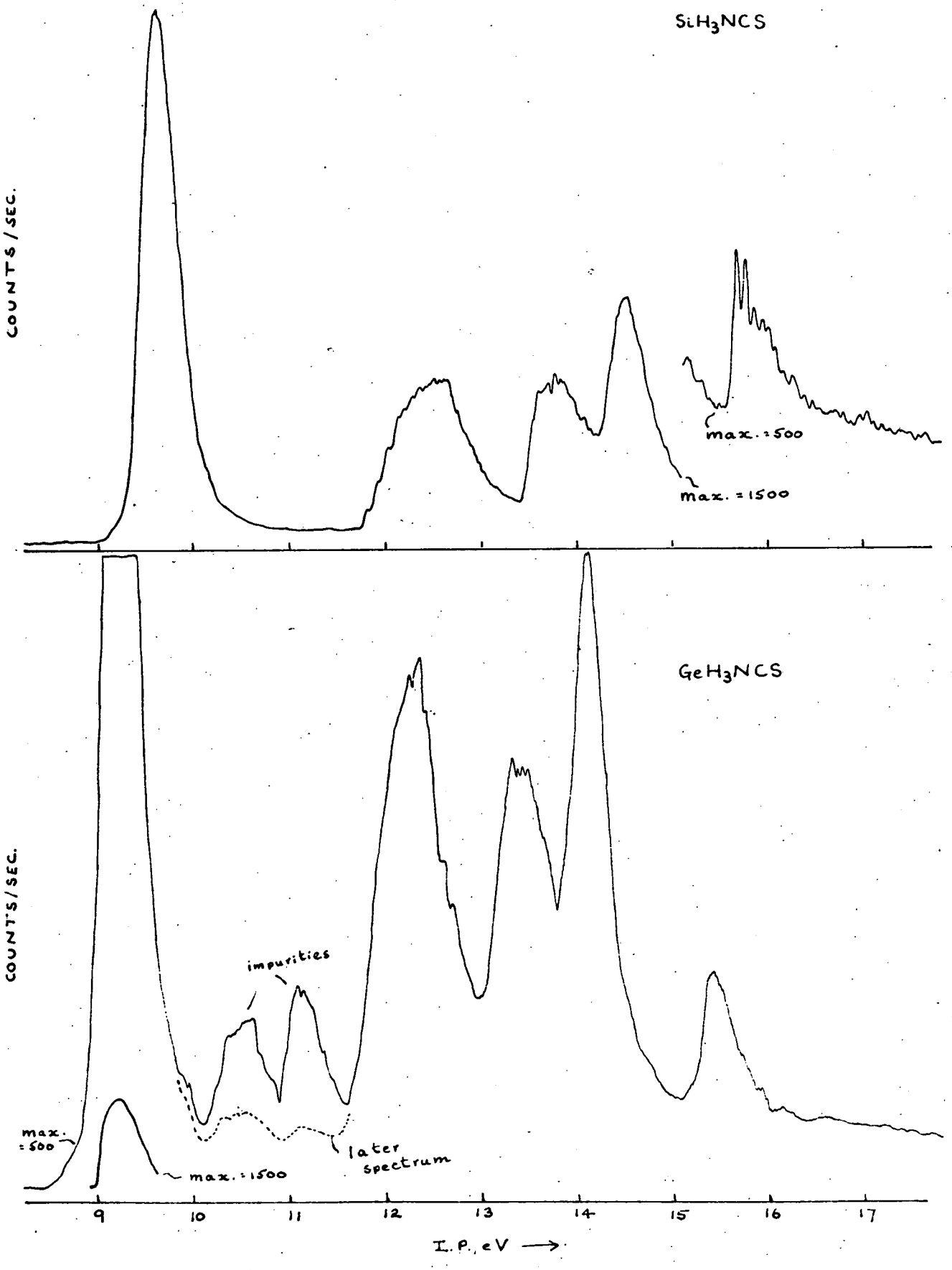

Figure 3.5 - Photoelectron spectra of MH_3NCS.

	Band number					
Compound	1	1a	2	3	4	5
HNCO	11.62N	12.30P	15.8P	17.50P	19.24P	-
HNCS	9.94	10.3P	13.31P	15.12	-	-
HN_3	10.72N	12.24P	15.37N	16.8	-	-
CH_3NCO	10.67N	11.20	14.7	16.1P	16.7	18.0
CH_3NCS	9.37	-	12.6	14.6	15.6P	17.5
CH_3N_3	9.81N	11.32	14.4	14.2	16.6	17.9
SiH_3NCO	11.10P	-	13.1P	15.7P	17.1	-
SiH_3NCS	9.54	-	12.5	13.9P	14.7	15.9
SiH_3N_3	10.33	11.00	13.0	15.0	16.2	-
GeH_3NCO	10.76	-	12.8	15.3	16.9	-
GeH_3NCS	9.14	-	12.3	13.4	14.1	15.5
GeH_3N_3	10.01	10.77	12.8	14.7	16.2	-
Me_3SiNCO	10.3	-	11.5	broad band with sharp		
Me_3SiNCS	9.3	-	11.0	one at 12.5eV extending		
Me_3SiN_3	9.7	-	11.2	to about 16eV.		

TABLE 3.1 - Ionisation potentials of observed bands in eV

(±0.02 or 0.1 eV depending on number of figures given)

Level	Vertical I.P. of corresponding band (eV)		
	CO_2	COS	N_2O
2π	13.79	11.19	12.89
1π	17.32	15.53	18.24
4σ	18.08	16.04	16.39
3σ	19.40	17.96	20.11

TABLE 3.2.

Compound	Energy level					
	$2\pi(a'')$	$2\pi(a')$	1π	4σ	3σ	Mp
HNCO	11.62	12.30	15.8	17.50	19.24	-
HNCS	9.94	10.3	13.31	15.12	-	-
HN_3	10.72	12.24	16.8	15.47	-	-
CH_3NCO	10.67	11.20	14.7	16.1	18.0	16.7
CH_3NCS	9.37	-	12.6	14.6	17.5	15.6
CH_3N_3	9.81	11.32	16.6	15.2	17.9	14.4
SiH_3NCO	11.10		15.7	17.1	-	13.1
SiH_3NCS	9.54		13.9	14.7	15.9	12.5
SiH_3N_3	10.33	11.00	16.2	15.0	-	13.0
GeH_3NCO		10.76	15.3	16.9	-	12.8
GeH_3NCS	9.14		13.4	14.1	15.5	12.3
GeH_3N_3	10.01	10.77	16.2	14.7	-	12.8

TABLE 3.3 - Ionisation potentials for molecular energy levels (in eV)

the highest energy levels for each is 2 π with a gap of over 3eV before the next level. The spectra of the hydrides HNCO, HNCS, HN_3 (table 3.1) each contain a pair of bands (1 and 1a) of ionisation potential 10 to 12eV, which are separated in each case from the next band by about 3eV. They were, therefore, assigned to the components 2 π (a') and 2 π (a") in a bent ion - derived from the 2 π level of the linear triatomic molecules.

The difference in vertical I.P. between the a' and a" components of the 2 π level is larger (1.5eV) for HN_3 than for HNCO (0.7eV) and HNCS (0.4eV). This is consistent both with a narrower angle in HN_3^+ than in $HNCO^+$ (as has been found for the neutral molecules[53]) and with greater concentration of the 2 π (a") component on the N atom bound to H in HN_3^+ than in $HNCO^+$ or $HNCS^+$. The shape of the component at lower I.P. is of the non-bonding type in each case while the component at higher I.P. is of bonding type. The second component was assigned as 2 π (a') which is involved in (NH) bonding, and the first component as 2 π (a") which cannot be involved in that bond.

The spectra of the MF_3 compounds contain one or two bands, designated 1 and 1a, in the region 9 to 12eV. Again these were assigned to the 2 π level or its two components. The spectra of all the azides showed two resolved components and hence all the ions are bent at nitrogen (as are the neutral molecules).

In the spectrum of methyl isocyanate two components were observed but only one was found in the spectra of silyl and

germyl isocyanates. Thus the ion CH_3NCO^+, like the neutral molecule, is bent at nitrogen but it seems that SiH_3NCO^+ and GeH_3NCO^+ may be linear or close to it. However, the limiting skeletal angle to allow resolution of the a' and a" components is not known.

The band corresponding to the 2 π level in the isothiocyanates is broad in all three cases and shows no splitting. It could, however, include a weaker component separated by 0.4eV (as in HNCS) or less from the main peak.

A band near 11eV in the spectra of the trimethyl silyl derivatives was assigned to the trimethyl silyl group, but at lower ionisation potential two bands were found in the spectrum of the azide and one band in those of the isocyanate and isothiocyanate. In the azide and isocyanate these bands were shifted by about 0.8eV to lower I.P. compared with the analogous bands in the silyl derivatives, presumably by interaction with the trimethyl silyl levels near 11eV. The shift of the 2 π band in the isothiocyanate was only 0.2eV, presumably because of the greater energy separation from the trimethyl silyl levels near 11eV.

At higher I.P. three further bands were observed in the spectrum of HNCO, and these were assigned to the 3σ, 4σ, and 1 π levels. Calculations of the energies of these levels[54] and comparison with the levels of CO_2 led, therefore, to the assignment of bands 2, 3, and 4 to the 1π, 4σ, and 3σ levels

respectively. No splitting was observed in the band assigned to the 1 π level. This may be due to the breadth of this band, because it arises from the excitation of a bonding electron, which may obscure a second component at higher I.P.

In HNCS only two further bands were observed and these were assigned by analogy with HNCO and COS to 1 π (at lower I.P.) and 4 σ (at higher I.P.)

In HN_3 band 2 was found to be non-bonding from its contour and was thus assigned to 4 σ, while band 3 which had a bonding contour was assigned to the 1 π level. This assignment was consistent with the order of levels found in N_2O in which 4 σ was found at lower ionisation potential than 1 π. The band assigned to 1 π in HN_3 again showed no discernible splitting.

In the MH_3 derivatives excitation from Mp would be expected to give rise to a band with two components for a bent ion and a single band for a linear ion in the same region as the bands due to 4 σ and 1 π. Between 12eV and 17.4eV each of these nine spectra contained three bands. These were assigned to 4σ, 1π, Mp and thus splitting of the 1 π and Mp bands into their components was not observed. The silyl and germyl compounds all gave a band around 13eV which was assigned to Mp by analogy with MH_4[51] and MH_3X[55] (where X = Cl, Br, I). Bands 3 and 4 in these compounds were assigned to 1 π and 4 σ assuming that these two levels retained the order found in the

hydrides (HQ). In the methyl compounds band 3 was narrow in each case compared with bands 2 and 4 and was assigned to 4σ. Assignment of Mp and 1π was then made depending upon whether 1π was expected to be at higher or lower I.P. than 4σ by analogy with the hydrides (HQ).

This simple assignment was sufficient for the interpretation of the observed spectra, although it takes no account of the mixing which takes place among all a' levels and among all a" levels. No splitting was observed of the Mp or 1π bands in the spectra of the methyl compounds, despite the splittings found in the 2π bands of methyl azide and methyl isocyanate.

In the methyl compounds and silyl and germyl isothiocyanates one further band (band 5) was observed. This was assigned to 3σ since in the silyl and germyl compounds M_s would be expected in this region and may well contribute to the observed band. The sharp fall in I.P. of this band from methyl to silyl isothiocyanate is difficult to explain unless involvement of the 3s orbital of silicon is taken into account.

The assignment of the observed bands to the expected molecular energy levels is given in table 3.3 and the trends in the derivatives of each pseudohalogen can be seen here.

3.5 Vibrational fine structure

Excitation of a ground state molecule to vibrationally excited states of the ion may give rise to vibrational fine structure in the observed bands of the photo-electron spectrum.

In the spectra of the pseudohalides under study vibrational fine structure was observed on almost every band for the hydrides, on the 2 π (a") band for the methyl compounds, and occasionally but not consistently on the bands of the silyl compounds. No fine structure was resolved on any bands in the spectra of the germyl and trimethyl silyl derivatives.

On the 2 π (a") band in HNCO, HN_3, CH_3NCO and CH_3N_3 typically non-bonding vibrational fine structure was observed, comparable with that observed on the 2 π bands in CO_2 and N_2O.[50] The frequencies found are shown in table 3.4. The two lower frequencies were assigned to the symmetric and antisymmetric pseudohalogen stretching vibration. The third frequency observed for HNCO and HN_3 was not affected by deuteration and was not, therefore, assigned as exclusively due to the (NH) stretching vibration. For HNCO it was assigned to the combination of the pseudohalide stretching vibrations and this assignment was in agreement with the observation of a similar frequency in CH_3NCO. For HN_3 this assignment was not very satisfactory, as agreement between the observed frequency and the arithmetic sum of the two vibrations was very poor. Various combinations are, however, possible as the infrared spectra of

Band	Compound	Vibrational Frequencies			
$2\pi(a'')$	HNCO	1080	1980	3200	
	DNCO	1130	2070	3230	
	CH_3NCO	1150	2180	3260	
	Assigned to	ν_s	ν_{as}	$\nu_s + \nu_{as}$	
	HN_3	840	1780	3000	
	DN_3	870	1890	3060	
	CH_3N_3	910	1820	-	
	Assigned to	ν_s	ν_{as}		
$2\pi(a')$	HNCO	Progression in 610 cm^{-1}			
	HNCS	" " 600 cm^{-1}			
	HN_3	" " 570 cm^{-1}			
1π	HNCO	" " 1120 cm^{-1}			
	HNCS	" " 850 cm^{-1}			
	SiH_3NCO	" " 790 cm^{-1}			
	SiH_3NCS	" " 490 cm^{-1}			
4σ	HNCO	" " 460 cm^{-1}			
	CH_3NCO	" " 700 cm^{-1}			
	HN_3	560	900	2340	2800
	DN_3	480	1000	2280	2800
	Assigned to	δ	ν_s	ν_{as}	$\nu_{as}+\delta$
3σ	HNCO	Progression in 1000 cm^{-1}			
	SiH_3NCS	2 peaks, separation 740 cm^{-1}			
	SiD_3NCS	2 peaks, separation 600 cm^{-1}			

Table 3.4 - Vibrational Structure (all intervals in cm^{-1}, ± 50 cm^{-1})

HN_3 and DN_3 in the region around 3300 cm.$^{-1}$ are quite complex. In HNCS and CH_3NCS the 2 π (a") bands are broader, probably because of spin-orbit coupling at sulphur, and no fine structure could be resolved.

The 2 π (a') bands for the three hydrides are all of typically bonding contour and all show a progression of about 600 cm.$^{-1}$ After deuteration of each, no fine structure could be resolved and thus the progressions were assigned to the (NH) deformation mode of the ions.

In HNCO, HNCS, SiH_3NCO, and SiH_3NCS, progressions were found on the 1 π bands. These were assigned to the symmetric pseudohalogen stretch, its frequency in the ion being reduced by the removal of a π bonding electron. This assignment was again in agreement with those made for CO_2 and COS.[50] For CH_3NCO and CH_3NCS no such simple progressions were observed. Perhaps mixing between 1 π and Mp is responsible for this as it would also explain the irregularities in 1 π band positions for the methyl compounds.

Only HN_3, HNCO, and CH_3NCO showed fine structure on the 4σ band. In HNCO the progression in 460 cm.$^{-1}$ is probably due to a deformation at nitrogen or carbon. A few peaks which were possibly part of a progression were observed for CH_3NCO but the band overlapped with the band assigned to excitation from the Mp levels.

The 4σ band in HN_3, as in N_2O,[50] has a sharp cut-off on

the low ionisation potential side but several vibrational levels were observed for the normal and deuterated species. These were assigned to vibrations of the ion by comparison with the vibrations of the ground state molecule. Similar assignment was possible for the 4 σ band of the ion N_2O^+ [50] by comparison with the vibrations of the molecule:

N_2O	1345	ν_s
	614	δ
	2251	ν_a
N_2O^+	1350	ν_s
	-	
	2460	ν_a

in which only the vibrations of the ion of the same symmetry as the level from which the electron was excited are activated. The assignments made for HN_3 were consistent with this. The assignments are shown in table 3.4.

A progression of 1020 cm.$^{-1}$, probably due to the symmetric pseudohalogen stretch, was observed on the 3σ band of HNCO. In SiH_3NCS this band showed two peaks of equal intensity followed by a much broader component. The separation of the two peaks decreased on deuteration and the feature was assigned, therefore, to excitation of the silyl rocking vibration, rather than to spin orbit coupling at sulphur.

A complicated structure observed on the Mp band of SiH_3NCO

was assigned to two overlapping progressions of 1100 cm.$^{-1}$, probably arising from the symmetric silyl deformation. The two progressions were probably caused by Jahn-Teller splitting as a similar feature was observed in the spectrum of silyl acetylene.[56] The separation of the two (0 - 0) transitions is 630 cm.$^{-1}$ The deuterated species showed an irregular structure on this band but two progressions could not be resolved. It is possible that the fine structure observed on the 4 σ band in CH_3NCO could also be explained in terms of overlapping vibrational progressions. This explanation would require the interchange of the assignments of Mp and 4σ, and the doubling in this case would be due to the a' and a" components of Mp since the ion CH_3NCO^+ is not linear.

3.6 Trends in ionisation potential

There are irregularities in the ionisation potentials of the pseudohalide levels when the group 4 atom is changed. Some of these effects can be correlated with interactions between the pseudohalide levels and the Mp levels of the group 4 atom. In the case of non-linear ions interactions between the metal p levels and all the pseudohalide levels are possible, but in the case of linear ions interactions are only possible with the 1π and 2 π pseudohalide levels.

If one accepts the assignment of the observed bands to excitation specifically from the Mp and pseudohalide levels it is possible to explain the variations in ionisation potential

Q	Levels	M = C	Si	Ge
NCO	2π(a") - Mp	-6.0		
	2π(a') - Mp	-5.5	-2.0	-2.0
	1π - Mp	-2.0	+2.6	+2.5
	4σ - Mp	-0.6	+4.0	+4.1
NCS	2π - Mp	-6.2	-3.0	-3.2
	1π - Mp	-3.0	+1.4	+1.1
	4σ - Mp	-1.0	+2.1	+1.8
N_3	2π(a") - Mp	-4.6	-2.7	-2.8
	2π(a') - Mp	-3.1	-2.0	-2.0
	4σ - Mp	+0.8	+2.0	-1.9
	1π - Mp	+2.2	+3.2	+3.4

Table 3.5 - Separation of Energy Levels (eV) in MH_3Q.

found - by estimating the magnitude of the interactions involved. However, interactions of this kind do not explain one important trend found in the ionisation potentials of the pseudohalide levels.

Table 3.6 shows the ionisation potentials of the 1 π and 2 π bands of the pseudohalides studied, giving an average in cases where two components (a' and a") were observed. It is clear from this data that except for 1 π of the azide the π levels of the silyl pseudohalides are lower in energy than those of their carbon analogues.

This trend cannot be explained by interactions with the Mp levels of carbon and silicon, as such interactions would be expected to lower the ionisation potential of the π levels of the silyl compounds more than those of the carbon ones.

To explain this trend one must include an interaction involving an unoccupied level of the group 4 atom. The interaction must be of π type since the effect is observed in both linear and non-linear ions. The most likely level to be involved is the 3d level (which is available only for silicon), since the observed effect is greater for silicon than carbon.

Such an interaction requires that the π levels of the silyl pseudohalides are involved in bonding. Comparison of the contours of the bands assigned to 1 π and 2 π in the spectra of the silyl and carbon compounds confirms the existence

Q	Level	M = C	Si	Ge
NCO	2π	10.93*	11.10	10.76
	1π	14.70	15.70	15.28
NCS	2π	9.37	9.54	9.14
	1π	12.58	13.90	13.40
N_3	2π	10.57*	10.67*	10.39*
	1π	16.60	16.22	16.16

* Mean of two components.

Table 3.6 - Vertical I.P.s of Levels in MH_3Q.

of this interaction.

The ionisation potentials of the bands observed in the spectra of the germyl compounds do not give clear evidence for similar bonding. The band contours, however, do show that the pseudohalide π levels are involved in bonding.

These conclusions are supported by a similar study of the series' MH_3X and MH_2X_2[55] (in which M = C, Si, Ge and X = F, Cl, Br, I) in which strong evidence was presented for $(p \rightarrow d)\pi$ bonding in the silyl and germyl species.

The first ionisation potential observed for the trimethyl silyl pseudohalides is lower than that observed in the methyl compounds (see tables 3.1 and 3.6). This does not rule out mixing between the π levels and the empty d orbitals of silicon since this region of the spectra of the trimethyl silyl derivatives is complicated by the trimethyl silyl bands at around 11eV. It is not possible, therefore, to draw any conclusions on the existence of such bonding in these molecules.

3.7 Discussion

The photoelectron spectra of the pseudohalide molecules studied give clear evidence for the existence of "π" bonding between the pseudohalide group and the group 4 atom when this is silicon or germanium.

The spectra do not, however, give any information on the

effect of this interaction on molecular geometry. The absence of splitting between the 2 π (a') and 2 π (a") bands merely indicates, if Koopman's theorem is accepted, that the ion formed by this excitation is linear, or nearly linear.

CHAPTER 4

SPECTROSCOPIC STUDIES OF THE PSEUDOHALIDES

4.1 Proton magnetic resonance spectra

Previous studies of the proton spectra of silyl and germyl pseudohalides have been mentioned, in Chapter 1. In these, the chemical shift of the observed resonance was used to decide which isomer (normal or iso) is present. The observed peaks could, however, represent equilibrium mixtures in which fast exchange was taking place between the two isomers. In order to investigate the existence of these exchange systems ^{15}N and ^{13}C substituted pseudohalides were prepared. Their spectra are reported in the following sections.

(a) Isotopically-substituted species

The proton spectra of silyl and germyl isocyanates and isothiocyanates containing 90% of ^{15}N were recorded in solution in cyclopentane. Also the proton spectra were recorded of silyl and germyl cyamides containing 60% of ^{13}C again in solution in cyclopentane. The form and assignment of these spectra are shown in figures 4.1 to 4.4, and tables 4.1 and 4.2 give the parameters obtained.

The spectra of silyl isocyanate and iso-thiocyanate obtained both show a small peak at 5.39 τ which had satellites with a coupling of $^1J(^{29}SiH)$ = 220.8 Hz. The amount of this species could be reduced to ca. 3 to 4% by distillation and the peaks were assigned to disiloxane which would be formed by hydrolysis of the silyl species. Since the peak occurs at an identical chemical shift in both species and with the same

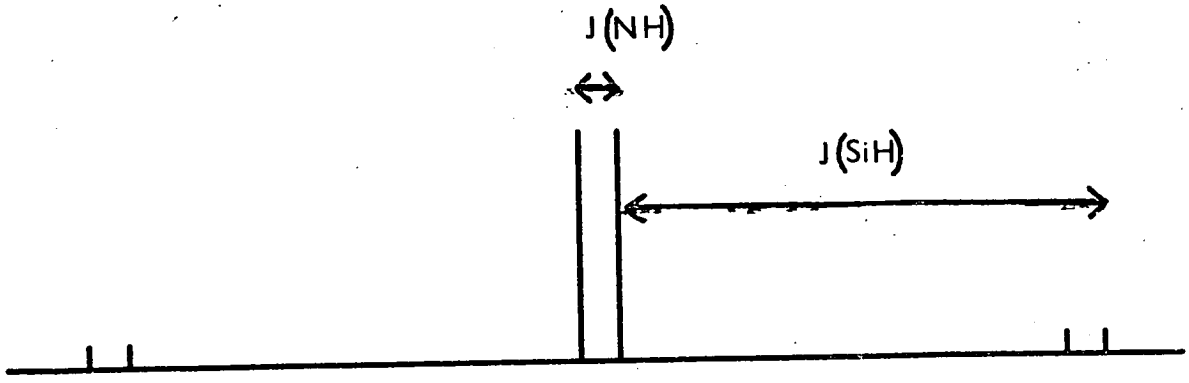

Figure 4.1 - ^{1}H-Spectrum of $SiH_3{}^{15}NCX$ where X = O_2S.

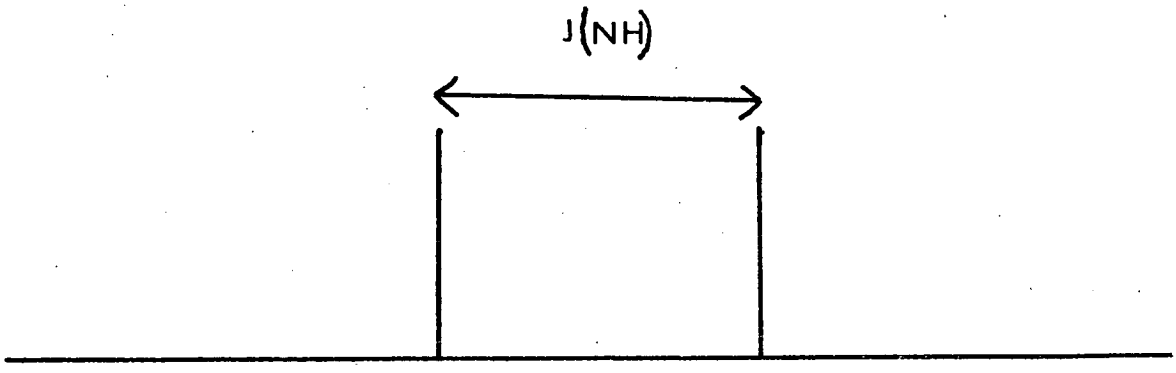

Figure 4.2 - ^{1}H-Spectrum of $GeH_3{}^{15}NCX$ where X = O_2S.

n.b. In all figures of n.m.r. spectra in this work (unless otherwise stated) frequency increases from right to left.

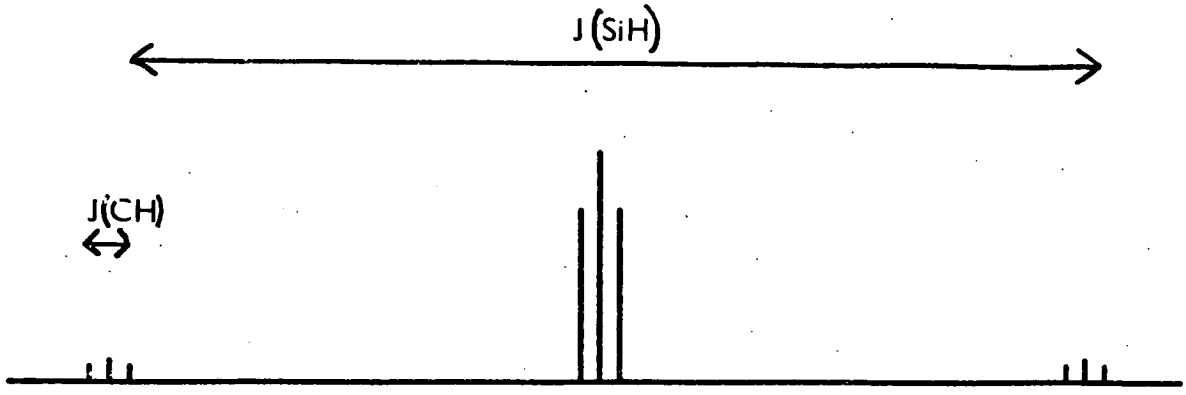

Figure 4.3 - ^{1}H-Spectrum of SiH_3CN containing 60% of ^{13}C.

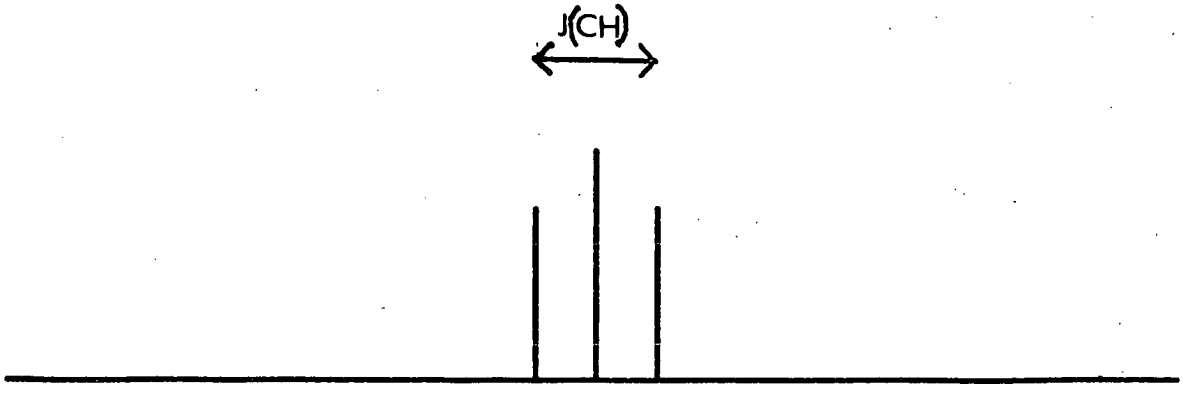

Figure 4.4 - ^{1}H-Spectrum of GeH_3CN containing 60% of ^{13}C.

Proton magnetic resonance parameters for the species' MH_3NCX

Compound	Chemical shift in p.p.m.(τ)	$^2J(^{15}NH)$ in Hz	$^1J(^{29}SiH)$ in Hz	$^1J(^{29}Si-^{15}N)$ in Hz
SiH_3NCS	5.53	-4.37	-234.6	+19.9
SiH_3NCO	5.55	-5.0	-230.6	+19.6
GeH_3NCS	4.82	$\pm$4.9	-	-
GeH_3NCO	4.96	$\pm$5.4	-	-

TABLE 4.1.

Proton magnetic resonance parameters for the species' MH_3CN

Compound	Chemical shifts in p.p.m.(τ)	$^2J(^{13}CH)$ in Hz	$^1J(^{29}SiH)$ in Hz	$^1J(^{29}Si-^{13}C)$ in Hz
SiH_3CN	6.17	+4.5	-232.5	-67
GeH_3CN	5.83	$\pm$6.4	-	-

TABLE 4.2.

Chemical shifts are quoted relative to T.M.S. (10.0 τ) as internal standard. The signs of coupling constants assume that $J(^{29}Si-H)$ is negative. All spectra were recorded in cyclopentane.

$^1J(^{29}SiH)$ it is most unlikely to be due to a small amount of the normal cyanate or thiocyanate as the chemical shifts of silyl protons are sensitive to the β-atom. No other peaks were observed in the spectra of the silyl species' with an estimated level of detection of $\sim$1% of the main resonance.

The spectra of germyl isocyanate and isothiocyanate obtained both show an impurity peak at 5.50τ which was 3 to 4% of the main resonance in all samples. Its chemical shift agreed with published values for germyl bromide and this halide was used to prepare both of these species'. Again the fact that the peak appears at an identical chemical shift in both spectra is good evidence that it is not due to a small amount of the normal cyanate or thiocyanate. Both of these species' were also prepared from germyl iodide and no peak was observed at 5.50 τ in these spectra (isotopically labelled isocyanates and isothiocyanates were not used in this experiment). No other peaks were observed in the spectra of the germyl species' and again the estimated level of detection was $\sim$ 1% of the main resonance.

The observation of coupling to ^{13}C and ^{15}N in all these spectra rules out the possibility of fast exchange between normal and iso-forms of the species'. The magnitudes of the coupling constants $J(^{29}Si-^{13}C)$ and $J(^{29}Si-^{15}N)$ found by spin tickling (see Part b) are consistent with the existence of the cyanates and thiocyanates in their iso-forms (N-bonded), and with the cyanides as normal-cyanides (C-bonded).

The ^{14}N chemical shift of germyl isocyanate[57] is further evidence for an N-bonded structure. The resonance lies 64 p.p.m. to high field of the free isocyanate ion, whereas all normal-cyanates resonate to low-field of this standard.

The existence of very small amounts of the other forms of these species ($\sim$1%) which are not involved in fast exchange cannot, however, be ruled out by these experiments.

The assumption that the splittings observed in the spectra of the isotopically substituted species were due to coupling to ^{15}N and ^{13}C was tested by spin-tickling experiments which are described in the following section.

The proton magnetic resonance spectrum of an impure sample of trimethyl silyl cyanide containing 90% ^{13}C has recently been recorded.[58] This showed two peaks which were assigned to the ^{13}C-cyamide (giving $^{3}J(^{13}CH) \sim 3$ Hz). These peaks are affected by irradiation in the region normal for the resonance of ^{13}C and thus fast exchange between normal and iso-forms is not possible.

(b) Spin-tickling experiments

SiH_3NCO

The ^{15}N and ^{29}Si spectra for silyl isocyanate are shown diagrammatically in figures 4.5 and 4.6 respectively. They assume that $J(^{29}SiH) > J(^{29}Si-^{15}N)$.

The spectra were not observed but the second radio-frequency

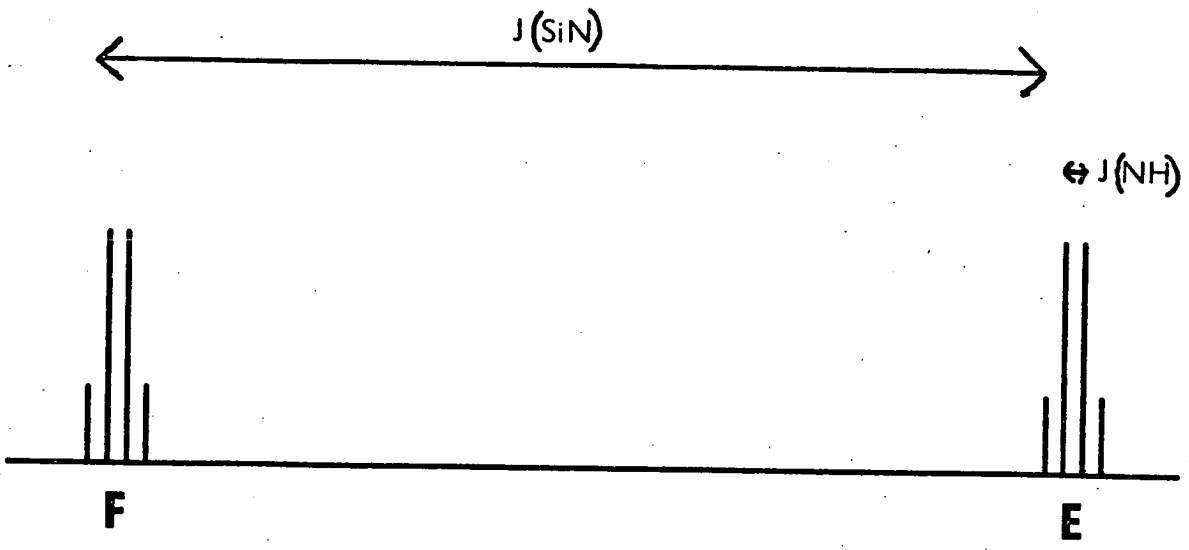

Figure 4.5 - ^{29}Si satellites in ^{15}N-spectrum of $SiH_3{}^{15}NCX$ where X = O, S.

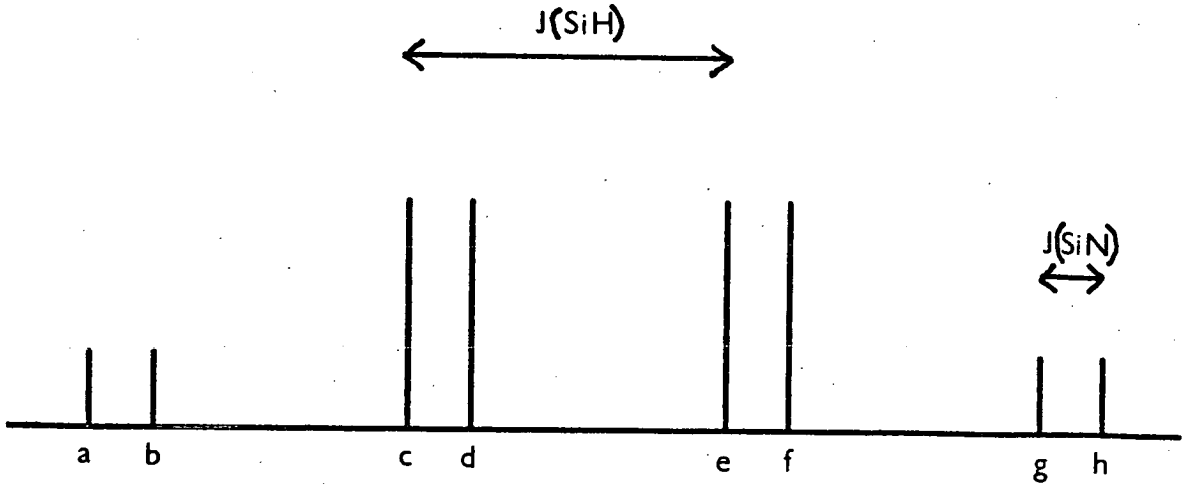

Figure 4.6 - ^{29}Si Spectrum of $SiH_3{}^{15}NCX$ where X = O,S.

source was used to scan these spectra while the proton spectrum was observed. Complete spin-decoupling could only be observed in the proton spectrum when a large amplitude radio-frequency was used. This did not allow precise measurement of the coupling constants, as decoupling was observed over a range of magnitudes for the radio-frequency. Thus the r.f. was normally of small amplitude and distortion of the proton-spectrum in the regions in which transitions were from spin-states which were being excited by the r.f. was observed.

In the simplest cases, in which a very small amplitude r.f. was used, the exciting frequency merely altered the populations of spin states without altering their energies. This effect was observed in the proton-spectrum as a change in the intensities of transitions to or from these spin states. This method was used in the double resonance spectra of silyl isocyanate with excitation at the frequencies of the ^{29}Si resonance.

Figure 4.7 shows the high-frequency ^{29}Si satellite in the proton-spectrum (see figure 4.1). At exciting frequencies of 19,865,589.2 Hz and 19,865,608.8 Hz the proton spectrum was perturbed as shown. The difference between these frequencies (19.6 Hz) must represent the spacing between 2 lines in the ^{29}Si spectrum (figure 4.6). Since $J(^{29}SiH)$ is known from the proton spectrum to be 230.6 Hz the splitting of 19.6 Hz must represent $^{1}J(^{29}Si-^{15}N)$. The relative signs of the coupling constants $^{1}J(^{29}Si-^{15}N)$ and $^{2}J(^{15}NH)$ are also given. Since the lower

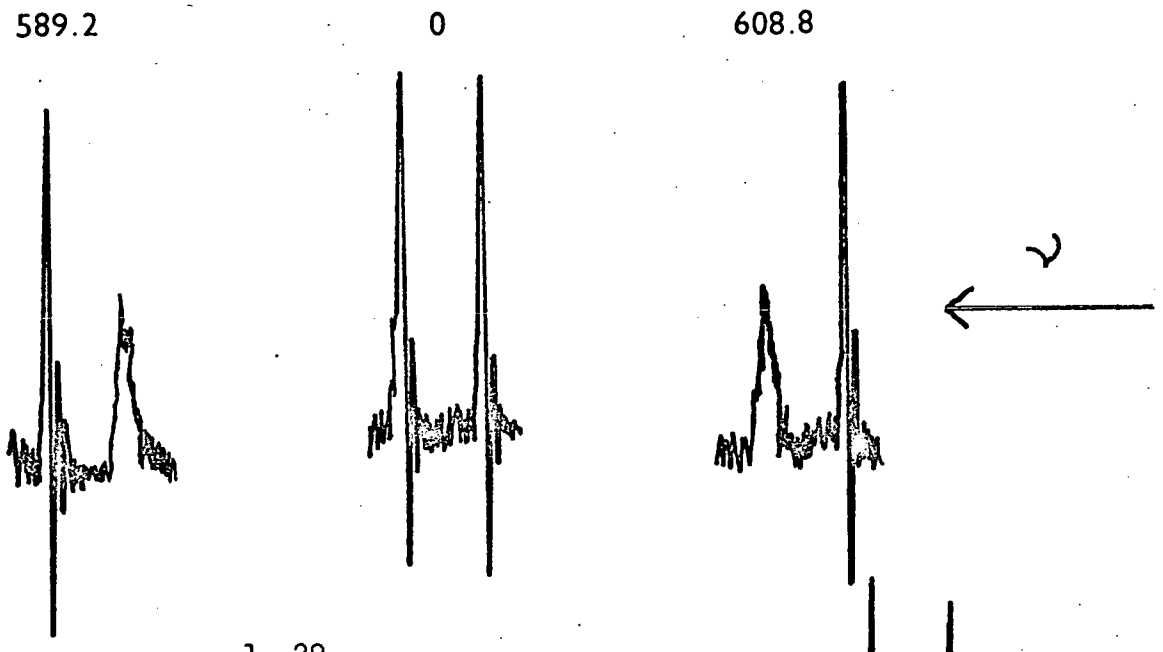

Figure 4.7 - $^{1}H(^{29}Si)$ in silyl isocyanate

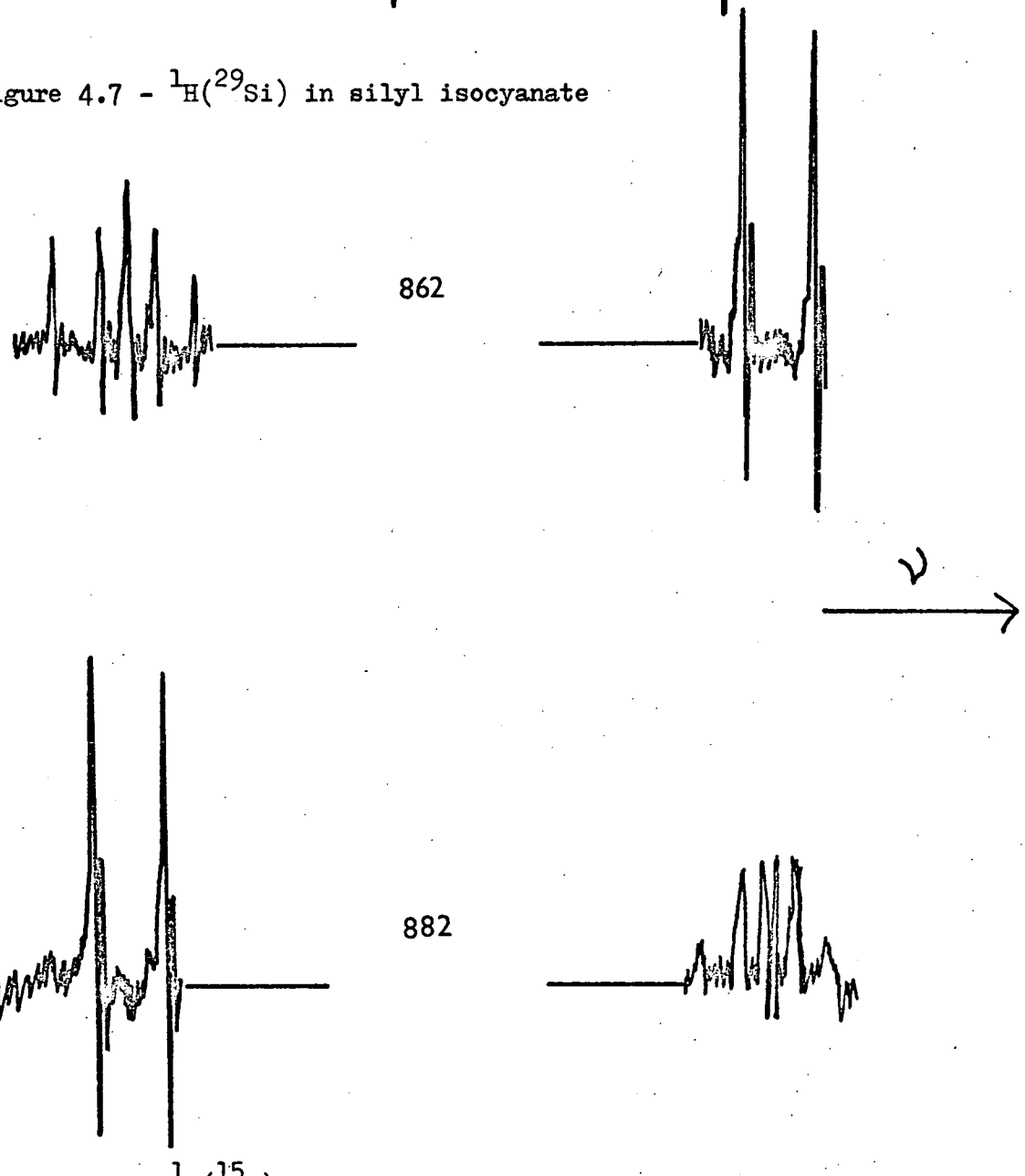

Figure 4.8 - $^{1}H(^{15}N)$ in silyl isocyanate

frequency line in the ^{29}Si spectrum represents a transition involving the same spin state as the lower frequency line in the ^{29}Si satellite in the proton spectrum the two reduced coupling constants must be of the same sign (see section (c)).

In order to relate these coupling constants to $^{1}J(^{29}SiH)$, which has been found to be in the range -200 to -400 Hz in all species studied, irradiation at frequencies in the ^{15}N resonance were carried out. Figure 4.8 shows the results of these experiments at the optimum frequencies found. Again two frequencies were found, about 20 Hz apart, which affected the proton spectrum. These, however, did not merely alter the intensities of the lines in the proton spectrum. The amplitude of the second r.f. was larger than that used to irradiate in the ^{29}Si region so that the signal was broad enough to excite all the lines in region E or region F (figure 4.5). Its amplitude was sufficient in this experiment to alter the energies of the spin-states involved and thus the effect observed on the proton-spectrum was complex. However, at the frequencies 10, 132, 862 and 10, 132, 882 perturbation of the ^{29}Si satellites in the proton spectrum was as shown in figure 4.8. The difference between these frequencies (20 Hz) again represents $^{1}J(^{29}Si-^{15}N)$ and, since the lower irradiating frequency perturbs the lower frequency ^{29}Si satellite in the proton spectrum, the reduced coupling constants $^{1}K(^{29}Si-^{15}N)$ and $^{1}K(^{29}SiH)$ must be of the same sign.

It seems likely that two of the three coupling

constants are negative, as listed in table 4.1.

SiH_3NCS

The ^{15}N and ^{29}Si- spectra for silyl isothiocyanate are of the same form as those of the isocyanate and are represented in figures 4.5 and 4.6. Again the perturbation of the proton-spectrum by irradiation at frequencies in the regions of the resonance of ^{15}N and ^{29}Si nuclei were observed.

Figure 4.9 shows the effect on the high and low frequency ^{29}Si satellites in the proton spectrum (see figure 1) of irradiating frequencies in the ^{15}N region. Since the lower irradiating frequency affects the lower frequency ^{29}Si satellite in the proton spectrum again the reduced coupling constants $^1K(^{29}Si\text{-}H_3)$ and $^1K(^{29}Si\text{-}^{15}N)$ must be of the same sign.

Since complete decoupling was not observed the best tickling frequencies had to be judged from the symmetry of the pattern of distortions found over the range of frequencies.

Observing the low frequency ^{29}Si satellites a symmetrical series of distortions is found around the tickling frequency 10,133,643 Hz - the corresponding pairs being 654 and 652, 655 and 651 etc. Similarly, observing the high frequency ^{29}Si satellite the pattern is symmetrical about the tickling frequency 10, 133, 672 Hz (which is very similar in its distortion to 653.)

In order to measure the difference between these two frequencies more accurately the amplitude of the second r.f. was

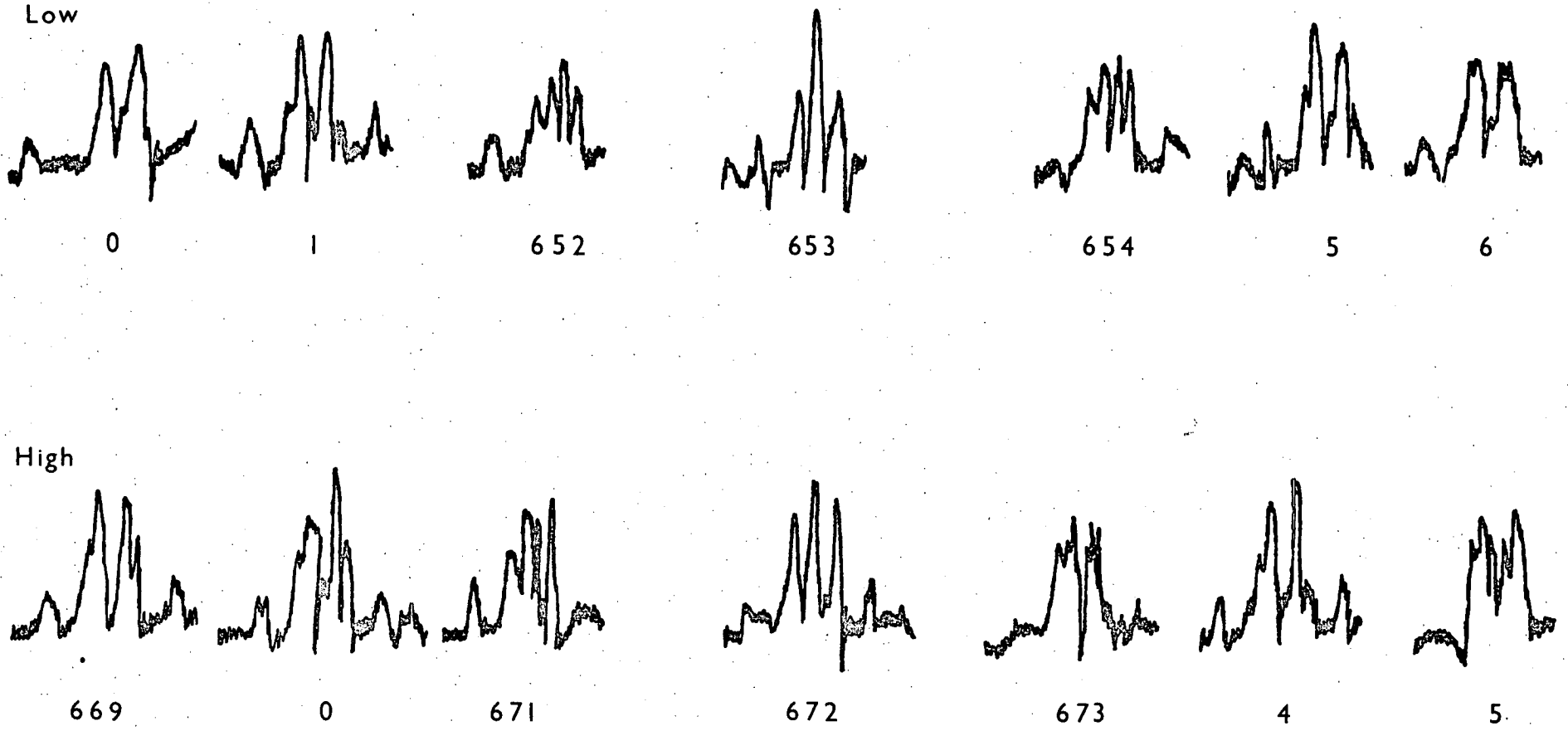

Figure 4.9 - ^{1}H (^{15}N) in silyl isothiocyanate.

reduced and the distortions of both satellites recorded over a smaller range of tickling frequencies around the two found. The optimum frequencies found were 10, 133, 671.8 and 10, 133, 652.6 Hz. This difference must represent a splitting in the ^{15}N spectrum (figure 4.5) which must be $^{1}J(^{29}Si-^{15}N)$ since $^{2}J(^{15}N-H_3)$ is known from the proton spectrum.

In order to relate the sign of $^{2}J(^{15}N-H_3)$ to the other two coupling constants spin-tickling of the ^{29}Si nucleus was also carried out. Only the higher frequency ^{29}Si satellite (shown in figure 4.10) was observed and the irradiating frequencies were assigned to lines in the ^{29}Si spectrum shown in figure 4.6.

The effect on the spectrum is tabulated below:

Irradiating frequency in Hz	Assignment (figure 4.6)	Collapse in ^{1}H-spectrum (figure 4.10)
19,866,045	a	B
19,866,020	b	A
19,865,810	c	B
19,865,790	d	A
19,865,590	e	B
19,865,560	f	A
19,865,340	g	B
19,865,320	h	A

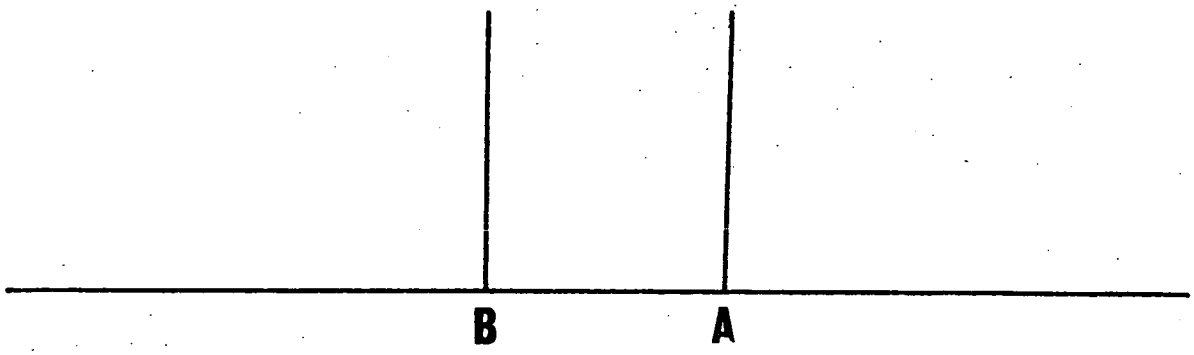

Figure 4.10 - High frequency ^{29}Si satellite in ^{1}H-Spectrum of $SiH_3{}^{15}NCS$ or $SiH_3{}^{13}CN$.

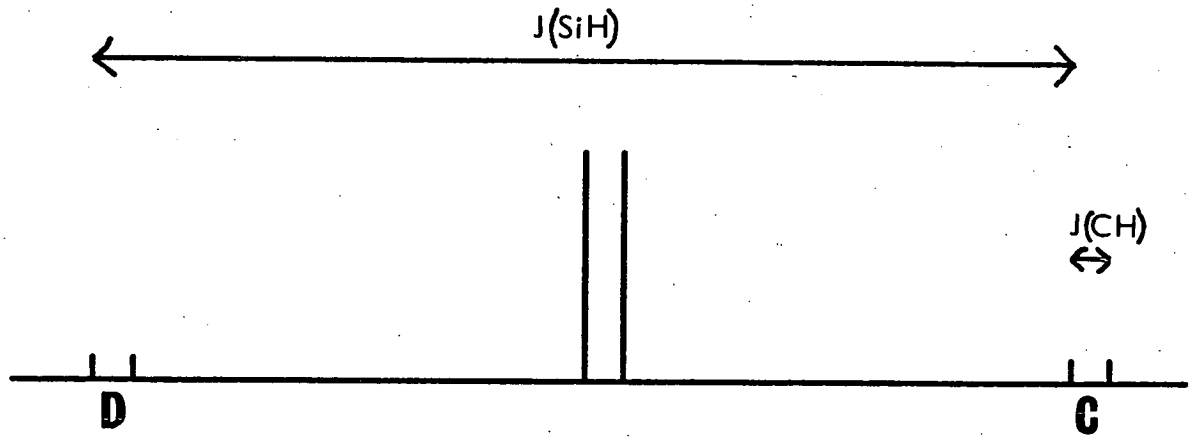

Figure 4.11 - ^{1}H-Spectrum of $SiH_3{}^{13}CN$.

A fairly large amplitude irradiating frequency was used and, therefore, coupling constants could not be measured accurately but the amplitude was kept constant throughout the series.

Again the lower irradiating frequency in each pair (b, d, f, h) collapsed the lower frequency line in the proton spectrum (A). Thus the reduced coupling constants $^{1}K(^{29}Si-^{15}N)$ and $^{2}K(^{15}N-H_3)$ must be of the same sign and the coupling constants are given in table 4.1.

SiH_3CN

The ^{1}H and ^{29}Si spectra of the molecules containing ^{13}C and the ^{13}C-spectrum of silyl cyanide are shown in figures 4.11 to 4.13 respectively.

A small amplitude r.f. was used for spin-tickling in the region of the ^{29}Si resonance (figure 4.12), and two frequencies - 19, 864, 958 and 19, 865, 025 Hz, were found which perturbed the lines A and B in the proton spectrum respectively (figure 4.10). Therefore, the reduced coupling constants $^{1}K(^{29}Si-^{13}C)$ and $^{2}K(^{13}CH_3)$ must be of the same sign and the splitting of 67 Hz must represent $^{1}J(^{29}Si-^{13}C)$.

Similarly, irradiation at two frequencies in the region of the ^{13}C resonance - 25, 147, 535 and 25, 147, 601.5 Hz (E and F in figure 4.13), was found to perturb the proton spectrum in the region C and D respectively (figure 4.11). The reduced coupling

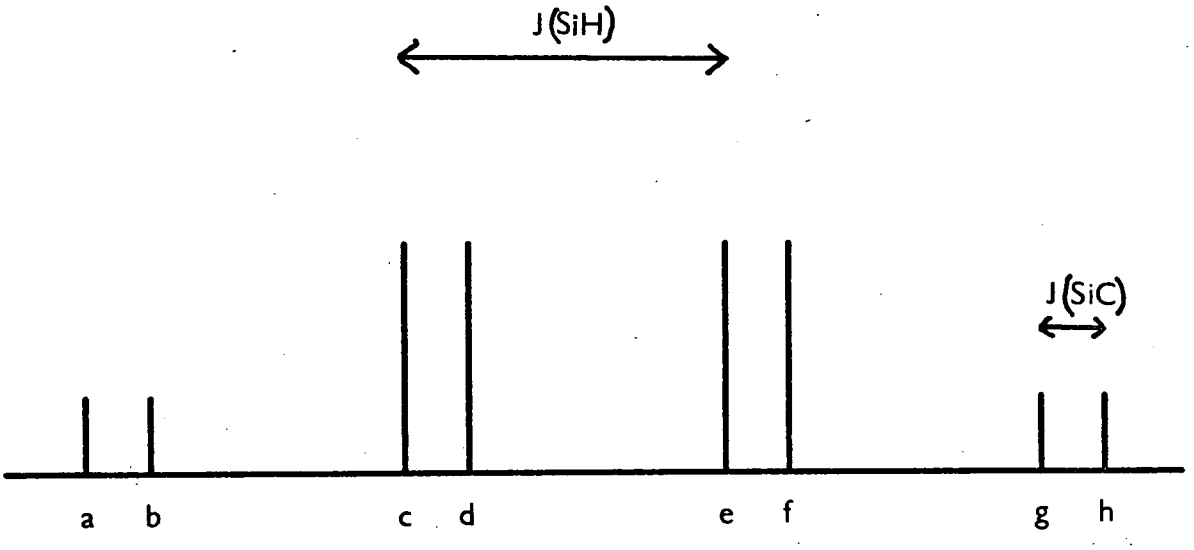

Figure 4.12 - ^{29}Si-Spectrum of $SiH_3{}^{13}CN$.

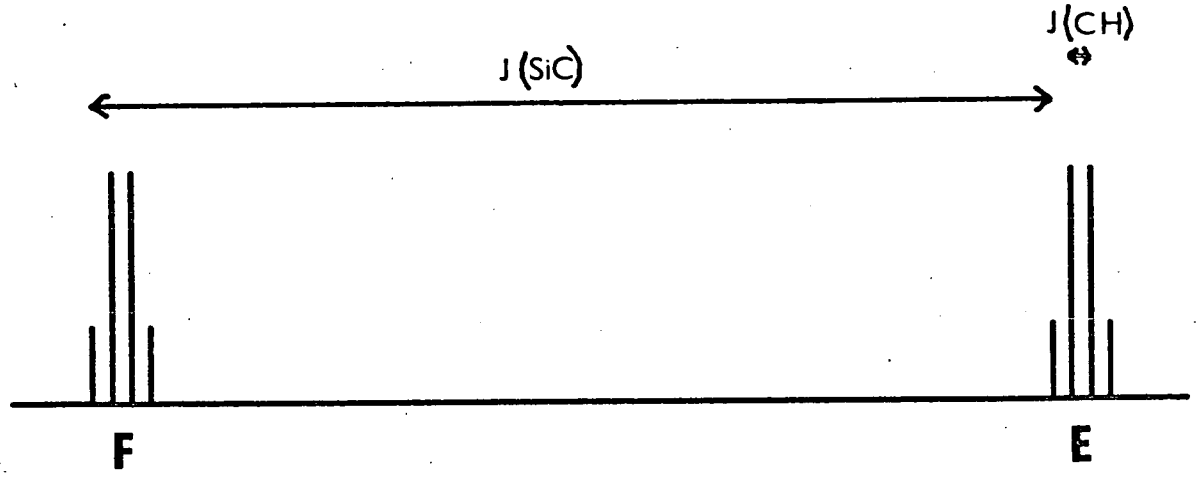

Figure 4.13 - ^{13}C-Spectrum of $^{29}SiH_3CN$.

constants $^{1}J(^{29}Si-^{13}C)$ and $^{1}J(^{29}Si-H)$ must therefore be the same sign, and the magnitude of $^{1}J(^{29}Si-^{13}C)$ found by tickling the ^{29}Si resonance is confirmed.

Two of the coupling constants were again taken to be negative as listed in table 4.1.

(c) Reduced coupling constants

In order to compare the coupling constants between different pairs of directly-bonded nuclei it is normal to use reduced coupling constants defined by the equation:-

$$K_{AB} = J_{AB} \times \frac{4\pi^2}{h} \times \frac{1}{\gamma_A \gamma_B}$$

for nuclei A and B, where J_{AB} = coupling constant, and γ_A and γ_B are magnetogyric ratios.

With the effects of magnetogyric ratios removed it is possible to observe trends in the (reduced) coupling constants which can be related to the bonding between the atoms.

Normally, the reduced coupling constants increase with the atomic numbers of the atoms [59] and substitution of increasingly electronegative atoms usually decreases the reduced coupling constants.[60]

Table 4.3 shows the reduced coupling constants for the coupling constants given in tables 4.1 and 4.2. The relative magnitudes for $^{1}K(^{29}Si-^{15}N)$ and $^{1}K(^{29}Si-^{13}C)$ are in agreement with the electronegativities of nitrogen and carbon given by the Allred-Rochow formula[61] (3.07 and 2.50 respectively). The magnitude of $^{1}K(^{29}Si-H)$ found is not in agreement with the electronegativity of hydrogen (2.30), however. This is probably due to the difference in atomic number between carbon and hydrogen - this effect being less important when comparing carbon with nitrogen.

(d) Chemical shifts of ^{15}N nucleus

It is possible in double resonance experiments to determine the chemical shifts of the nuclei being irradiated from measurement of the tickling frequencies used to perturb the proton spectrum. The exact operating conditions of the instrument must, however, be recorded in order to make the necessary corrections to the observed frequency. (The routine alterations of the machine settings used change the magnitude of the irradiating frequency required.) If the conditions used are known, the irradiating frequency can be corrected to allow comparison with the locking frequency, and the chemical shift found from that of the lock sample used (usually tetramethyl silane). Many calibrations of tetramethyl silane are now available using the accepted standards for each magnetic nucleus. The normal standard for ^{15}N is tetramethyl ammonium iodide.[62]

Compound	$^1K(^{29}SiH)$	$^1K(^{29}Si^{13}C)$	$^1K(^{29}Si^{15}N)$	$^2K(^{15}NH)$	$^2K(^{13}CH)$
SiH_3NCO	+96.58	-	+81.10	+4.11	-
SiH_3NCS	+98.38	-	+82.34	+3.62	-
SiH_3CN	+97.50	+111.75	-	-	+1.49
GeH_3NCO	-	-	-	$\pm$4.44	-
GeH_3NCS	-	-	-	$\pm$4.03	-
GeH_3CN	-	-	-	-	$\pm$2.12

All values of K are in the units 10^{19} NA^2m^{-3}.

TABLE 4.3 - Reduced coupling constants for the species' MH_3CN and MH_3NCX.

The ^{15}N chemical shift of only one of the pseudohalides studied (silyl isocyanate) was calculated and related to this standard. Several other species have recently been studied,[63] however, and are given in table 4.4.

From table 4.4 it is clear that the ^{15}N nucleus is very sensitive to its environment, and that the electronegativity of the groups attached to nitrogen have a very great effect on its chemical shift.

4.2 Infrared Spectra

The spectra of all the pseudohalides in this work have been recorded previously and are discussed in Chapter 1. The spectra described in this section are of isotopically substituted silyl isocyanate and isothiocyanate, and germyl isocyanate. They were recorded to determine the magnitudes of the fundamental frequencies not observed directly,(in particular the low-frequency skeletal bend), by a study of some of the combination bands. Most of the vibrational modes involving (SiH) and (GeH) have, therefore, been omitted.

The silyl compounds belong to the point group C_{3v}, and germyl isocyanate, since it is not linear (see discussion in Chapter 5), belongs to the point group C_s.

The silyl compounds have ten normal modes of vibration - five of symmetry class a_1 and five degenerate modes of class e. Germyl isocyanate, however, has 15 normal modes of vibration -

Compound	^{15}N chemical shift
PF_2NH_2	-21.4
SiH_3NHPF_2	-14.1
SiH_3NCO	+33.7
$(SiH_3)_2NH$	+69.0
$(SiH_3)_3N$	+79.9

TABLE 4.4. ^{15}N-chemical shifts in p.p.m.* from $(CH_3)_4N^+I^-$

* A positive chemical shift represents a shift to high field.

five of symmetry class a" and ten of symmetry class a'. The in-plane modes (a') correspond to the five a_1 modes of C_{3v} and one component of each of the degenerate (e) modes. Thus the degenerate modes of C_{3v} are split in C_s into two components. Since this splitting was not observed in any of the bands in the spectrum of germyl isocyanate, the spectra of all three species will be discussed in terms of a C_{3v} model.

The observed spectra are presented in tables 4.5 to 4.7 together with the numbering of the normal modes for each compound. For combination bands of fundamentals whose isotopic shifts with ^{15}N substitution are measured, calculated and experimental shifts are tabulated.

Table 4.8 summarises the combination bands observed in the region 2300 to 4000 cm.$^{-1}$ for the three compounds.

The assignments are now discussed:

(a) Silyl isothiocyanate

The previous assignment of the very strong band at 2039 cm.$^{-1}$ as $2\,\nu_3{}^{18}$ was supported by its isotopic shift compared with that of the fundamental ν_3. The absence of bands in the region 230 to 400 cm.$^{-1}$ showed, however, that the assignment[18] of $2\,\nu_9$ to the band at 567 cm.$^{-1}$ was not possible. It seems likely that this band should be assigned to $\nu_9 + \nu_{10}$ and that ν_9 is masked by the band at 505 cm.$^{-1}$ (ν_5). It is quite possible for the combination $\nu_9 + \nu_{10}$ to be of greater

Observed frequencies ^{14}N	^{15}N	Isotopic shift (^{14}N-^{15}N)	Assignment	Calculated shift
3119			$\nu_2 + \nu_3$	
2920				
2840				
2649//	2615//	34	$\nu_2 + \nu_9 + \nu_{10}$	29
2600//	2569//	31	$\nu_2 + \nu_5$	24
2540//	2520//	20	$2\nu_3 + \nu_5$	22
2106	2081			
2095	2071	24	ν_2	-
2083	2059			
2039//	2018//	21	$2\nu_3$	22
1888//	1890//	0	$2\nu_7$	-
1415//				
1090				
1034//	1023//	11	ν_3	-
567	562	5	$\nu_9 + \nu_{10}$	-
505	505	0	ν_5	-

The fundamental frequencies of the molecule are:-

ν_1	$\nu(SiH)_s$	ν_6	$\nu(SiH)_a$
ν_2	$\nu(CN)$	ν_7	$\delta(SiH)_a$
ν_3	$\nu(CS)$	ν_8	$\rho(SiH)$
ν_4	$\delta(SiH)_s$	ν_9	Skeletal bending
ν_5	$\nu(SiN)$	ν_{10}	Skeletal bending

The symbol // denotes a band with parallel contour.

TABLE 4.5 - Infrared frequencies for silyl isothiocyanate.

Observed frequencies ^{14}N	^{15}N	^{2}H	Isotopic shift (^{14}N - ^{15}N)	Assignment	Calculated shift
3846	-	3840	-	$\nu_1 + \nu_3 + 2\nu_{10}$	-
3747	3699	3749	49	$\nu_1 + \nu_3$	28
3688//	3659	3034	29	$\nu_2 + \nu_3$	-
3540	-	3537	-	$\nu_1 + 2\nu_5$	-
3149	3150	-	-1	$\nu_2 + \nu_4$	-
2986	2965	2978	21	$\nu_1 + \nu_5 + \nu_{10}$	-
2927//	2914	2916	13	$\nu_1 + \nu_5$	2
2424	2407	2415	17	$\nu_1 + 2\nu_{10}$	-
2300	2297		3	ν_1	-
1448//	1423//		25	ν_3	-
1239	1260		-21	$2\nu_5$	-2
-	1070		-		-
619	620		-1	ν_5	-
582	579		3	ν_9	-

The fundamental frequencies of the molecule are:

ν_1	$\nu(NCO)_a$	ν_6	$\nu(SiH)_a$
ν_2	$\nu(SiH)_s$	ν_7	$\delta(SiH)_a$
ν_3	$\nu(NCO)_s$	ν_8	p (SiH)
ν_4	$\delta(SiH)_s$	ν_9	skeletal deformations
ν_5	$\nu(SiN)$	ν_{10}	skeletal deformations

TABLE 4.6 - Infrared frequencies for silyl isocyanate.

Observed frequencies ^{14}N	^{15}N	Isotopic shift	Assignment	Calculated shift
3742	-	-	$\nu_1+\nu_3+2\nu_{10}$	-
3663	3632	31	$\nu_1+\nu_3$	27
3628	3598	30	$\nu_2+\nu_3+2\nu_{10}$	-
3530//	3520//	10	$\nu_2+\nu_3$	19
2974	2965	9	$\nu_2+\nu_4$	3
2927	2918	9	$2\nu_3$	32
2849	2842	7	$\nu_1+\nu_5+2\nu_{10}$	-
2758	2740	18	$\nu_1+\nu_5$	17
2372	2344	28	$\nu_1+2\nu_{10}$	-
2270	2259	11	ν_1	-
2124//	2121//	3	ν_2	-
1406	1390	16	ν_3	-
861//	861//	0	ν_4	-
656 ⊥	645 ⊥	11	ν_8	-
495	489	6	ν_5	-

⊥ denotes a band of perpendicular contour.

The fundamental frequencies of the molecule are:-

ν_1	$\nu(NCO)_a$	ν_6	$\nu(GeH)_a$
ν_2	$\nu(GeH)_s$	ν_7	$\delta(GeH)_a$
ν_3	$\nu(NCO)_s$	ν_8	$\rho(GeH)$
ν_4	$\delta(GeH)_s$	ν_9	skeletal deformations
ν_5	$\nu(GeN)$	ν_{10}	skeletal deformations

TABLE 4.7 - Infrared frequencies for germyl isocyanate.

Assignment	SiH_3NCO	SiD_3NCO	$SiH_3{}^{15}NCO$	GeH_3NCO	$GeH_3{}^{15}NCO$	SiH_3NCS	SiD_3NCS	$SiH_3{}^{15}NCS$
$\nu_1+\nu_3+2\nu_{10}$	3846	3840	-	3742	-	-		-
$\nu_1+\nu_3$	3747	3749	3699	3663	3632	3119	-	-
$\nu_2+\nu_3+2\nu_{10}$	-	-	-	3628	3598	-		-
$\nu_2+\nu_3$	3688//	3034	3659	3530//	3520//	-		-
$\nu_1+2\nu_5$	3540	3537	-	-	-	-		-
$\nu_2+\nu_4$	3149	-	3150	2974	2965	-		-
$2\nu_3$	-	-	-	2927	2918	2039	2025	2018
$\nu_1+\nu_5+2\nu_{10}$				2849	2842	-		-
$\nu_1+\nu_5+\nu_{10}$	2986	2978	2965					
$\nu_1+\nu_5$	2927//	2916	2914	2758	2740	2600//	2581	2569//
$\nu_1+\nu_9+\nu_{10}$	-	-	-	-	-	2649//	2623	2615//
$2\nu_3+\nu_5$	-	-	-	-	-	2540//	2534	2520//
$\nu_1+2\nu_{10}$	2424	2415	2407	2372	2344	-		-

The numbering of the assignments relate to those of silyl and germyl isocyanates (silyl isothiocyanate numberings have been altered to correspond)

TABLE 4.8 Combination bands for silyl isocyanate and isothiocyanate and germyl isocyanate in the range 2300 to 4000 cm. $^{-1}$

intensity than the fundamental ν_9 since this combination (but not ν_9) has a component of the same symmetry class as the band ν_5. Fermi resonance may then account for the intensity of the combination. Since the band at 567 cm.$^{-1}$ is much weaker than ν_5 it seems likely that the interaction between the two is not strong and thus ν_{10} may be about 60 cm.$^{-1}$.

Further evidence comes from the band at 1090 cm.$^{-1}$ which could be assigned as $\nu_3 + \nu_{10}$ - leading again to a magnitude of about 70 cm.$^{-1}$ for ν_{10}. The infrared spectrum of silyl isothiocyanate has recently been recorded in solution in hexane[64] in the region 25 to 250 cm.$^{-1}$. A band at 93 cm.$^{-1}$ was observed and this must be assigned to ν_{10}.

It is strange that ^{15}N substitution produces no shift of ν_5 (the (SiN) stretching mode). It is possible that the presence of ν_9 under this band hides the shift expected. Recent calculations based on an electron diffraction and infrared study of difluoro(isocyanato)phosphine and difluoro (isothiocyanato)phosphine[65] have shown, however, that the band assigned to the (PN) stretch in these molecules has contributions from several other modes. In fact, in both cases the contribution of (PN) stretching in this vibrational mode of the molecules is quite small.

(b) Silyl isocyanate

The bands observed in the spectrum of the deuterated species

from 2400 to 4000 cm.$^{-1}$ are included in table 4.6 to show which bands involve the (SiH) modes. Assignment of the other combination bands is, therefore, easier.

From the intensity of the band at 2424 cm.$^{-1}$ in the ^{14}N compound it seems likely that it is involved in fermi resonance with the fundamental ν_1. The combination was previously assigned[66] $\nu_1 + \nu_{10}$ but this does not have a component of a_1 symmetry and could not, therefore, interact with ν_1. It seems more likely that the combination is $\nu_1 + 2\nu_{10}$ which gives a magnitude of 62 cm.$^{-1}$ for ν_{10}. Two other bands were observed which may involve ν_{10} (3846 cm.$^{-1}$ and 2986 cm.$^{-1}$) and lend some support to the assignment. Further support is derived from the assignment of these combinations in other isocyanates.[67-69].

(c) Germyl isocyanate

Assignments could not be made to all the combination bands observed without involving the low-frequency skeletal bend ν_{10}. As in silyl isocyanate a band is observed above the (NCO) asymmetric stretch whose intensity may be explained by fermi resonance with ν_1. Again the assignment $\nu_1 + 2\nu_{10}$ is made on symmetry grounds and this gives a magnitude of 51 cm.$^{-1}$ for the fundamental ν_{10}. A band was observed at 115 cm.$^{-1}$ in a spectrum of liquid germyl isocyanate[16] and this may also be assigned ν_{10}. The assignment of the band at 2372 cm.$^{-1}$ as a combination involving ν_{10}[17] was discounted[16] in the absence of

a corresponding difference band (ca. 2168 cm.$^{-1}$). In view of the two (GeH) bands in this region it is not surprising that a weak difference band is not observed. No difference band was observed in silyl isocyanate, but in difluoro(isocyanato)phosphine[65] a series of bands is reported:

$\nu_1 + 2\ \nu_8$

$\nu_1 + \nu_8$

ν_1

$\nu_1 - \nu_8$

where ν_8 is the skeletal bending frequency in this molecule.

In difluoro(isothiocyanato)phosphine[65] even $\nu_1 + 3\ \nu_8$ is observed. A similar series is found around the (NCN) asymmetric stretch in digermyl carbodiimide.[26]

In germyl isocyanate several other combinations were observed involving ν_{10} (table 4.7). The spectrum has been discussed in terms of a C_{3v} model in order to make comparison easier with the silyl species. The complexity of the band contour of ν_3 was previously taken[71] to indicate the non-linear structure. However, the band contour of ν_3 in silyl isocyanate is also complex, although it may be in this case due to an interaction with the overtone 2 ν_8.

4.3 Mass spectra

The spectra were recorded of silyl isothiocyanate and germyl

cyamide to demonstrate the incorporation of ^{15}N and ^{13}C. The cracking patterns of silyl isocyanate and silyl isothiocyanate are also reported, however.

(a) Germyl cyanide

The mass spectrum was recorded at 70 eV of the sample of ^{13}C-substituted germyl cyanide used in the proton magnetic resonance studies described in Section 4.1. The sample was estimated to contain 60% ^{13}C from its proton spectrum.

Peaks were observed in the $^{e}/_{m}$ regions 104 to 96 and 78 to 70 and their approximate relative intensities are given in table 4.9. The presence of both ^{13}C and ^{12}C can be seen from the range of peaks - 96 to 104. These can only be explained by a series of species from $^{70}Ge^{12}CN$ to $^{74}GeH_3{}^{13}CN$. The peak at 78 is probably due to $^{74}GeH_4$.

(b) Silyl isothiocyanate

Exact mass measurement was carried out on the parent ions for both ^{14}N and ^{15}N samples. The magnitudes found were:

$SiH_3{}^{14}NCS$ 88.9753 (calculated 88.9755)

$SiH_3{}^{15}NCS$ 89.9720 (calculated 89.9726)

The cracking pattern found at 70eV is shown in figure 4.14, the fragments being identified by comparison of the ^{14}N and ^{15}N compounds. Weak metastable ions at 41.8 and 42.8 in the ^{15}N spectrum showed the origins of the unexpected peak at 61. The exact mass of the 61 peak was measured to check its assignment

e/m	Approx. relative intensity
104	10
103	10
102	60
101	60
100	100
99	30
98	50
97	25
96	15
78	10
77	10
76	85
75	50
74	150
73	50
72	110
71	20
70	55

TABLE 4.9 - Mass spectrum of germyl cyanide.

- 60.9563 (calculated 60.9568).

At 70eV the peaks at 54 and 61 in the ^{14}N spectrum were of about equal intensity. At lower eV, however, the 54 peak was much more intense than the 61 peak.

(c) Silyl isocyanate

The exact mass of the parent ion was measured and was found to comprise:

72.9982	$^{28}SiH_3NCO$	(calculated 72.9984)
72.9899	$^{29}SiH_2NCO$	(calculated 72.9901)
72.9787	$^{30}SiHNCO$	(calculated 72.9796)

The cracking pattern found at 70eV is shown in figure 4.15. No metastable ions were observed and thus only the likely origins of the ions observed are given. At 70eV the intensities of the peaks were approximately:

$$(42) = (44) = (43) > (45) = (54)$$

At low eV this pattern was altered:

$$(43) = (44) > (42) = (45) = (54)$$

The fragmentation of the peaks (70) and (71) seems to be less at the lower ionising voltage.

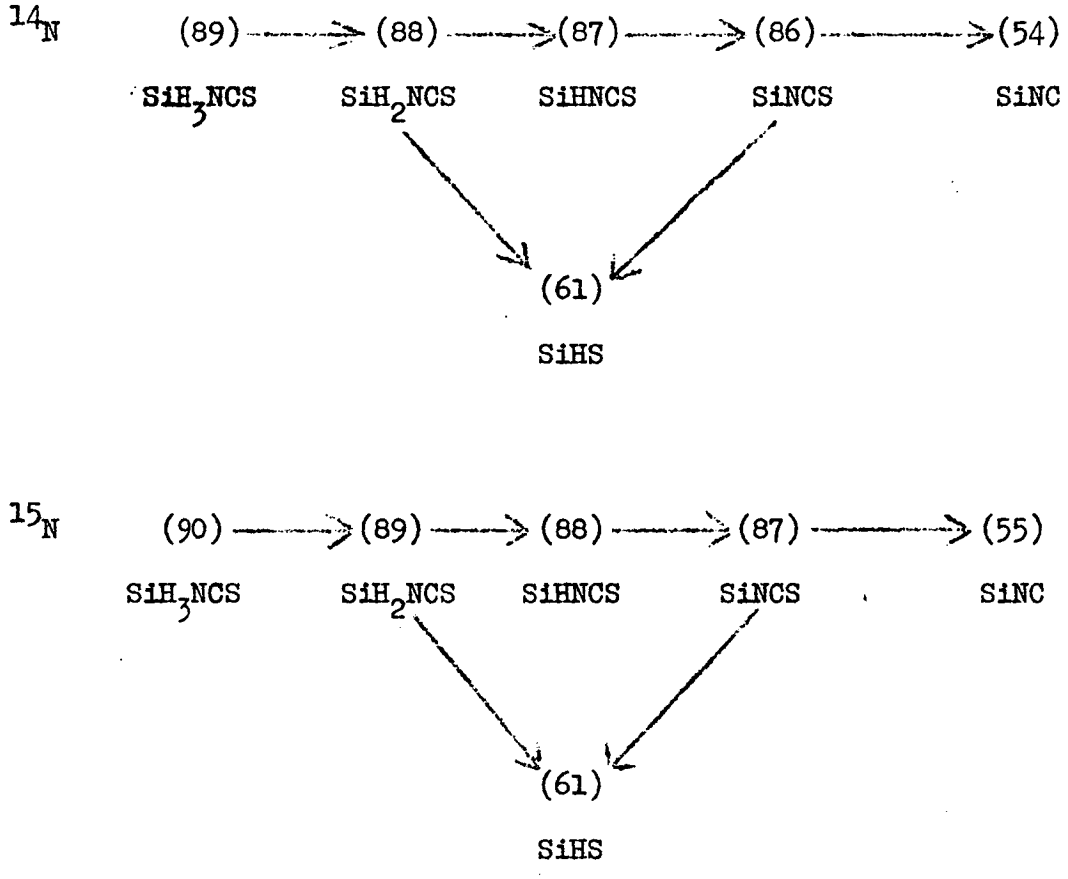

FIGURE 4.14 - Cracking pattern for silyl isothiocyanate.

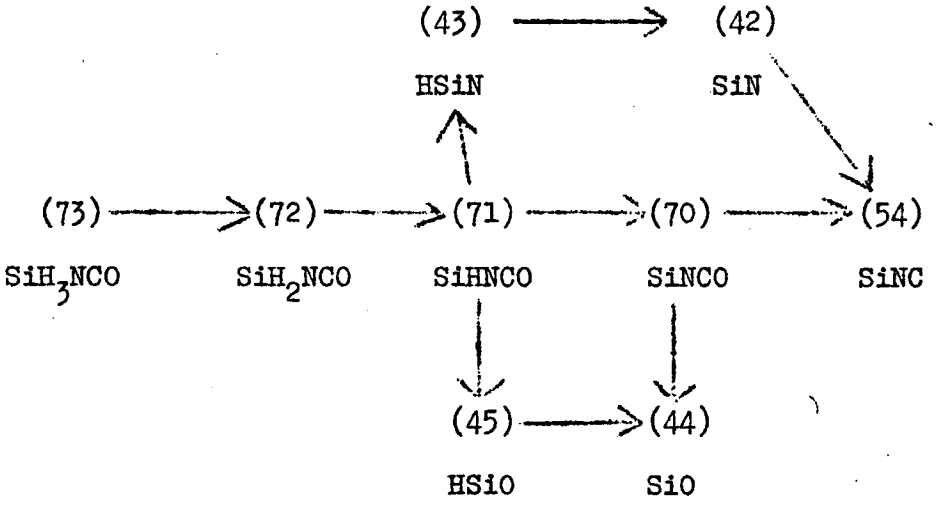

FIGURE 4.15 Cracking pattern for silyl isocyanate.

CHAPTER 5

MOLECULAR STRUCTURES AND BONDING

It was evident in Chapter 1 that definitive structural information is rarely obtained from the application of one technique. A combination of the results of several investigations, together with a comparison with those obtained for very similar molecules, is required.

As in Chapter 1 the structural information obtained is discussed with reference to the two main features of the structures of these molecules - the donor site, the angle at the donor atom. From these some idea of bonding differences may be deduced.

5.1 Donor site.

The proton magnetic resonance spectra (Chapter 4) show quite clearly that each pseudohalide studied exists almost completely in one form - as isocyanate, isothiocyanate, and n-cyanide. If the other isomer is present, it is present in concentrations of less than 1% of the predominant isomer, and is not involved in fast exchange with it.

It seems very likely, therefore that the bands in the infrared, in some cases assigned to the other isomer, are combination bands. Their intensity can be explained in all cases by fermi resonance and the magnitudes of skeletal bending frequencies obtained assuming this assignment are reasonable compared with estimates by other techniques (see Section 5.3).

The electron diffraction structure determination of digermyl carbodiimide is definitive proof that the molecule does not

have a cyanamide structure. In view of the similarity of the infrared spectra of the silyl[24,25] and germyl[25,26] compounds and their dissimilarity with the spectrum of the methyl compound,[23] is seems likely that the assignment of a carbodiimide structure to the silyl species and a cyanamide structure to the methyl species were correct.

5.2 Geometrical structure

Before one can interpret differences in bonding between the silicon, germanium, and carbon compounds it is necessary to explain the differences in the bond angles found for the methyl pseudohalides.

Despite the fact that the azide and isocyanate groups are isoelectronic very different bond angles are observed in the methyl compounds[11] (117° and 140° respectively). In resonance terms this may be explained by considering the possible canonical forms for the two species:-

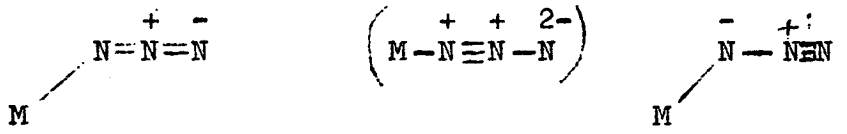

(I) (II) (III)

and

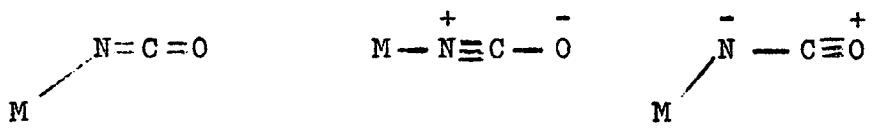

(I) (II) (III)

For the azide there will be very little contribution from structure (II) because of the unstable charge distribution. The main contribution will be from (I) because of the inductive effect of the methyl group. Thus one expects an angle at nitrogen of about 120° and $r(N_2N_3) < r(N_1N_2)$.

In the isocyanate, (II) may now make a significant contribution and this would explain the wider angle of 140° found. The inclusion of (II) also predicts that $r(NC) < r(CO)$. This is in agreement with experimental measurements (table 5.1), as are the predicted relative magnitudes of r(NN) in methyl azide. It should be noted, however, that the exact measurement of bond lengths within the pseudohalide group by electron diffraction is not simple because of the overlapping of peaks in the radial distribution curves. However, the differences discussed in the following section are regarded as large enough to be significant. The parameters obtained for several pseudohalides by electron diffraction are shown in table 5.1.

The bond angles found in germyl isocyanate and azide are very similar to those found in the methyl compounds. In germyl isocyanate, however, $r(NY) > r(YZ)$. This could only be explained by an increase in the contribution of (III) compared with the methyl compound. In view of the electronegativities of carbon and germanium this is unlikely, and a second consequence of inclusion of (III) would be a narrower angle at nitrogen. Since this is not observed this explanation is unsatisfactory.

This argument is reinforced by the parameters given in

Y	C	C	C	C	C	C	C	N	N
Z	O	O	O	O	O	O	O	N	N
X	H	H	H	Me	F	F	Cl	H	H
M	C	Si	Ge	Si	C	Si	Si	C	Ge
Species	CH_3NCO	SiH_3NCO	GeH_3NCO	Me_3SiNCO	CF_3NCO	SiF_3NCO	$SiCl_3NCO$	CH_3N_3	GeH_3N_3
r(MN)	1.450	1.703	1.831	1.76	1.470	1.648		1.468	1.855
r(NY)	1.168	1.216	1.190	1.20	1.210	(mean of	1.219	1.216	1.245
r(YZ)	1.202	1.164	1.182	1.18	1.170	(1.18))	1.139	1.130	1.134
$\hat{MNY}$	140	152	141	150	126	161	138	117	119
Reference	11	14	-	35	70	73	75	11	-

TABLE 5.1 Bond lengths and angles in the pseudohalides (MX_3NYZ) from electron diffraction measurements

table 5.1 for CF_3NCO[70] and SiH_3NCO[14]. The parameters of CF_3NCO can be explained by an increase in the contribution of (III) which would be stabilised by the electron-withdrawing CF_3 group. The greater difference between r(NC) and r(CO) in the silyl compound shows that the effect is probably connected with a widening of the angle at nitrogen.

It is also difficult to explain the longer r(NY) in germyl azide than in methyl azide. This would also require a larger contribution from (III) which is not supported by the bond angle found.

These effects can be satisfactorily explained by including two other canonical forms in which germanium is involved in multiple bonding:-

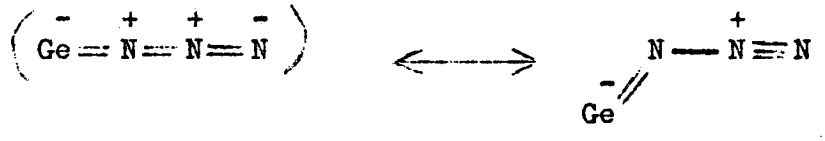

(IV) (V)

and

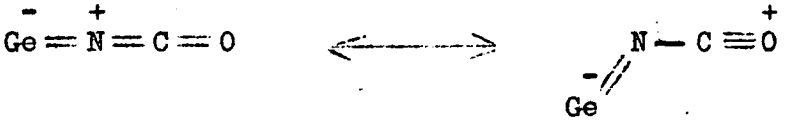

(IV) (V)

Structure (IV) will make little contribution to the azide but the inclusion of (V) can explain the long $r(N_1N_2)$ without altering the angle at nitrogen substantially.

In the isocyanate there may be substantial contribution

from (IV) and (V). The magnitudes of r(NC) and r(CO) may be explained by approximately equal contributions from (II) and (V) and the narrowing of the angle at nitrogen caused by inclusion of (V) may be counteracted by the contribution from (IV). Thus the overall structure would be

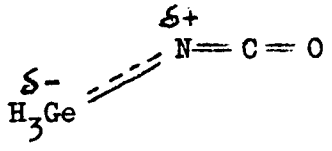

where the (GeN) bond corresponds to 1.4 bonds and $\delta+$ and $\delta-$ are $\pm$ 0.4.

The predicted bond angle would then be 144°.

In silyl isocyanate the contributions from (IV) and (V) appear to be greater, producing a shorter r(CO), a longer r(NC) and a wider angle at nitrogen. Similarly, comparing silyl[14] and methyl isothiocyanate[11] r(NC) is longer, (CS) is shorter, and the angle at nitrogen wider in the silyl compound. The application of shrinkage corrections to the bond angles quoted above and in table 5.1 will be discussed in Section 5.3. These corrections reinforce the argument proposed.

It seems, therefore, that (p → d) π bonding explains the bond lengths and angles found in the germyl pseudohalides. Its existence is confirmed by the photoelectron spectra reported in Chapter 3. The ionisation potentials and band shapes for the silyl compounds and the band shapes of the germyl compounds were explained by this interaction. No information was obtained, however, on the effect of the bonding on molecular geometry. The

presence or absence of splitting in the bands assigned to the pseudohalide π -levels merely gave information on the shapes of the ions formed on excitation.

5.3 Shrinkage

In order to assess the extent of the effect on molecular geometry of π -bonding, the parameters determined by electron diffraction are not sufficient. For example, the skeletons of silyl isocyanate and isothiocyanate are known from their microwave spectra[13,20] to be linear, but the angles found by electron diffraction are 152° and 164°. The discrepancy occurs because the angles given by electron diffraction are time-averages. They are deduced from the distances between non-bonded atoms. The skeletal bending vibration at nitrogen in these molecules causes the time-average for the (Si .. O) or (Si .. S) distance to be shorter than when the molecule is in its equilibrium position and thus the angle deduced is less than 180°. The shrinkages in these molecules are severe for two reasons - the amplitude of the skeletal bending vibration is large, and the equilibrium angle in these molecules is 180°.

The shrinkage caused by a bending vibration is zero for an equilibrium angle of 90°, and at a maximum for an angle of 180°. Figure 5.1 shows the effect on the angle measured by electron diffraction of the same vibrational amplitude for equilibrium angles from 90° to 180°. The amplitude was chosen so that an observed angle of 160° (silyl isothiocyanate)

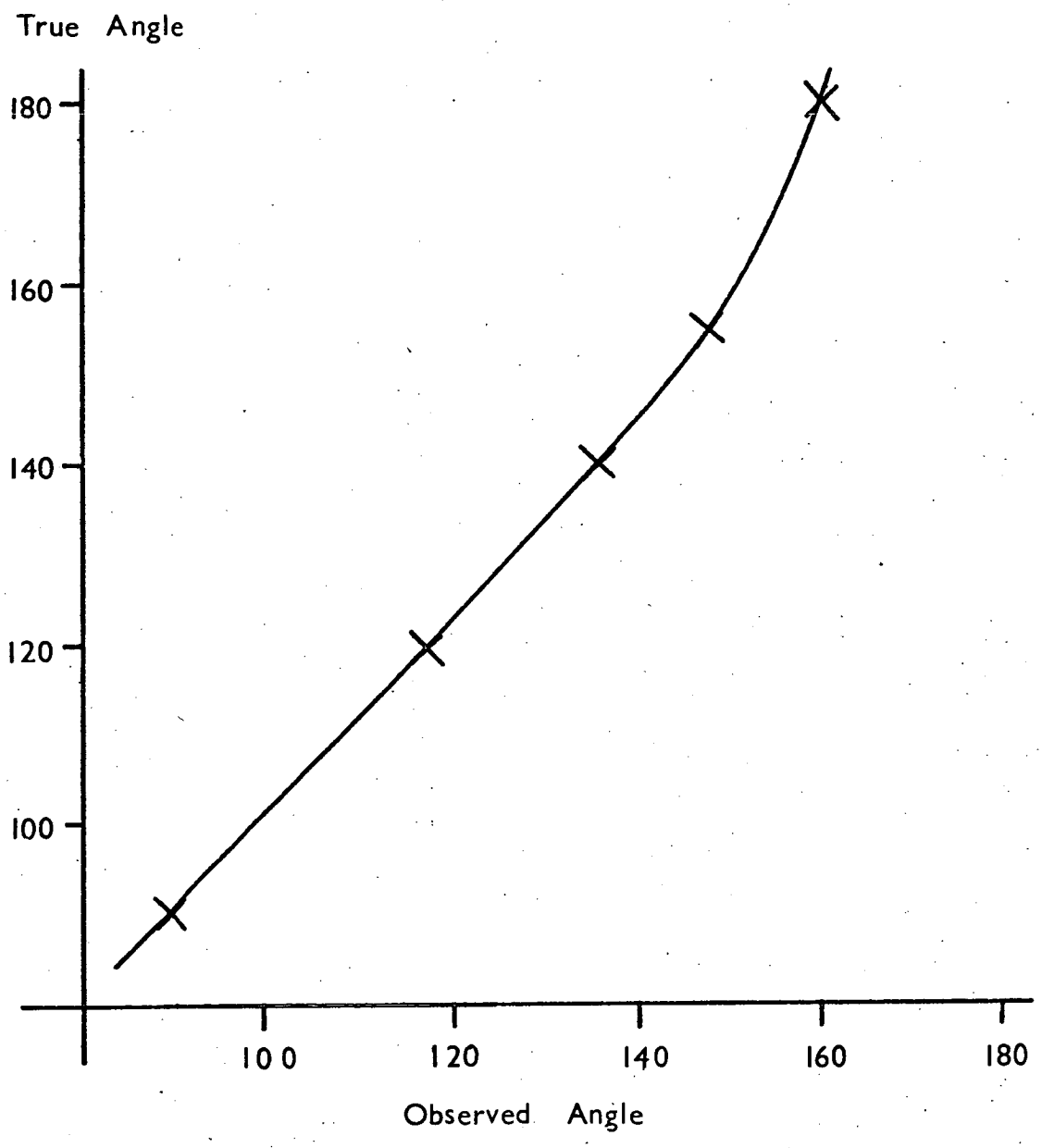

Figure 5.1 - Effect of shrinkage for equilibrium angles from 90° to 180°.

corresponds to a true angle of 180°.

In order to determine the equilibrium angles for any molecule, therefore, all the vibrational amplitudes must be known. Calculations of the shrinkages expected from the vibrational frequencies of difluorophosphine isocyanate and isothiocyanate[65] have been carried out. The shrinkages found were only 4° for observed angles in the region 130° to 140°, even although the skeletal bending frequencies are quite low.

Direct measurement of the skeletal bending frequency is very rarely possible in pseudohalides, and various methods have been used to estimate them. Microwave spectra may yield information on these vibrations, as the spectra of molecules in excited states may be observed. Estimates of the frequency by this method, however, assume that the vibration is harmonic.

For silyl isocyanate and isothiocyanate the electron diffraction data itself has been used to characterise the shape of the potential well for the skeletal bending vibration.[71] The asymmetry of the peaks due to r(Si.. O) and r(Si.. S) suggest potential wells which differ for the two molecules - that of silyl isothiocyanate is harmonic, while that of silyl isocyanate is anharmonic and has two minima at angles of 159°, but the barrier between these is lower than the first vibrational level ($\sim$ 20 cm.$^{-1}$). The anharmonicity found for silyl isocyanate is in agreement with the microwave spectrum in which lines were observed which could not otherwise be assigned. The estimates of ν_{10} differ from those made from the microwave spectra,

however, by a factor of two. The magnitude for ν_{10} in both these molecules, however, seems to be in the range 40 - 100 cm.$^{-1}$.

The infrared spectra described in Chapter 4 suggest that ν_{10} has the magnitudes:-

SiH_3NCS	60 to 90 cm.$^{-1}$
SiH_3NCO	60 to 70 cm.$^{-1}$
GeH_3NCO	50 to 60 cm.$^{-1}$

Thus despite the discrepancies found between the estimates of ν_{10} for silyl isocyanate and isothiocyanate, it seems that the magnitude of ν_{10} in germyl isocyanate is fairly similar to that in the silyl compounds.

Germyl isocyanate, therefore, appears to be non-linear, with an equilibrium angle of about 145°. This was estimated from the graph in figure 5.1, which assumes a harmonic vibration of about the same amplitude as that found in silyl isothiocyanate (calculated on the basis of the required shrinkage). It is interesting to note that this graph predicts that if silyl isocyanate had a harmonic potential well with the same vibrational amplitude as silyl isothiocyanate, the shrinkage would predict an equilibrium angle of 159°.

This estimate of the equilibrium angle in germyl isocyanate requires a very similar shrinkage to that found in the difluorophosphine pseudohalides. Also if the bond lengths found by the electron diffraction study (reported in Chapter 2) are combined with the results of the preliminary microwave study of

germyl isocyanate[33] an equilibrium bond angle of about 144° is predicted.

No microwave study or estimate of ν_{10} is available for silyl isoselenocyanate, but from the observed electron diffraction angle, and by comparison with the isocyanate and isothiocyanate, it seems likely that this molecule is also linear in its ground state.

The angle at nitrogen found for digermyl carbodiimide is very similar to that in germyl isocyanate, and combination bands involving ν_{10} suggest a value of about 50 to 60 cm.$^{-1}$. The shrinkage which must be applied in this case would thus be very similar to that for germyl isocyanate. Application of shrinkage corrections to the dihedral angle of 75° suggests that the molecule has an allene conformation, like the difluorophosphine compound.

Germyl azide is known to be non-linear[30], and since the angle measured by electron diffraction is 123°, shrinkage corrections are likely to be small.

5.4 π-bonding in the pseudohalides.

A possible explanation of the geometric differences found between methyl and silyl compounds has recently been proposed.[72] It suggests that the difference in molecular shape between trisilylamine and trimethylamine can be explained by the greater mixing of the non-bonding (π) and lowest antibonding level in the silicon species. The energy of the antibonding level in the

two compounds depends on the electron releasing properties of the methyl and silyl groups. The greater electron releasing ability of the silyl group lowers the energy of the antibonding level, and increases mixing.

This explanation is contrary to recent structural information on perfluoro-silyl isocyanate[73] and perfluorodisiloxane.[74] The bond angle widening of the silyl compounds compared with the methyl compounds is increased in the perfluoro compounds.

It seems therefore that the bond lengths and angles found for the methyl, silyl and germyl pseudohalides can only be explained by the existence of π -bonding between the silicon and germanium atoms and the pseudohalide groups. Characterisation of the potential wells for silyl isocyanate and isothiocyanate has suggested, however, that the energy differences required to produce the observed angles in these molecules and their methyl analogues are small.

REFERENCES

1. Linton, Nixon. J.Chem.Phys. 28, 990(1958).
2. Beachell J.Chem.Phys. 28,991(1958).
3. Bither, Knoth, Lindsey, Sharkley J.A.C.S. 80,4151(1958)
4. Linton, Nixon Spec.Acta. 10,299(1958).
5. Goldfarb, Zafonte J.Chem.Phys. 41,3653(1964).
6. Ebsworth, Frankiss. J.C.S.(A) 661 (1963).
7. Frankiss. Spec.Acta 26 A,859(1970)
8. Eyster, Gillette J.Chem.Phys.8,369(1940)
9. Hirschmann, Kinseley, Fassel Spec.Acta 21,2125(1965).
10. Eyster, Gillette, Brockway J.A.C.S.62,3236(1940).
11. Anderson,Rankin,Robertson J.Mol.Struc., in press.
12. Ebsworth, Mays J.C.S.4844(1962).
13. Gerry, Thomson, Sugden Nature 211,846(1966).
14. Glidewell, Robiette, Sheldrick. Chem.Phys.Lett., in press.
15. Srivastava, Griffiths, Onyszchuk Can.J.Chem. 40,739(1962).
16. Griffiths, J.Chem.Phys. 48,278(1968).
17. Mackay, Stobart Spec.Acta. 26 A,373(1970).
18. Ebsworth, Mould, Taylor, Wilkinson, Woodward. Trans.Farad.Soc. 58,1069(1962).
19. Ebsworth, Turner J.Phys.Chem. 67,805(1963).
20. Jenkins, Kewley, Sugden Trans.Farad.Soc. 58,1284(1962).
21. Davidson, Woodward, Mackay, Robinson Spec.Acta. 23 A,2383(1967).
22. Ebsworth, Mays J.C.S. 3893(1963).
23. Kahovec, Kohlrausch Z.Physik Chem. B37,421(1937).
24. Ebsworth, Mays J.C.S. 4879(1961).

25. Ebsworth, Mays — Spec.Acta. 19,1127(1963).

26. Cradock, Ebsworth — J.C.S.(A) 1423(1968).

27. Ebsworth, Mays — J.C.S.(A) 3450(1964).

28. Ebsworth, Jenkins, Mays, Sugden. — Proc.Chem.Soc. 21(1963).

29) 30) Cradock, Ebsworth — J.C.S.(A) 1420(1968).

31. See references 8 and 9.

32. Curl, Rao, Sastry, Hudgeson — J.Chem.Phys. 39,3335(1963)

33. Ramprassad, Varma, Nelson — J.A.C.S. 90,6247 (1968).

34. Thayer, Strommer — J.Organomet.Chem. 5,383(1966).

35. Kimura, Katada, Bauer. — J.A.C.S. 88,416(1966).

36. Beagley, Clark, Hewitt. — J.C.S.(A) 658(1968).

37. Rankin, Robiette, G.M.Sheldrick, W.S.Sheldrick, Aylett, Ellis, Monaghan — J.C.S.(A) 1224(1969).

38. Hedberg, Iwasaki — Acta.Cryst. 17,529(1964).

39. Cox, Bonham. — J.Chem.Phys. 47,2599(1967).

40. Bartell. — J.Chem.Phys. 23,1219(1955)

41. Hamilton — Acta.Cryst. 18, 502(1965).

42. Strandberg, Wentink, Hill — Phys.Rev. 75,827(1949).

43. Bak, Sloan, Williams — ibid. 80,101(1950).

44. Cross, Brockway — J.Chem.Phys. 3,821(1935).

45. Finbak, Hassel — Arch.Math.Naturv. B,44 No.3.

46. As 14.

47. I.Karle, J.Karle — J.Chem.Phys. 17,1052(1949).

48. Rankin — J.C.S. Dalton 869(1972).

49. Koopmans — Physica 1, 104(1934).

50. Brundle, Turner — Int.J.Mass.Spec.Ion Phys. 2,195(1969).

51. Brundle, Robin, Basch — J.Chem.Phys. 53, 2196(1970).

Cradock. — J.Chem.Phys. 55, (1971).

52. Eland — Phil.Trans. 268,87(1970).

53. Kewley, Sastry, Winnewisser — J.Mol.Spec. 10,418(1963).

Winnewisser, Cook. — J.Chem.Phys. 41,999(1964).

54. Radom, Hehre, Pople — J.A.C.S. 93,289(1971).

55. Cradock, Whiteford — Trans.Farad.Soc. 67, 3425(1971).

56. Cradock, Ebsworth — Unpublished observation.

57. Chew, Darbyshire, Logan — Chem.Comm. 1708(1970).

58. Arnold. — Personal communication.

59. Lynden-Bell and Harris, Nelson — "N.M.R." p.107.

60. Ibid. p.110.

61. Allred J.I.N.C. 5,264(1958).

62. Baker. J.Mag.Resonance 4,142(1971).

63. Rankin Personal communication.

64. Ebsworth Personal communication from C.G.Carlson.

65. Rankin, Cyvin J.C.S. Dalton 1277(1972).

66. Mays Ph.D. Thesis (Cambridge).

67. Miller, Carlson Spec.Acta. 17, 977(1961).

68. Goubeau, Grabner Chem.Ber. 93,1379(1960).

69. Koster Spec.Acta. 24, 395(1968).

70. Rankin Personal communication (preliminary study).

71. As 14, and Cyvin, Burnvoll, Robiette Chem.Phys.Lett. 11,263(1971).

72. Bartell J.Chem.Ed. 45, 754(1968).

73. Airey, Glidewell, Robiette, G.M.Sheldrick. J.Mol.Struc. 8,435(1971).

74. Airey, Glidewell, Rankin, Robiette, Sheldrick, Cruickshank. Trans.Farad.Soc. 66,551(1970).

75. Hilderbrandt, Bauer J.Mol.Struc. 3,325(1969).

76. Beard, Dailey J.A.C.S. 71,929(1949).

77. Rankin Personal communication.

78. Kimura, Kubo J.Chem.Phys. 30,151(1959).

79. Kasai, Myers. Ibid., 30, 1096(1959).

80. Pierce, Hayashi Ibid., 35, 479 (1961).

81. Beecher J.Mol.Spec. 21,414(1966).

82. Almenningen, Bastiansen, Ewing, Hedberg, Traetteberg. Acta.Chem.Scand. 17, 2455(1963).

83. Almenningen, Hedberg, Seip ibid., 17,2264(1963).

84. Almenningen, Fernholt, Seip ibid., 22, 51(1968).

85. Glidewell, Rankin, Robiette, Sheldrick, Beagley, Cradock. J.C.S.(A), 315(1970).

86. Murdoch, Rankin, Glidewell J.Mol.Struc. 9,17(1971) and this work.

87. Beagley, Robiette, Sheldrick J.C.S.(A) 3002(1968).

88. Hamilton "Statistics in physical science" Ronald Press, N.Y.(1964).

89. Bartell, Higginbotham J.Chem.Phys. 42, 851(1965).

90. Kilb, Pierce	ibid. 27, 108(1957).
91. Laurie	ibid. 30, 1210(1959).
92. Eisch, King	"Organometallic Syntheses" Academic Press (1965), p.172.
93. Eisch, King	ibid., p.124.
94. Eisch, King	ibid., p.125.
95. Jolly	J.A.C.S. 83,335(1961).
96. Dennis, Judy	ibid., 51, 2321(1929).
97. Cradock	Ph.D. Thesis, Cambridge, (1966).
98. Fritz, Kummer	Z.Anorg.Chem. 308, 105(1961).
99. Thompson	Ph.D.Thesis, Cambridge (1965).
100. Stock, Somieski	Ber., 54,740(1921).
101. West, Thayer	Inorg.Chem.,3,899(1964).
102. Cradock, Ebsworth	J.C.S.(A) 1423(1968.
103. Cradock, Ebsworth	J.C.S.(A) 1226(1967).
104. Ebsworth, Mays	J.C.S. 3893(1963).
105. Cradock, Ebsworth, Davidson, Woodward	J.C.S.(A) 1229(1967).
106. Amberger, Boeters	Ang.Chem.Int. 1,52(1962).
107. Norman, Wingleth	Chem.Comm. 1218(1967).
108. Norman	Chem.Comm. 812(1968).
109. Brauer	"Handbook of Preparative Inorg.Chem." Acad.Press p.527(1965).
110. Finholt, Helling, Imhof, Neilsen, Jacobson.	Inorg.Chem. 2,504(1963).

SECTION II

CHAPTER 6

SILYL AND GERMYL PHOSPHINE COMPLEXES

6.1 Summary

The second section of this thesis describes the preparation, spectroscopic properties, and some reactions of silyl and germyl phosphine complexes. All the complexes studied were derivatives of molybdenum hexacarbonyl in which one or more carbonyl groups have been replaced by the phosphine. The phosphines used were all derived from phosphine by substitution of one, two, or three hydrogen atoms by silyl or germyl groups.

6.2 Phosphine

Phosphine has long been known to react with diborane[1] but it was only recently that a correct description of the product of this reaction was made. The product was originally thought to be ionic and the structure proposed for it was $(PH_4)^+ (H_2BPH_2BH_3)^-$. The application of several spectroscopic techniques has now shown[2] that the compound is a simple molecular adduct - PH_3BH_3. Phosphine forms similar adducts with boron trifluoride[3] and the aluminium halides.[4]

Many transition metal complexes of phosphine are also now known but most of these have only been prepared in the last few years. Phosphine was known to form 1:1 adducts with titanium tetrahalides[5] and copper (II) halides[6] at low temperatures. These, however, are unstable even at low temperatures and it is thought that the bonding between the metal and phosphorus is merely based on σ-donation and involves very

little π -back donation. The first stable transition metal derivative of phosphine to be isolated was a bridged dimeric complex of vanadium[7] in which two (PH_2) groups were assumed to bridge between the vanadium atoms - $(CO)_4V(PH_3)_2V(CO)_4$. The first monomeric phosphine complex[8] to be prepared was also a derivative of vanadium carbonyl - $C_5H_5V(CO)_3PH_3$. Phosphine complexes have now been isolated for the metals:

Mn, Cr, Mo, W, Fe, V, Ni, Rh, Co.[9]

6.3 Preparation

Normally two methods can be employed for preparing these complexes. Either a carbonyl group may be replaced directly by the phosphine ligand using ultra-violet irradiation or strong heating, or the complex can be prepared from a starting material which contains a labile ligand which can be replaced by the phosphine under mild conditions. In the second method the denticity of the labile ligand in the starting compound usually determines the number of phosphine ligands in the product.

In this work only the latter method was attempted since mild conditions were required by the nature of the phosphine ligands. The study was also restricted to molybdenum complexes as previous work had shown that these compounds react faster than those of the other group six metals.

Suitable starting materials for preparing mono-, bis-, and tris-phosphine complexes were:-

N-methyl pyridinium molybdenum pentacarbonyl iodide, norbornadiene molybdenum tetracarbonyl, and cyclohepta-1,3,5 - triene molybdenum tricarbonyl.

All three complexes are octahedral and the stereochemistry of each is known. The structure of the second was deduced from ^{13}C-nuclear magnetic resonance spectroscopy[10], and that of the third was determined by X-ray crystallography.[11] The compounds react with phosphines to yield octahedral species in which the symmetry of the starting compound (C_{4v}, C_{2v}cis), or C_{3v}(cis)) is retained.

It appears that two mechanisms are possible in the formation of the mono-complex.[12,13] One of these postulates a seven coordinate intermediate and leads to the mono-phosphine product. This is the mechanism involved when the concentration of the phosphine is high. When the phosphine concentration is low another mechanism is implied by the kinetic data and involves a five coordinate intermediate formed by loss of carbon monoxide. It leads, therefore, to an initial product in which the halogen is retained and the phosphine has replaced one carbonyl group. This product may then react with further phosphine to produce a bis-substituted phosphine carbonyl.

Only a seven coordinate intermediate has been proposed[14] in the formation of the tris complex which leads to the cis-substituted product.

No kinetic studies have been published on the tetracarbonyl starting compound used in this work. Data on its cyclooctatetraene analogue[15] has again suggested two mechanisms involving five and seven coordinate intermediates, respectively, but both of these lead to the cis product.

For all three starting compounds chosen, substituted carbonyls can be obtained of molybdenum with phosphine itself -

$Mo(CO)_5\ PH_3$ 16, 17, 20, 9

$Mo(CO)_4\ (PH_3)_2$ 18, 19, 21, 22, 9

$Mo(CO)_3\ (PH_3)_3$ 20, 9

Transition metal complexes of many substituted phosphines have also been prepared and are well characterised. For example, methyl phosphine forms a similar series of molybdenum carbonyl complexes to those listed above.[9]

6.4 Silyl and germyl compounds

Silyl and germyl compounds in which this group is directly bound to a group 6 atom have been found to exhibit properties which are not those that would be predicted from a knowledge of their corresponding methyl compounds. The donor strength of the group 6 atom was shown to be less than in the methyl compounds.[23] This is the reverse of that expected on the basis of the electronegativities of carbon, silicon, and germanium. The observations were explained in terms of a π -interaction between the vacant 'd' orbitals of the group 4 atom and the lone pairs on the group 6 atom.

This explanation has been supported recently by a study of the photo-electron spectra of the compounds $(MH_3)_2Y$ and MH_3SH, in which M = C, Si, Ge; Y = O, S, Se, Te.[24] All the bands in these spectra could be assigned to excitation from the expected molecular energy levels. The band in the spectra assigned to excitation from the/

lone pair orbitals of the group 6 atom was very sharp in the methyl compounds but was broad in all the silyl and germyl compounds. This is strong evidence that the lone pair electrons of the group 6 atom are non-bonding in the methyl compounds but that they are taking part in bonding to silicon and germanium. The ionisation potentials of these bands are also consistent with the existence of 'π -type' bonding in all the silyl and germyl compounds. This evidence lends direct support to the previous investigations of donor strength of the group 6 atom, as comparisons in these studies could have been hampered by differences in solvation behaviour of the complexes.

The structures found for the molecules $(MH_3)_2Y$ (in which M = C, Si, Ge and Y = O, S, Se)[25] by electron diffraction favour substantial π-bonding in the silicon and germanium molecules only when Y = O. The molecular parameters found show no evidence for such interactions in the other species (see table 1.2).

A similar situation is found in molecules in which silicon and germanium are bonded to elements of group 5. The structures determined by electron diffraction for trisilylamine[26] and trigermylamine[27] contain a planar heavy atom skeleton. Since this is the most favourable conformation for maximum overlap of the empty d orbitals of the group 4 atoms with the lone pair orbital on the nitrogen atom, the molecular shapes were explained in terms of such an interaction. Similar studies of trisilyl phosphine[28] and trigermyl phosphine [29] have shown that their

heavy atom skeletons are not planar and have given molecular parameters close to those expected in the absence of π - bonding. This could well be explained by a greater overlap of the 2p orbital of nitrogen than the 3p orbital of phosphorus with the 3d and 4d orbitals of silicon and germanium.

A recent study of the photoelectron spectra of the molecules $(MH_3)_3X$[30] (where X = N, P, As and M = C, Si, Ge) has shown that the formally non-bonding electrons on X are more tightly held in the silicon and germanium compounds than in the carbon analogues for all cases of X. Although the existence of π-bonding in all the silicon and germanium species is a consistent explanation of this data it need not be invoked in all cases. The use of photoelectron spectroscopy to determine molecular energy levels for a series of compounds depends on the assumption that Koopmans' theorem is equally valid for all the members of the series. In this case, for example, it is possible that there is a difference in molecular geometry between the ions $(CH_3)_3P^+$ and $(SiH_3)_3P^+$ which is not found in the neutral molecules and that such a situation does not exist when X is nitrogen.

Equally, the electron diffraction data does not rule out the existence of weak π-bonding in the molecules in which X is phosphorus, and the extent of such bonding necessary to produce the changes in ionisation potential found in the photoelectron spectra is not known. It has also been suggested[31] that the lone pair may be predominantly 's' in character and that

delocalisation may take place involving the d_{z^2} orbitals of silicon where the Z axis is taken as along the (SiP) bond. This would be described as ($\sigma \rightarrow d$) π bonding.

An estimate of the base strength of these phosphines may still, therefore, be the most reliable means of assessing the extent of such bonding.

A study of the reactions of trisilyl phosphine[31] showed no evidence for nucleophilic character and was, therefore, consistent with delocalisation of the 'lone pair' electrons. Further support was provided by the absence of adduct formation with boron trifluoride.[32]

Monosilyl phosphine, however, does form an adduct with diborane exactly analogous to that formed by methyl phosphine.[33] The adduct is only stable at low temperatures, but its existence shows that silyl phosphine is capable of exhibiting donor properties.

The preparation of transition metal complexes of silyl and germyl phosphines described in this work demonstrates further the existence of donor properties of all these phosphines.

6.5 Exchange reactions

Silyl and germyl phosphines will undergo exchange reactions with silyl and germyl halides. The reactions are equilibria and the position of equilibrium in each case depends on the particular halide used. No evidence has been reported

for the existence of mixed silyl and germyl phosphines.

These reactions have been used to prepare isotopically labelled species[34] and also to prepare trigermyl phosphine. This species could not be prepared directly by the same method as trisilyl phosphine[35], and had to be prepared from it by exchange.

Exchange reactions of this kind were, therefore, attempted using silyl and germyl phosphine complexes. The results of these investigations are reported in Chapter 7.

CHAPTER 7

THE PREPARATION AND REACTIONS OF COMPLEXES OF SILYL AND GERMYL PHOSPHINES.

7.1 General methods of preparation

Three general methods were employed in preparing the complexes. These are summarised and discussed below, although the experimental details of each method are given at the end of Section II.

The methods were:

(a) $L + IMo(CO)_5^- \xrightarrow{T.H.F.} LMo(CO)_5 + I^-$

(b) $2L + C_7H_8Mo(CO)_4 \xrightarrow{\text{hydrocarbon}} L_2Mo(CO)_4 + C_7H_8$

(c) $3L + C_7H_8Mo(CO)_3 \xrightarrow{\text{hydrocarbon}} L_3Mo(CO)_3 + C_7H_8$

All the reactions successfully employed go to completion on standing at room temperature. In reaction (a) the iodide formed (N-methyl pyridinium iodide) is insoluble in tetrahydrofuran (T.H.F.) and its precipitation assists in driving the reaction to completion and was a useful guide to the progress of the reaction.

The phosphines (L) were always used in excess of the stoichiometric requirements so that they could be removed, together with the hydrocarbon products of reactions (b) and (c), by pumping on the reaction mixture.

In reaction (a) the two products can easily be separated by decantation before the removal of the solvent.

The preparative reactions were all carried out in vacuo using dry solvents and the products handled either under vacuum or in an inert atmosphere of dry, oxygen-free nitrogen.

The products were characterised by their infrared and nuclear

magnetic resonance spectra which are discussed in chapter 8.

7.2 Preparation of the phosphine complexes

(a) L is trigermyl phosphine

The mono-, bis-, and tris-phosphine complexes were all prepared by the methods already discussed. The proton magnetic resonance spectrum of the tris-complex, however, showed the presence of free trigermyl phosphine in all the samples prepared. It is possible that this complex is unstable even in solution but it may be that its formation is an equilibrium reaction.

(b) L is trisilyl phosphine

Both the mono-, and bis-phosphine complexes were prepared as described. The infrared spectrum of the mono-complex contained a weak sharp band at 1011 $cm.^{-1}$ which was thought to be a (PH) deformation. It seems likely that this was caused by the hydrolysis of a small amount of the product under the conditions used to obtain an infrared spectrum. No evidence was found for a compound containing (PH) in the proton magnetic resonance spectrum.

(c) L is silyl phosphine or trimethyl silyl phosphine

Bis-substituted complexes could be prepared with both ligands but attempts to prepare mono-complexes by the method given in Section 7.1 led to the formation of the species $PH_3Mo(CO)_5$ only. This product was identified by its infrared and proton magnetic resonance spectra.[9]

(d) L is germyl phosphine

Neither the mono- nor the bis-phosphine complex could be prepared. In both cases germyl phosphine disproportionated and several products were formed.

In the attempt to prepare the mono-phosphine complex the proton magnetic resonance spectrum detected all the possible disproportionation products as ligands:

$(GeH_3)_3P$, $(GeH_3)_2PH$, GeH_3PH_2, PH_3,

although phosphine and trigermyl phosphine predominated.

No attempt was made to separate these products and no evidence was obtained whether the disproportionation of the phosphine takes place during or after coordination.

(e) Mixed phosphine complexes

An attempt was made to prepare a bis-substituted complex containing two different phosphine ligands. The preparative method for the bis-complex was used but an equimolar mixture of the two phosphines was added - phosphine and silyl phosphine. The relative concentrations of the three products measured from a proton magnetic resonance spectrum were approximately:

bis-silyl phosphine complex	1
silyl phosphine/phosphine complex	2
bis phosphine complex[9]	1

The rates of substitution for the two phosphines are, therefore, very similar and this suggests that there is little

difference in donor strength between silyl phosphine and phosphine.

No attempt was made to separate the substances formed in this experiment but, as the silyl peaks in the proton spectrum of the bis-silyl phosphine complex overlapped with those of the mixed complex, some means of separation was required.

The reaction was, therefore, carried out using a ratio of 10 parts phosphine to 1 part of silyl phosphine. Under these conditions the amount of bis-silyl phosphine complex formed should have been about 1%. Since its p.m.r. spectrum contains many lines none of this product was detected. This product mixture allowed observation of the silyl and (PH_2) parts of the spectrum of the mixed complex (Chapter 8).

The reaction was repeated with the phosphine concentrations reversed to observe the PH_3 part of the spectrum. This was not necessary, however, when the spectrum was recorded at 220 MHz. The spectrum of the mixed complex could then be measured in the presence of the large excess of the bis-phosphine complex as the peaks due to the two species did not overlap in any region of the spectrum.

A similar experiment was tried using silyl phosphine and trifluorophosphine in equimolar quantities. The proton spectrum of the products was very complicated and could not be attributed to the expected products. Silyl phosphine and trifluorophosphine to not react under the conditions used and, therefore, this reaction was unexplained.

7.3 Exchange reactions

Since no monogermyl phosphine complexes could be prepared directly (Section 7.2) exchange of the silyl groups in the coordinated silyl phosphines was investigated.

Bis-germyl phosphine molybdenum tetracarbonyl was prepared by reaction of germyl fluoride on the silyl analogue in solution in benzene at room temperature. Exchange was complete and the product was identified by its infrared and p.m.r. spectra (Chapter 8). The same product was also obtained from bis-trimethyl silyl phosphine molybdenum tetracarbonyl by exchange with germyl fluoride.

The mixed germyl phosphine/ phosphine complex was similarly prepared from the silyl species. This reaction was carried out in the presence of the bis-phosphine complex from which the silyl compound has not been separated (see Section 7.2) and the product was identified by its p.m.r. spectrum only. The carbonyl region of the infrared of the product mixture is swamped by the bis-phosphine complex but the vibrations of the germyl phosphine ligand were observed. The pattern of these vibrations is extremely similar to that of the bis-germyl phosphine complex and thus identification of the product as the mixed complex from infrared was not possible.

Since no evidence was found for the disproportionation of the ligands it seems likely that the disproportionation of germyl phosphine reported in Section 7.2 took place during the coordination of the ligand.

7.4 Discussion

Previous evidence for the absence of nucleophilic character in trisilyl phosphine[31] is contradicted by the existence of the phosphine complexes described. All the phosphines studied exhibit donor properties, although the only measure of the ease of donation is the comparison between silyl phosphine and phosphine which was based, however, only on kinetic evidence. All the complexes, however, are stable at room temperature (except perhaps tris-trigermyl phosphine molybdenum tricarbonyl) and their spectra showed no decomposition over several days.

In view of the other complexes prepared, the failure to prepare mono-complexes of silyl, germyl, or trimethyl silyl phosphine suggests that a non-ionic starting material may have been more successful.

The behaviour of germyl phosphine was unexpected when compared with that of difluorophosphine.[9] This compound is unstable to disproportionation and at room temperature the reaction below takes place slowly:

$$3\ PF_2H \longrightarrow 2\ PF_3 + PH_3$$

However, under similar conditions to the attempted preparation of bis-germyl phosphine molybdenum tetracarbonyl, this phosphine reacts to form only one product - $(PF_2H)_2\ Mo(CO)_4$.

As was found in the preparation of trigermyl phosphine,[35] germyl analogues of silyl compounds had to be prepared from them

by exchange. The exchange used to prepare trigermyl phosphine was interesting in that no mixed silyl and germyl phosphines were observed during the reaction. It seems that these species are either very reactive or unstable to disproportionation. Further investigation of exchange in phosphine complexes could lead to the formation of these mixed phosphines coordinated to molybdenum and stabilised as difluorophosphine.

A preliminary experiment did show that trigermyl phosphine was displaced from its mono-complex by excess trifluorophosphine. $PF_3Mo(CO)_5$ was identified from its vapour phase infrared spectrum[36]. The existence of the free phosphine as the other product was not shown. It is possible, however, that mixed coordinated phosphines, if formed, could be displaced by trifluorophosphine and their subsequent behaviour studied.

CHAPTER 8

SPECTROSCOPIC PROPERTIES OF THE PHOSPHINE COMPLEXES

8.1 Infra-red spectra

All the infrared spectra were recorded in solution and their assignments were made assuming them to be produced by free molecules of the species' studied. In all cases the complexes were assumed to be octahedral.

Many reviews have been published of the spectra of substituted carbonyl complexes[25-7] and it is generally accepted that satisfactory assignment of the carbonyl stretching vibrations may yield the overall symmetry of the molecule.

For bis andtris substituted carbonyl complexes more than one stereochemistry is possible and the arrangement of the carbonyl groups affects the carbonyl stretching region of the spectrum. The complexity of the molecules studied does not allow complete assignment of the observed bands to the normal vibrational modes of the molecules. Thus information on the stereochemistry of the molecules was derived only from the carbonyl stretching region of the spectra.

Tentative assignments have been made, however, for many other bands by correlation, by comparison with other similar molecules,[9] and by comparison with the fundamental vibrational frequencies of the free phosphines.[20,21,35].

The observed spectra of the complexes prepared are summarised in tables 8.1 to 8.3. Table 8.4 shows the number and symmetry class of infrared bands in the carbonyl stretching region (ca. 1800 to

Assignment	[a] $(GeH_3)_3$ P $Mo(CO)_5$	[b] $[(GeH_3)_3 P]_2$ $Mo(CO)_4$	[a] $[(GeH_3)_3 P]_3$ $Mo(CO)_3$
ν(GeH)	2062	2084 m	2075
		2066 m	2065
ν(CO)	2079 w (A_1)	2022.5 s (A_1'')	1945
	1955 vs (E)	1952.0 s (A_1')	1858
	1927 w (A_1)	~1922 vs (B_2)	
	1986 vw (B)	1889.5 s (B_1)	
δ (GeH)	864 w	865.0 w	865
	817 w	824.0 m	813
	795 w		788
	784 m	813.0 m	781
	775 m	762.5 s	
	766 m		
δ (CO)	615 vw	612.5 w	
	604 w	580.0 w	
	588 w		
ν(GeP)	371 w	~379,358 vw	

a. Solution in cyclopentane b. Solution in n-pentane

TABLE 8.1 Infra-red spectra of trigermyl phosphine complexes

Assignment	[a] $(SiH_3)_3$ P $Mo(CO)_5$	[b] $(SiH_3PH_2)_2$ $Mo(CO)_4$
ν(PH)	-	2327
ν(SiH)	2172	2169
ν(CO)	2081 w (A_1)	2028 m (A_1'')
	1958 vs (E)	1940 s (A_1')
	1929 w (A_1)	1917 vs (B_2)
	1986 vw (B)	1897 vw
δ(PH)	(1011 w)	1062
		1008
δ(SiH)	962 w	941
	943 w	926
		908
		881
ρ(SiH_3)		743
		(788 vw)
δ(CO) and ν(SiP)	618 vw	612
	606 w	588
	590 w	549
	385 vw	439
	374 vw	403
		382

a. Solution in cyclopentane

b. Solution in benzene

TABLE 8.2 - Infra-red spectra of silyl phosphine complexes.

Assignment	[a] $(GeH_3PH_2)_2 Mo(CO)_4$
ν(PH)	2300 w
ν(GeH)	2070-2100 m
ν(CO)	2023 s (A_1'')
	1912 vs (A_1' and B_2)
	1891 vs (B_1)
δ(PH)	1068 m
	1009 w
δ(GeH)	879 m
	869 m
	804 m
	773 w
ρ(GeH_3)	728 s
	735 sh
δ(CO)	609 m
	584 s
	409 w
ν(GeP)	383 m

a. Solution in benzene.

TABLE 8.3 - Infra-red spectra of germyl phosphine complexes.

2000 $cm.^{-1}$) of the spectrum expected for each possible stereochemistry of the molecules.[37] It is based on the selection rules governing allowed vibrational transitions.

In the spectrum of species' $LMo(CO)_5$ one extra weak band (B_1) is usually observed in the cases in which L is a phosphine. This arises from a lowering of the molecular symmetry to C_s (from C_{4v}) by the three-fold symmetry of the ligand.

The preparation of bis-phosphine complexes from the same starting compound as that used in this study always led to cis complexes[9] by retention of the configuration of the starting compound. All the spectra of the bis-complexes reported in tables 8.1 to 8.3 except bis (monogermyl phosphine) molybdenum tetracarbonyl contained four carbonyl stretching bands in agreement with a cis-configuration of C_{2v} symmetry. The spectrum of the germyl compound was recorded in solution in benzene (unlike the other complexes) and this solvent broadens the carbonyl bands. It seems likely that this complex is also cis and that the fourth band is masked by the solvent-broadening of the other three.

The starting compound used to prepare the tris-complex has also led to the formation of cis-phosphine complexes[9,14]. The spectrum of the complex prepared is consistent with a cis complex although the observation of only two bands is not definitive.

8.2 Proton magnetic resonance spectra

The nuclear magnetic resonance data obtained from the proton

Formula	Stereochemistry	Symmetry	Active vibrational modes
$Mo(CO)_5 L$	-	C_{4v}	$2A_1 + E$
$Mo(CO)_4L_2$	cis	C_{2v}	$2A_1 + B_1 + B_2$
	trans	D_{4h}	E_u
$Mo(CO)_3L_3$	cis	C_{3v}	$A_1 + E$
	trans	C_{2v}	$2A_1 + B$

TABLE 8.4 - Infra-red active vibrations for carbonyl complexes.

Compound	$\tau(H_3)$ in τ	$^2J(PH)$	Solvent
$(GeH_3)_3 P$	5.96	16.1	Cyclopentane
$(GeH_3)_3 PMo(CO)_5$	5.62	16.9	do.
$[(GeH_3)_3P]_2 Mo(CO)_4$		16.5	n-pentane
$[(GeH_3)_3P]_3 Mo(CO)_3$	5.63	ca.15.6	cyclopentane
$(SiH_3)_3 P$	6.08	17.1	do.
$(SiH_3)_3 PMo(CO)_5)$	5.83	14.9	do.

TABLE 8.5 - Proton magnetic resonance spectra of trisilyl and trigermyl phosphine complexes.

spectra of the complexes prepared is given in tables 8.5 and 8.6. Tables 8.7 to 8.9 contain similar data obtained for other phosphine complexes, and table 8.10 gives data on the free phosphines.

In the following discussion the complexes are grouped dependent on the number of phosphine ligands present in the molecule.

(a) Mono-substituted pentacarbonyls $[LMo(CO)_5]$

Proton spectra were obtained for the species in which $L = (SiH_3)_3P$ and $(GeH_3)_3P$. In both cases the spectra consist of two sharp lines and therefore $\delta(H_3)$ and $^2J(PH_3)$ could be measured directly. The resonances of both complexes are to low field of those of the free ligand indicating stronger shielding of the protons in the complex. The magnitude of $^2J(PH_3)$ is very little affected by coordination and, in fact, its change was in opposite directions in the two species:-

For $(SiH_3)_3P$ $\quad J(\text{complex}) < J(\text{free phosphine})$,

and for $(GeH_3)_3P$ $\quad J(\text{complex}) > J(\text{free phosphine})$.

It is very difficult to interpret such changes in coupling constants in terms of electronic or geometric changes in the phosphine on coordination, as the magnitudes of coupling constants depend not only on the ground states of the molecules but also on excited states and their mixing with the ground state. In view of the very smallchange which takes place in $^2J(PH_3)$ on coordination in all the complexes studied, no attempt has been made to interpret it.

Compcund	$\delta(H_3)$	$\delta(H_2)$	$\delta(PH_3)$	$^1J(PH_2)$	$^1J(PH_3)$	$^2J(PH_3)$	$^3J(PH_2)$	$^3J(PH_3)$	$^3J(HH)$	$^2J(PP^1)$	Solvent
SiH_3PH_2	6.39	8.45	-	184.5	-	16.4	-	-	5.2	-	Benzene
GeH_3PH_2	6.50	8.76	-	180.2	-	15.2	-	-	4.8	-	do.
$(SiH_3PH_2)_2Mo(CO)_4$	6.38	7.89	-	301	-	14.9	9	-	4.5	27	do.
$(GeH_3PH_2)_2Mo(CO)_4$	6.34	7.73	-	(299.7)	-	17.0	(9)	-	4.3	n.o.	do.
$SiH_3PH_2 \backslash PH_3 / Mo(CO)_4$	6.36	7.86	7.20	310	322	15.0	9.8	10.0	4.8	Small 6	do.
$GeH_3PH_2 \backslash PH_3 / Mo(CO)_4$	6.28		7.20		301	16.2		10.5	4.3	Small	do.

TABLE 8.6 ^1H - spectra of silyl and germyl phosphine complexes

Compound	δ(H) in τ	J(PH) in Hz	J(PH') in Hz	J(PP') in Hz	Solvent	Ref.
PH_3	8.45	186.6	-	-	Benzene	9
$PH_3Mo(CO)_5$	7.55	326	-	-	Benzene	49
	6.22	332	-		Acetone	9
$(PH_3)_2Mo(CO)_4$	7.61	314	10.75	-24.8	Benzene	49
	6.30	318.8	10.2	-20.4	Acetone	49
$(PH_3)_3Mo(CO)_3$	6.46	307	10.2	-	Acetone	9
	6.41	313	10	-	Dioxan	49

Table 8.7 - ^1H n.m.r. of phosphine complexes.

Compound	δ(H) in τ	δ(H') in τ	J(PH) in Hz	J(PH') in Hz	J(HH') in Hz	Solvent	Ref.
$CH_3'PH_2$	7.5	9.0	187	3.99	7.98	None	52
$CH_3'PH_2Mo(CO)_5$	5.61	8.45	328.1	-8.8	7.0	Acetone	9
	-	-	353.06	-6.95	8.34	None	9
$(CH_3'PH_2)_2Mo(CO)_4$	5.82	8.57				Acetone	9
$(CH_3'PH_2)_3Mo(CO)_3$	5.72	8.50				Acetone	9

Table 8.8 - ^{1}H-n.m.r. of methyl phosphine complexes.

Compound	δ(H) in τ	δ(H') in τ	J(PH) in Hz	J(PH') in Hz	Solvent	Ref.
$Me_3'SiPH_2$	8.77	9.63	180.8	6.8	Benzene	50
$(Me_3'SiPH_2)_2Mo(CO)_4$	8.76	9.57	292	6.54	Benzene	9

Table 8.9 - ^{1}H-n.m.r. of trimethyl silyl phosphine and a complex.

Compound	δ(H) in τ	δ(H') in τ	J(PH) in Hz	J(PH') in Hz	J(HH') in Hz	Solvent	Ref.
PH_3	8.45	-	186.6	-	-	Benzene	9
$CH_3^{\bullet}PH_2$	7.5	9.0	187	3.99	7.98	None	52
$SiH_3^{\bullet}PH_2$	8.69	6.27	180	16.2	5.1	None	34,53
*	+5.83	+3.41	185	16.4	5.3	Chloroform	54
	8.45	6.39	184.5	16.4	5.2	Benzene	-
$(SiH_3')_2PH$	9.60	6.30	184.0	17.5	5.1	None	55
*	+6.60	+3.38	185.8	17.0	5.1	Chloroform	54
$(SiH_3')_3P$	-	6.08	-	17.1	-	Cyclopentane	-
$GeH_3^{\bullet}PH_2$	8.59	6.33	180	15.3	4.8	None	34,53
	8.76	6.50	180.2	15.2	4.8	Benzene	-
$(GeH_3')_2PH$	9.22	6.12	171	15.9	4.7	T.M.S.	56
	-	6.12	-	15.7	4.7	Cyclopentane	-
$(GeH_3')_3P$	-	5.96	-	16.1	-	Cyclopentane	-

* These chemical shifts are given in p.p.m. to high field of the solvent used (Chloroform).

Table 8.10 - ^{1}H-n.m.r. of free phosphines.

(b) Bis-substituted tetracarbonyls $[L_2Mo(CO)_4]$

The spectra of all these species are second order because of the presence of the two phosphorus atoms of the same chemical shift, and the fact that $J(PP^1) \neq 0$.

Since the spin systems are more complex the parameters were more difficult to obtain from the spectra. Different methods were used to obtain the parameters from the spectra of species of different spin systems and thus the analyses of these spectra are discussed separately.

(i) $(SiH_3PH_2)_2Mo(CO)_4$

100MHz spectrum

At this frequency the spectrum obtained was very complicated and its overall appearance is shown in figure 8.1(a). The region labelled "A/C" is more complicated than the rest of the spectrum and in the regions "B" and "D" the observed lines are equally spaced with the same interval in the two regions. It seemed likely that this regular spacing was due to coupling between the protons on silicon and those on phosphorus within the same phosphine ligand and that the lines observed in legion B were the high-field half of the SiH resonance. It was not possible to determine any of the other coupling constants or even the chemical shifts directly from the main spectrum.

The ^{29}Si satellites were identified, however, and they appear to be first order. From the satellite spectrum (shown in figure

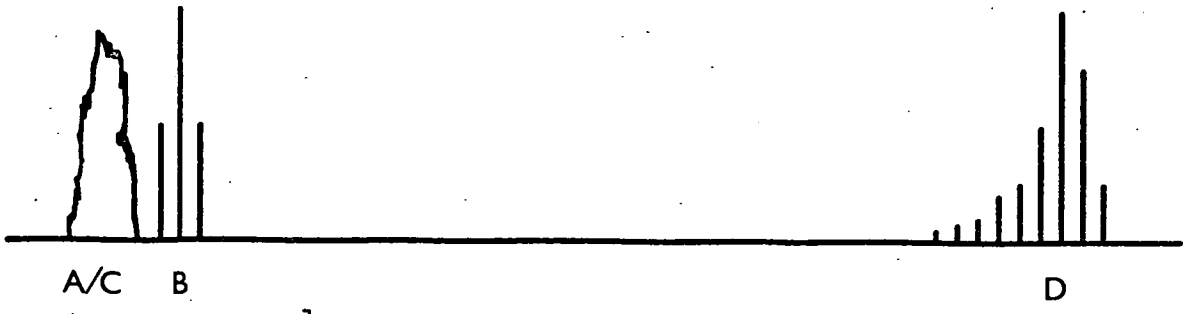

Figure 8.1(a) - ^{1}H-spectrum of $(SiH_3PH_2)_2Mo(CO)_4$ at 100 MHz.

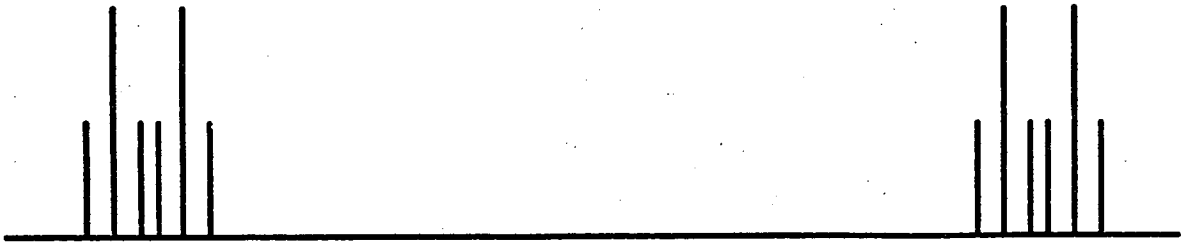

Figure 8.1(b) - ^{29}Si satellite spectrum of figure 8.1(a).

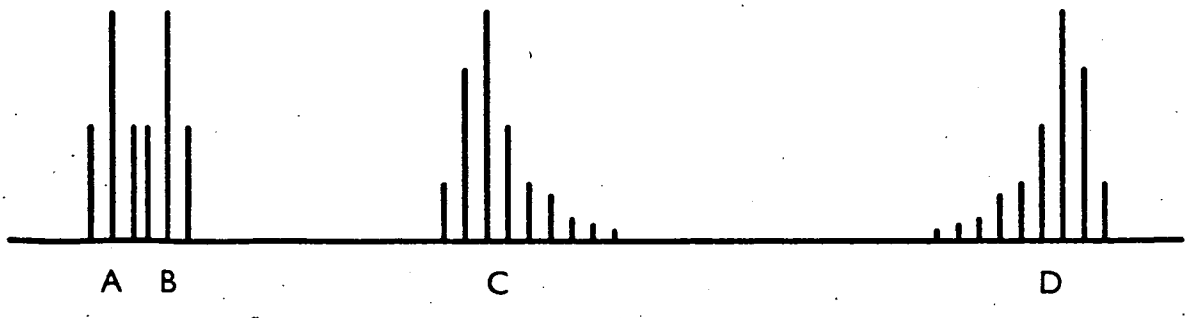

Figure 8.2 - ^{1}H-spectrum of $(SiH_3PH_2)_2Mo(CO)_4$ at 220 MHz.

8.1(b)) it was thus possible to measure $\delta(SiH_3)$, $^2J(PH_3)$, $^3J(HPSiH)$ and $^1J(^{29}SiH)$ directly. These values were used to simulate the Si<u>H</u> part of the main spectrum, and the calculation showed that the high-field half of the Si<u>H</u> resonance is first order in the observed spectrum (B in figure 8.1(a)) and the complexity of the region A/C is therefore due to the proximity of the low-field half of the P<u>H</u> resonance (C) and the low-field half of the Si<u>H</u> resonance (A).

220MHz spectrum

This spectrum is very much less complicated as a consequence of the greater chemical shift difference between the low-field Si<u>H</u> and low-field P<u>H</u> resonances at this operating frequency (see figure 8.2). The silyl resonance A,B appears first order and several parameters could be measured directly - $\delta(SiH_3)$, $^2J(PH_3)$, $^3J(HSiPH)$. The magnitudes of these are in good agreement with those obtained from the ^{29}Si satellite spectrum described in the previous section. The interaction of the low-field half of the P<u>H</u> resonance and the low-field half of the Si<u>H</u> resonance at 100MHz was taken to show that $^2J(PH_3)$ and $^1J(PH_2)$ are of the same sign. This result was confirmed at 220MHz - irradiation at a frequency corresponding to the high-field half of the P<u>H</u> resonance (D in figure 8.2) was found to collapse the (HSiPH) coupling in the high-field half of the Si<u>H</u> resonance (B). Similarly, irradiation at the frequency C was found to collapse the splitting in A.

The same decoupling experiment was carried out on silyl phosphine itself and again $^2J(PSiH)$ and $^1J(PH)$ were found to have

the same sign. Unfortunately, no ^{29}Si satellites of the (PH) resonance in either the free or coordinated phosphine could be detected. Observation of these would have allowed the signs of the coupling constants to be related to $^{1}J(^{29}SiH)$ in each case by double irradiation. Thus comparison would have been possible between the free and coordinated phosphine. It seems likely, however, that $^{2}J(PSiH)$ and $^{1}J(PH)$ do not change sign on coordination to molybdenum, and thus the change in $^{2}J(PSiH)$ is very small.

The appearance of the spectrum is shown in figure 8.2 and it can be seen that the phosphine resonance (C and D) is still complex although symmetrical. The resonance 'C' (of figure 8.2) is shown in figure 8.3 (below). This spin system is bound to produce a second-order spectrum because the silyl and the $-PH_2$ groups are chemically but not magnetically equivalent. In Haigh's notation[38] the spin system is denoted $\lceil AM_3X_2\rfloor_2$; in the following discussion nuclei which are chemically but not magnetically equivalent are distinguished by a prime as in the system of notation of Corio.[39]

The first order appearance of the silyl resonance was assumed to be a consequence of the fact that $^{4}J(PH_3)$ is negligibly small and therefore that the spectrum is not "deceptively simple". The corresponding parameter for the phosphine part of the resonance - $^{3}J(PH_2)$ - would be expected to be of the order of 10Hz and a second-order treatment was thus required for its analysis, based on the full spin system of the nuclei - $\lceil AM_3X_2\rfloor_2$, where A = P, $M_3 = SiH_3$, and $X_2 = PH_2$.

It was assumed throughout the assignment of the spectrum

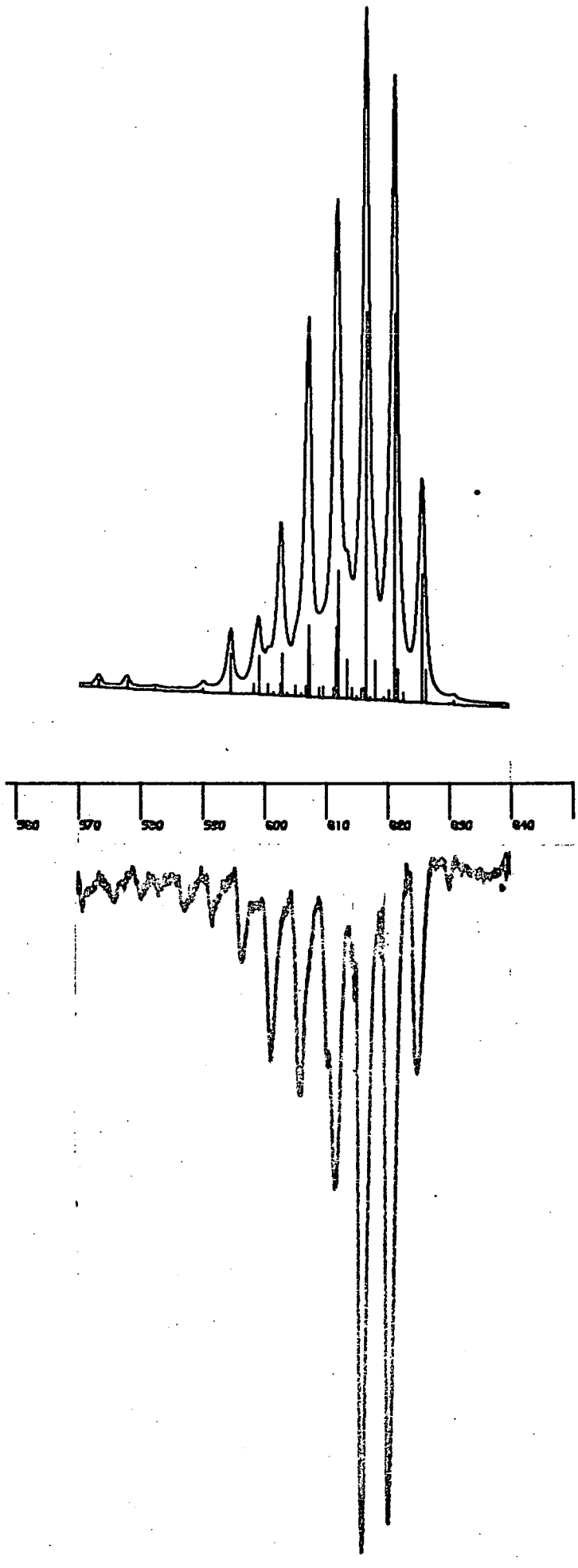

Figure 8.3 - Calculated and experimental spectra of $(SiH_3PH_2)_2Mo(CO)_4$.

observed that $J_{XX'}$ and $J_{MM'}$ are both effectively zero; this is a condition of the validity of the equations employed in the analysis. The final agreement between observed and calculated spectra is shown in figure 8.3, and is good evidence for the validity of these assumptions.

The spin system on which the equations used in this analysis were originally based is $[AX]_2$, whose solution is well known[40]. It is characterised by six parameters - ν_A, ν_X, J_{AX}, $J_{AX'}$, $J_{AA'}$, $J_{XX'}$; $J_{AX} = J_{A'X'}$ and $J_{AX'} = J_{A'X}$ because of the symmetry, and there are therefore sixteen symmetrised spin functions. The transition energies for the X spectrum can thus be calculated with their relative intensities, and are given in table 8.11 in terms of the above parameters and the parameters K, L, M, N, which are defined in table 8.11. This solution depends upon the assumption that:

$$J_{AX}, J_{AX'} \ll \nu_o \delta_{AX}$$

Mixing then only occurs between two pairs of spin states.

The 'X' spectrum in this case is identical to the 'A' spectrum and each consists of 12 lines. The overall picture of this is shown in figure 8.4 for the situation:

$$J_{AX} \gg J_{AX'} > 0 \text{ and } J_{XX'} \gg J_{AA'} > 0$$

The degenerate pairs of transitions 1, 2 and 3,4 have half the total intensity of the spectrum.

The 'X' part of an $[AX]_2$ spectrum will always contain:

(a) Two strong absorptions separated by 'N' and centred on

Spin function	A	X	Diagonal element($-\frac{1}{4}K$)
ψ_1	$\alpha\alpha$	$\alpha\alpha$	$\nu_A + \nu_B + \frac{1}{2}N$
ψ_2	$2^{-\frac{1}{2}}(\alpha\beta+\beta\alpha)$	$\alpha\alpha$	ν_B
ψ_3	$\alpha\alpha$	$2^{-\frac{1}{2}}(\alpha\beta+\beta\alpha)$	ν_A
ψ_4	$\beta\beta$	$\alpha\alpha$	$-\nu_A + \nu_B - \frac{1}{2}N$
ψ_5	$\alpha\alpha$	$\beta\beta$	$\nu_A - \nu_B - \frac{1}{2}N$
ψ_6	$2^{-\frac{1}{2}}(\alpha\beta-\beta\alpha)$	$2^{-\frac{1}{2}}(\alpha\beta-\beta\alpha)$	$-K$
ψ_7	$2^{-\frac{1}{2}}(\alpha\beta+\beta\alpha)$	$2^{-\frac{1}{2}}(\alpha\beta+\beta\alpha)$	0
ψ_8	$2^{-\frac{1}{2}}(\alpha\beta+\beta\alpha)$	$\beta\beta$	$-\nu_B$
ψ_9	$\beta\beta$	$2^{-\frac{1}{2}}(\alpha\beta+\beta\alpha)$	$-\nu_B$
ψ_{10}	$\beta\beta$	$\beta\beta$	$-\nu_A-\nu_B+\frac{1}{2}N$
ψ_{11}	$2^{-\frac{1}{2}}(\alpha\beta-\beta\alpha)$	$\alpha\alpha$	$\nu_B-\frac{1}{2}(K+M)$
ψ_{12}	$\alpha\alpha$	$2^{-\frac{1}{2}}(\alpha\beta-\beta\alpha)$	$\nu_A-\frac{1}{2}(K-M)$
ψ_{13}	$2^{-\frac{1}{2}}(\alpha\beta+\beta\alpha)$	$2^{-\frac{1}{2}}(\alpha\beta-\beta\alpha)$	$-\frac{1}{2}(K-M)$
ψ_{14}	$2^{-\frac{1}{2}}(\alpha\beta-\beta\alpha)$	$2^{-\frac{1}{2}}(\alpha\beta+\beta\alpha)$	$-\frac{1}{2}(K+M)$
ψ_{15}	$2^{-\frac{1}{2}}(\alpha\beta-\beta\alpha)$	$\beta\beta$	$-\nu_B-\frac{1}{2}(K+M)$
ψ_{16}	$\beta\beta$	$2^{-\frac{1}{2}}(\alpha\beta-\beta\alpha)$	$-\nu_A-\frac{1}{2}(K-M)$

where $K = J_{AA'} + J_{XX'}$

$L = J_{AX} - J_{AX'}$

$M = J_{AA'} - J_{XX'}$

$N = J_{AX} + J_{AX'}$

Table 8.11a- States for, the spin system $(AX)_2$.

Transition		Energy rel. to ν_A	Rel. intensity
$\psi_2 \rightarrow \psi_1$	1	$\frac{1}{2}N$	2
$\psi_4 \rightarrow \psi_2$	2	$\frac{1}{2}N$	
$\psi_{10} \rightarrow \psi_8$	3	$-\frac{1}{2}N$	2
$\psi_8 \rightarrow \psi_5$	4	$-\frac{1}{2}N$	
$\psi_6 \rightarrow \psi_3$	5	$\frac{1}{2}K+\frac{1}{2}(K^2+L^2)^{\frac{1}{2}}$	$\sin^2\theta_s$
$\psi_9 \rightarrow \psi_7$	6	$-\frac{1}{2}K+\frac{1}{2}(K^2+L^2)^{\frac{1}{2}}$	$\cos^2\theta_s$
$\psi_7 \rightarrow \psi_3$	7	$\frac{1}{2}K-\frac{1}{2}(K^2+L^2)^{\frac{1}{2}}$	$\cos^2\theta_s$
$\psi_9 \rightarrow \psi_6$	8	$-\frac{1}{2}K-\frac{1}{2}(K^2+L^2)^{\frac{1}{2}}$	$\sin^2\theta_s$
$\psi_{14} \rightarrow \psi_{12}$	9	$\frac{1}{2}M+\frac{1}{2}(M^2+L^2)^{\frac{1}{2}}$	$\sin^2\theta_a$
$\psi_{16} \rightarrow \psi_{13}$	10	$-\frac{1}{2}M+\frac{1}{2}(M^2+L^2)^{\frac{1}{2}}$	$\cos^2\theta_a$
$\psi_{13} \rightarrow \psi_{12}$	11	$\frac{1}{2}M-\frac{1}{2}(M^2+L^2)^{\frac{1}{2}}$	$\cos^2\theta_a$
$\psi_{16} \rightarrow \psi_{14}$	12	$-\frac{1}{2}M-\frac{1}{2}(M^2+L^2)^{\frac{1}{2}}$	$\sin^2\theta_a$

where $\frac{\cos 2\theta_s}{\sin 2\theta_s / 1} = \frac{K}{L/(K^2+L^2)^{\frac{1}{2}}}$ and $\frac{\cos 2\theta_a}{\sin 2\theta_a / 1} = \frac{M}{L/(M^2+L^2)^{\frac{1}{2}}}$

Table 8.11b- Allowed transitions for $(AX)_2$.

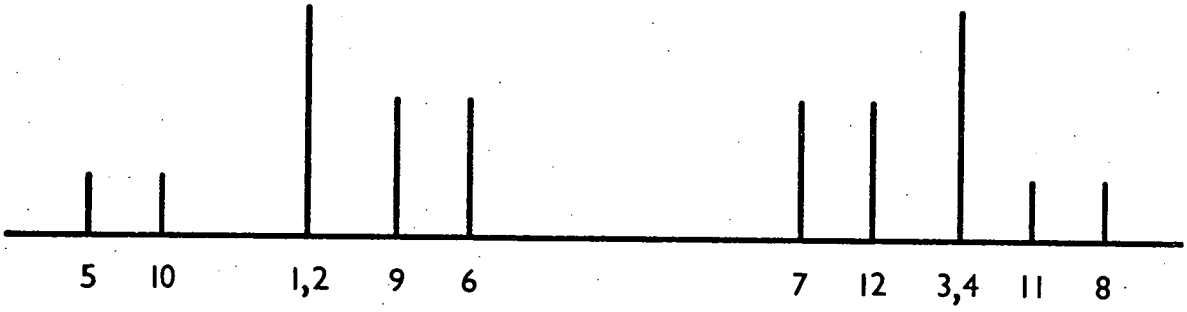

Figure 8.4 - 'X' spectrum for the spin system $\lceil AX \rfloor_2$.

the resonance frequency of X - $\nu_o \delta_x$.

(b) Two pairs of symmetrical quartets centred on the resonance frequency of X with the inner lines of each quartet always more intense.

Observation of these features of the spectrum allows direct measurement of L and N, K and M separately but distinction between K and M cannot be made.

Analyses of the spin systems $[AX_2]_2$[41] and $[AX_3]_2$[42,43] have also been achieved without recourse to computers and many of the formulae derived for these systems apply to the general spin system $[AX_n]_2$. Harris[44] has published general equations for this spin system which apply to the 'X' spectrum when $J_{XX'} = 0$. The main feature of these spectra is the intense doublet of separation 'N', symmetrical about ν_x, corresponding to the 1, 2 and 3,4 transitions in the $[AX]_2$ spectrum. In all cases this doublet comprises half the total intensity since it originates from all transitions from half of the A and A' spin states. All other allowed transition energies of the 'X' nuclei are, in fact, given by one equation:

Eq. (1) $$\epsilon_X - \epsilon_{X-1} = \pm \tfrac{1}{2}((\mathcal{N}^2L^2 + J_{AA'}^2)^{\frac{1}{2}} \pm ((\mathcal{N} - 1)^2L^2 + J_{AA'}^2)^{\frac{1}{2}})$$

These energies are relative to ν_X and $\mathcal{N}$ can take any integral value between 1 and 'n' inclusive. This part of the spectrum is also symmetrical about ν_x and for each value of $\mathcal{N}$ there are two pairs of lines - an "inner" and "outer" pair. The "inner" pair is given when the signs are opposite and the "outer" pair when

the signs are the same. The relative intensities of these pairs of lines depend only on the relative magnitudes of L and $J_{AA'}$ - the "inner" pairs for each value of χ will always be more intense than the "outer" pairs.

These general equations have been used as the basis for calculation of a similar series of equations for the spin system $\lfloor AMX_n \rfloor_2$[45] in which it was assumed that $J_{XX'} = 0$ and $J_{MM'} = 0$. The addition of the 'M' nucleus to the $\lfloor AX_n \rfloor_2$ spin system splits the doublet of separation N (now N_{AX}) in the 'X' spectrum into two doublets of separation $N_{AX} \pm N_{MX}$ with $\frac{1}{4}$ the total intensity of the 'X' spectrum and a series of doublets, with another $\frac{1}{4}$ of the total intensity, whose separations are given by:

Eq. (2) $$N_{AX} \pm (\chi^2 L_{MX}^2 + J_{MM'}^2)^{\frac{1}{2}} \pm ((\chi - 1)^2 L_{MX}^2 + J_{MM'}^2)^{\frac{1}{2}}$$

The remaining series of doublets from the 'X' spectrum of $\lfloor AX_n \rfloor_2$ given in Eq. (1) is split into two series' of doublets whose separations are given in the equations:

Eq. (3) $$N_{MX} \pm (\chi^2 L_{AX}^2 + J_{AA'}^2)^{\frac{1}{2}} \pm ((\chi - 1)^2 L_{AX}^2 + J_{AA'}^2)^{\frac{1}{2}}$$

and

Eq. (4) $$L_{MX} \pm ((L_{AM} + \chi L_{AX})^2 + J_{AA'}^2)^{\frac{1}{2}} \pm ((L_{AM} + (\chi - 1) L_{AX})^2 + J_{AA'}^2)^{\frac{1}{2}}$$

where

$$N_{xy} = /J_{xy} + J_{xy'}/$$

and

$$L_{xy} = /J_{xy} - J_{xy'}/$$

and, x and y may be A, M, or X.

The overallchange in the 'X' spectrum on going from $[AX_n]_2$ to $[AMX_n]_2$ is shown in table 8.12.

These calculations have now been extended to the spin system $[AM_nX_y]_2$ [46] in which again it was assumed that $J_{MM'} = 0$ and $J_{XX'} = 0$. In this case the 'N' doublet of Harris is split into a series of doublets of separation:

Eq. (5) $N_{AX} + 2kJ_{MX} + 2lJ_{MX'}$

in which k and l can take values from $\frac{n}{2}$ to $-\frac{n}{2}$.

The total intensity of these lines is half the total intensity. Thus the 'n' M nuclei were found to cause a first order splitting - the line positions being dependent on the magnitudes of J_{MX} and $J_{MX'}$. The relative intensities can also be found from a first order analysis of the splitting. The remaining half of the intensity of the 'X' spectrum goes into a series of doublets whose separations are given by:

Eq. (6) $2kJ_{MX} + 2lJ_{MX'} \pm (((k-1)L_{AM} + \chi L_{AX})^2 + J_{AA'}^2)^{\frac{1}{2}}$

$\pm (((k-1)L_{AM} + (\chi - 1)L_{AX})^2 + J_{AA'}^2)^{\frac{1}{2}}$

in which k and l can take any value from $\frac{n}{2}$ to $-n/2$ and χ can take values from y to (1-y). This, therefore, gives several series' of doublets dependent on (k - l) and χ which are all split in a first order sense by the 'n' M nuclei. The relative intensities are again in agreement with this interpretation.

Analysis of the phosphine resonance of bis(monosilyl phosphine) molybdenum tetracarbonyl was thus possible using these equations.

$[AX_n]_2$	$[AMX_n]_2$
Main doublet of separation N ($\frac{1}{2}$ total intensity)	Main multiplet of separation $N_{AX} \pm N_{MX}$ ($\frac{1}{4}$ total intensity)
	Series of lines in χ given by Eq.(2) ($\frac{1}{4}$ total intensity)
Inner/Outer series of doublets given by Eq. (1) ($\frac{1}{2}$ total intensity)	Inner/outer series in χ given by Eq.(3) ($\frac{1}{4}$ total intensity)
	Further series in χ given in Eq.(4) ($\frac{1}{4}$ total intensity)

TABLE 8.12 'X' spectrum of $(AMX_n)_2$ spin system.

The spectrum was analysed and could be satisfactorily assigned assuming $J_{MX'} = J_{AM'} = 0$ although this simplification was not incorporated into the equations. Use was made of computing facilities in the determination of the parameters from this part of the observed spectrum. The equations given above for the $[AM_nX_y]_2$ spin system were written as a subroutine in Edinburgh Fortran[47] used in a line shape program[48] and a spectrum for any given parameters could either be calculated or plotted. A flow diagram of the program as it was used is shown in figure 8.5. The main program was designed to refine the parameters supplied to obtain the least-squares best fit to the experimental spectrum but success in the passing over of information from the subroutine (HOBBIT) to the main program was never achieved. Variation of the input parameters for the calculated spectrum had thus to be performed manually.

From this assignment the magnitudes of several parameters were found:

$$^1J(PH_2),\ ^3J(PH_2),\ ^2J(PP'),\ ^3J(HH).$$

$\delta(PH_2)$ could be measured directly since the resonance is symmetrical; $^3J(HH)$ agreed in magnitude with the value found from the silyl resonance. The relative signs of $^1J(PH_2)$ and $^3J(PH_2^1)$ were found but no information was obtained about the sign of $^2J(PP')$ as this term always appeared squared in the equations.

The equations which were used in the analysis of the spectrum are based on several assumptions. They were employed, however,

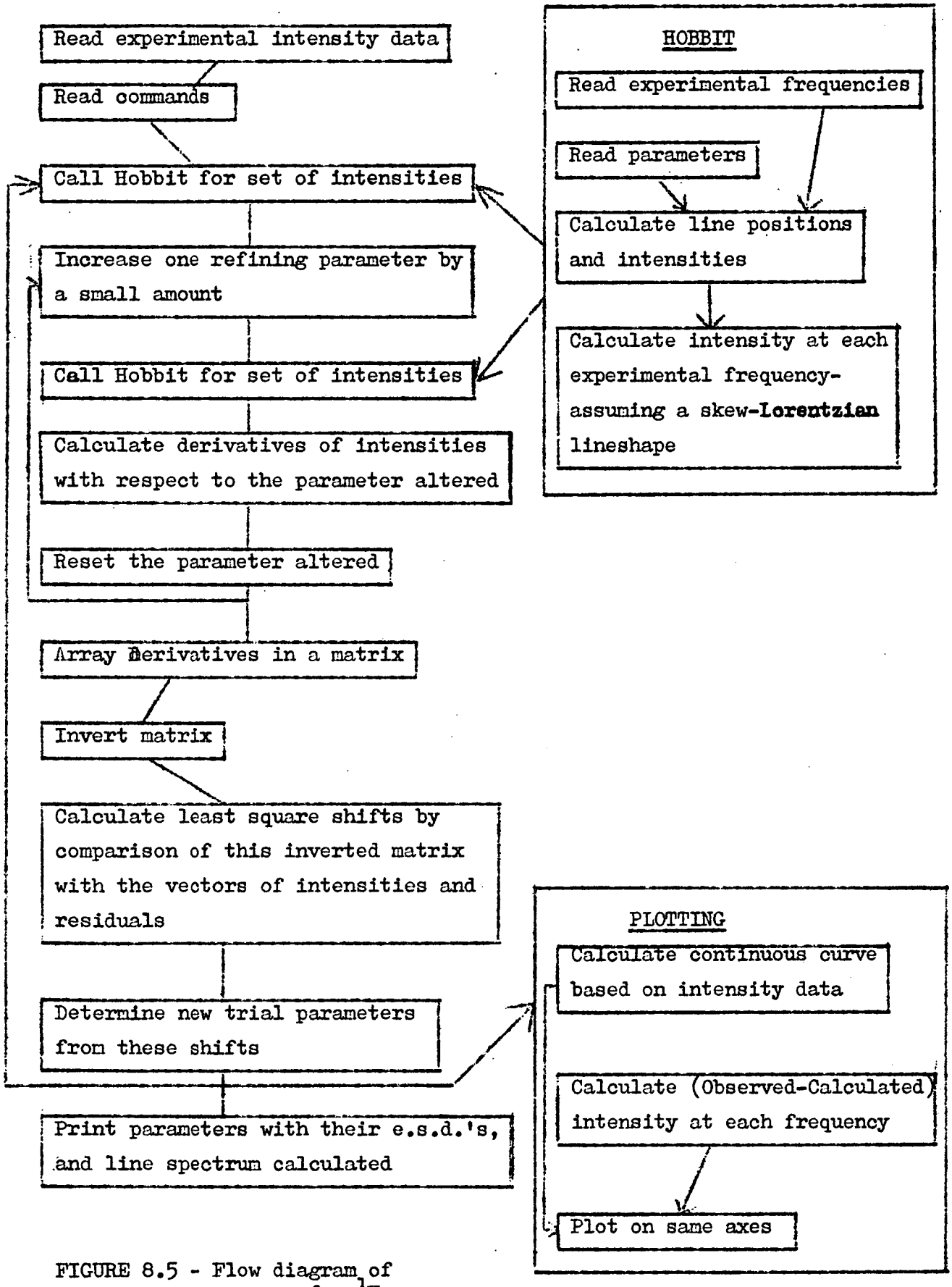

FIGURE 8.5 - Flow diagram of program for ^{1}H - n.m.r.

because the spin system was too large to be handled by the least-squares refinement program available[48] due to the size of the matrices involved.

(ii) $(GeH_3PH_2)_2Mo(CO)_4$

220 MHz Spectrum

The signal to noise ratio in the spectra obtained for this species was not as high as in the spectra of the silyl species and it was not considered possible to assign the observed spectrum completely. The spin system of the nuclei is the same as for the silyl complex, and the overall patterns of the spectra were so similar that it seemed reasonable to make the same assumptions in this case.

The parameters $\delta(GeH_3)$, $^2J(PH_3)$, and $^3J(HH)$ could be measured directly from the germyl resonance, and $\delta(PH_2)$ was measured using the symmetry of the (PH_2) resonance. No attempt was made to measure $J(PP')$ or to separate $^1J(PH_2)$ and $^3J(PH_2)$ which are quoted as a sum. Double resonance experiments showed that again $^2J(PH_3)$ and $^1J(PH_2)$ are the same sign.

(iii) $((GeH_3)_3P)_2\ Mo(CO)_4$

60 MHz spectrum

The spectrum of this species comprised only a simple doublet. $\delta(GeH_3)$ could be measured directly and the separation of the two lines was taken to be $^2J(PH_3)$, since $^4J(PH_3)$ was likely to be very

small.

(iv) Discussion

The chemical shifts of all the protons in the phosphines move downfield on coordination although these shifts are small for the protons not directly bound to phosphorus. The increased shielding on coordination is in agreement with the mono-substituted complexes and with other phosphine complexes (see tables 8.7 to 8.9).

The coupling constants are changed very little on coordination, except $^{1}J(PH_2)$ which is increased from ca. 180 to $>$ 300 Hz. This change is also found in other phosphine complexes and in complexes of 'PH_3' itself.

In both the monosilyl and monogermyl phosphine complexes $^{2}K(PH_3)$ and $^{1}K(PH_2)$ were found to be the same sign. Since both are (PH) reduced coupling constants the coupling constants (J) must also be the same sign.

(c) Bis-substituted tetracarbonyls $[LL'Mo(CO)_4]$

The spectra of these species were always observed in the presence of a large excess of $(PH_3)_2Mo(CO)_4$ whose proton spectrum under these conditions is known.

(i) $SiH_3PH_2(PH_3)Mo(CO)_4$

220 MHz spectrum

It was assumed from its appearance that this spectrum was

first order and assignments were made on this basis. All the parameters except $J(PP')$ could then be measured directly. $J(PP')$ has no effect on the proton spectrum if it is first order. Figure 8.6 shows the pattern of the observed spectrum and its assignment.

100 MHz spectrum

The spectrum observed at this frequency was complex because of the proximity of the low-field halves of the silyl and (PH_2) resonances. Double irradiation was carried out at this frequency and showed that in this case also $^2J(PH_3)$ and $^1J(PH_2)$ are of the same sign.

The perturbation caused by the proximity of the two resonances discussed above allowed $J(PP')$ to affect this spectrum. An attempt was made to compute the spectrum using the least-squares refinement program[48] previously mentioned. The spin-system of this complex was too large for the program and was reduced to:

$SiH_3PH_2 - Mo(CO)_4 - P'H'$

Inclusion of the H' was found to have no observable effect on the computed spectrum and thus the model was further reduced to:

$SiH_3PH_2 - Mo(CO)_4 - P'$

By comparison of the computed and observed spectra an estimate of $J(PP')$ was made.

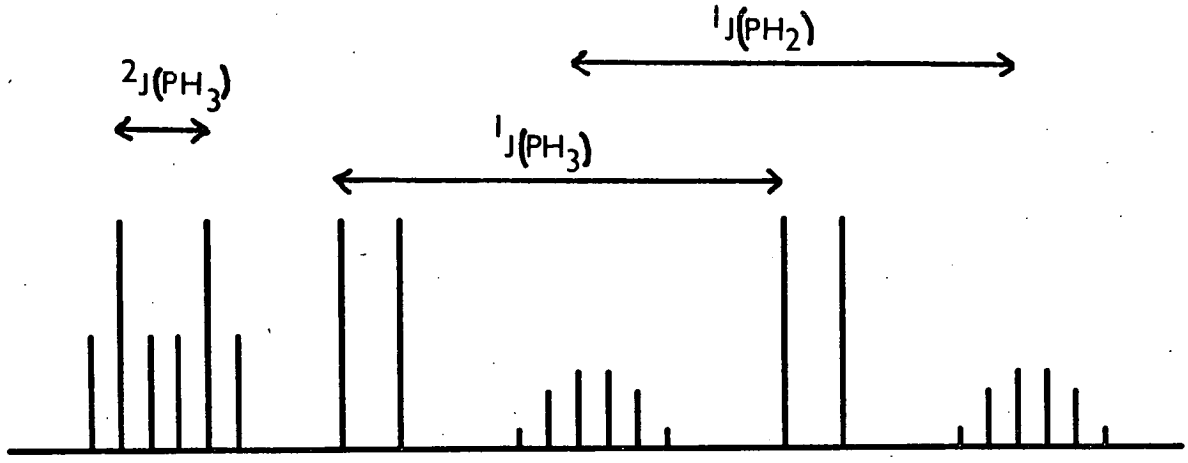

Figure 8.6 - ^{1}H-spectrum of $SiH_3PH_2(PH_3)Mo(CO)_4$ at 220 MHz.

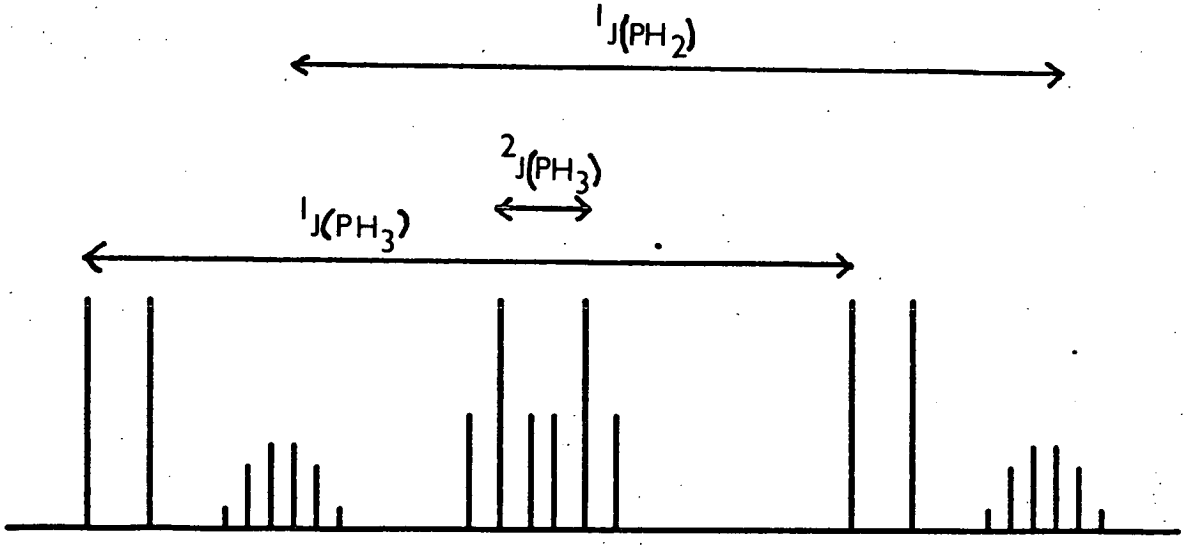

Figure 8.7 - ^{1}H-spectrum of $GeH_3PH_2(PH_3)Mo(CO)_4$ at 60 MHz.

(ii) $GeH_3PH_2(PH_3)Mo(CO)_4$

100 MHz spectrum

For the same reasons as the analogous silyl complex, this spectrum is very complex. Its overall pattern is very similar to that of the silyl species but no attempt was made to assign the spectrum.

60 MHz spectrum

The parameters were measured directly from this spectrum in the absence of a spectrum at 220 MHz. The pattern of this spectrum is shown in figure 8.7. Because of overlapping with the spectrum of $(PH_3)_2Mo(CO)_4$ only the parameters $\delta(GeH_3)$, $\delta(PH_3)$, $^1J(PH_3)$ and $^3J(PH_3)$ were measured.

(iii) Discussion

The chemical shifts and coupling constants found for these mixed phosphine complexes are very similar to those reported for the bis-phosphine complexes $[L_2Mo(CO)_4]$. The magnitude of J(PP') found for the silyl complex is less than that found for the bis-monosilyl phosphine complex. It seems, in these complexes, that when the chemical shift difference between the two phosphorus atoms in large coupling between them is small. For example:

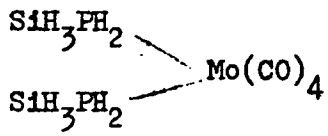

$J(PP') = \pm 27$

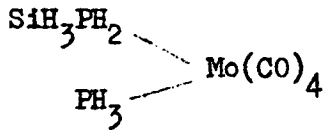

$J(PP')$ ca. 6

and

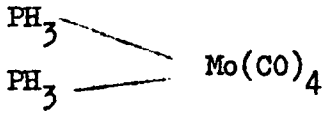

$J(PP') = -20.4$Hz [9]

$J(PP') = 0$ [9]

(d) Tris-substituted tricarbonyls $[L_3Mo(CO)_3]$

Only one of these complexes was prepared - $[(GeH_3)_3P]_3Mo(CO)_3$. The spectrum at 60 MHz always contained a broad doublet and a sharp doublet. From its chemical shift and separation the sharp doublet was attributed to free trigermyl phosphine, and the broad doublet to the complex. The broadness of the lines observed for the complex was to be expected in view of its spin system and only $\delta(GeH_3)$ could be measured. The magnitude quoted for $^2J(PH_3)$ is the separation of the two lines and is only an apparent coupling constant - the separation will depend also on coupling to the other phosphorus atoms. It is not known whether the free phosphine observed in the spectrum was a decomposition product or

whether the formation of the complex is an equilibrium reaction.

It seems likely from the quasi-first order nature of the spectrum that the assignment of the complex to a cis-configuration from its infrared spectrum is correct.

EXPERIMENTAL

References given in this Appendix refer to the list given at the end of Section I of the thesis.

EXPERIMENTAL

(a) Experimental methods

A conventional pyrex vacuum system with greased taps was used to handle all volatile compounds. Quantities of these were measured by pressure in calibrated volumes - pressures being measured with a spiral gauge. The amounts of less volatile compounds were found by weighing in a greaseless tap ampoule. Solids were also weighed and were handled under dry, oxygen-free nitrogen in a dry bag. Reactions were carried out either in a breakseal ampoule or a greaseless tap ampoule.

Volatile compounds were purified by trap to trap distillation and their purity checked by measurement of vapour pressure and by their infrared and nuclear magnetic resonance spectra. The incorporation of ^{13}C and ^{15}N was shown from exact mass measurements in mass spectra.

(b) Instruments

A Perkin-Elmer 457 infrared spectrometer (range 4000 - 250 $cm.^{-1}$)was used for low-resolution spectra, and for high resolution a Perkin-Elmer 225 (range 5000-200 $cm.^{-1}$) was used. Proton magnetic resonance spectra were recorded on a Varian Associates HA 100 and a Schlumberger decade frequency meter and generator (type FSX 3000) was used for spin-tickling experiments. Mass spectra were obtained at various ionising voltages on an A.E.I. M.S.909.

Photoelectron spectra were recorded in the range 6 to 21.2 eV on a Perkin-Elmer PS16 spectrometer using the helium line at 584 Å for excitation. Samples were admitted through a stainless steel needle valve from a vacuum system fitted with Quickfit Rotaflow taps.

The instruments used to obtain electron diffraction data are described in Section 2.1.

(c) Solvents

Solvents used were purified as follows:

Cyclopentane - distilled through flamed molecular sieve.

Monoglyme and diglyme - shaken with potassium and anthracene until a dark blue colour formed, then distilled.

Dimethyl ether - distilled off $LiAlH_4$ and passed through a trap at -78°C.

Benzene - sodium wire.

Tetramethyl silane - distilled through flamed molecular sieve.

Tetrahydrofuran - passed through Al_2O_3 and distilled off $LiAlH_4$.

Ammonia - condensed several times on to sodium.

n-Pentane was used without purification.

(d) Preparations (from Section I)

The methods used to prepare the starting materials and the samples of pseudohalides used in the spectroscopic studies are shown in table 1.

The preparations of the isotopically substituted pseudo-

Compound	Method	Reference
GeH_4	$GeO_2 + BH_4^-$	95
GeH_3Br	$GeH_4 + HBr + AlBr_3$	96
GeH_3Cl	$GeH_3Br + HgCl_2$	-
GeH_3F	$GeH_3Br + PbF_2$	-
GeH_3I	$GeH_3Cl + HI$	97
SiH_3Br	$PhSiCl_3 + LiAlH_4$, then HBr	98
SiD_3Br	Supplied by E.A.V.Ebsworth	-
SiH_3I	$(SiH_3)_3N + HI$	99
$(SiH_3)_3N$	$SiH_3Cl + NH_3$	100
Me_3SiN_3	$NaN_3 + Me_3SiCl + AlBr_3$	101
$(Me_3Si)CN_2$	Me_3SiCl + Ag salt	102
GeH_3NCO	GeH_3Br + Ag salt	15
GeH_3N_3	$Me_3SiN_3 + GeH_3F$	103
GeH_3NCS	GeH_3Br + Ag salt	21
SiH_3NCO	$SiH_3I + GeH_3NCO$	-
SiH_3NCS	SiH_3Br + Ag salt	20
SiH_3NCSe	SiH_3I + Ag salt	104
$(GeH_3)_2CN_2$	$GeH_3F + (Me_3Si)_2CN_2$	103

TABLE 1 - Preparation of pseudohalides and starting materials.

halides were performed using very small quantities and, therefore, the streaming methods used to prepare pseudohalides were unsuitable. Exchange of silyl and germyl groups was used whenever possible as these reactions are often quantitative. The small quantities involved also created problems of separation and this influenced the method selected to prepare each species (see table 2).

The reactions between a halide and a silver salt were carried out in a greaseless tap ampoule by repeatedly freezing the halide onto the silver salt and allowing the mixture to warm to room temperature. The silver salts were first mixed with dry powdered glass to increase their bulk and minimise decomposition of the products. For the pseudohalides containing ^{15}N and ^{13}C the halide was used in small excess, but for those containing ^{2}H the silver salt was in excess.

Exchange reactions were carried out using equal quantities of the two reactants.

Germylcyanide was the only pseudohalide to be prepared by a completely new method. $H^{13}CN$ was prepared by reaction between HBr and the silver salt by the method described. The $H^{13}CN$ (0.0062 g.) was added to digermyl carbodiimide (0.0233 g.) in a greaseless tap ampoule and the mixture warmed to room temperature for 10 minutes. No non-condensable gas was produced and the volatile products were distilled through a trap at -46°C. The fraction stopping (0.0174 g.) was shown to be germyl cyanide from its magnetic resonance and infrared spectra.

Compound	Method	Yield (%)
$GeH_3{}^{15}NCO$	GeH_3Br + Ag salt	67
$GeH_3{}^{15}NCS$	GeH_3Br + Ag salt	64
$GeH_3{}^{13}CN$	HCN + $GeH_3NCN\,GeH_3$	76
$SiH_3{}^{15}NCO$	SiH_3I + GeH_3NCO	quantitative
SiD_3NCO	SiD_3Br + GeH_3NCO	-
$SiH_2{}^{15}NCS$	SiH_3Br + Ag salt	88
SiD_3NCS	SiD_3Br + Ag salt	-
$SiH_3{}^{13}CN$	SiH_3Br + Ag salt	-

TABLE 2 - Preparation of isotopically substituted pseudohalides.

The fraction passing -46°C (0.0048 g.) was shown by infrared to be hydrogen cyanide and a trace of germyl cyanide. A small amount (0.0082 g.) of an involatile pale yellow solid was also formed. The yield of germyl cyanide was therefore 76%.

The silver salts used to prepare the pseudohalides were prepared from potassium and sodium salts supplied by Dr. D.I. Nicholls. The silver salts were precipitated by mixing approx. neutral solutions of the potassium salts and silver nitrate. They were washed with water, alcohol, and diethyl ether, then dried by pumping.

(e) Preparations and reactions (from Section II)

The molybdenum complexes used as starting materials were prepared by methods previously described -

$(C_5H_5NCH_3)(Mo(CO)_5I)$ [92] A

nor - $C_7H_8Mo(CO)_4$ [93] B

$C_7H_8Mo(CO)_3$ [94] C

The methods used to prepare the phosphine ligands are shown in table 3. The preparations of the silyl and germyl halides used are given in table 1. The preparations of the mono-, bis- and tris-phosphine complexes are now described using the symbols above to represent the molybdenum starting compound. In each case the phosphine was distilled into an ampoule containing the starting material in the solvent given and the mixture warmed to room temperature for the time

Compound	Method	Reference
$(GeH_3)_3P$	$GeH_3Br + (SiH_3)_3P$	105
$(SiH_3)_3P$	$SiH_3Br + KPH_2$	106
GeH_3PH_2	$LiAl(PH_2)_4 + GeH_3Br$	107
SiH_3PH_2	$LiAl(PH_2)_4 + SiH_3Br$	108
Me_3SiPH_2	$LiAl(PH_2)_4 + Me_3SiCl$	-
PH_3	$Ca_3P_2 + H_2O$	109
$LiAl(PH_2)_4$	$LiAlH_4 + PH_3$	110

TABLE 3 - Preparation of phosphines.

specified.

All the complexes prepared were involatile and thus once isolated they were dissolved in a suitable solvent for identification by their infrared and nuclear magnetic resonance spectra (see Chapter 8).

References to the text are given for each experiment.

$LMo(CO)_5$

(i) 82.6 mg. A (0.18 m moles) and 0.24 m moles $(GeH_3)_3P$ in T.H.F. for 3 hours (Section 7.2(a)).

(ii) 87.5 mg. A (0.2 m moles) and 0.25 m moles $(SiH_3)_3P$ in T.H.F. for 2 hours. (Section 7.2(b)).

(iii) 91.0 mg. A (0.2 m moles) and 0.25 m moles SiH_3PH_2 in T.H.F. for 6 hours. The only product of this reaction was $PH_3Mo(CO)_5$. (Section 7.2(c)).

(iv) 128.5 mg. A (0.28 m moles) and 0.3 m moles GeH_3PH_2 in T.H.F. for 4 hours. Several products were identified from this reaction. (Section 7.2(d)).

In these preparations the product remained in solution and this solution was decanted off the solid formed before the solvent was removed.

$L_2Mo(CO)_4$

In all the following preparations the solvent and excess phosphine were removed by pumping.

(v) 63.5 mg. B (0.2 m moles) and 0.45 m moles $(GeH_3)_3P$ for 4 hours (Section 7.2(a)).

(vi) 60.6 mg. B (0.2 m moles) and 0.45 m moles of SiH_3PH_2 for $2\frac{1}{2}$ hours in benzene. (Section 7.2(c)).

(vii) 61.8 mg. B (0.2 m moles) and 0.45 m moles GeH_3PH_2 overnight in n-pentane. Several products were identified by nuclear magnetic resonance from this reaction (Section 7.2(d)).

$LL'Mo(CO)_4$

(viii) 59.4 mg. B (0.2 m moles) and 0.2 m moles SiH_3PH_2 and 0.2 m moles PH_3 in n-pentane for 2 hours. The mixture of products obtained is described in Section 7.2(e).

(ix) 240.0 mg. B (0.8 m moles) and 1.5 m moles PH_3 and 0.16 m moles SiH_3PH_2 in benzene for 3 hours. Again the products obtained from this reaction are discussed in Section 7.2(e).

$L_3Mo(CO)_3$

(x) 44.5 mg. C (0.16 m moles) and 0.5 m moles $(GeH_3)_3P$ in n-pentane for 8 hours. A small amount of brown solid remained in the reaction vessel after decantation of the pentane solution (Section 7.2(a)).

Two of the germyl phosphine complexes were prepared by exchange reactions from other phosphine complexes (see Section 7.3). Exchange was carried out by adding excess of the germyl halide to a solution of the phosphine complex in

benzene. The addition was made either directly into an n.m.r. tube which was then sealed, or in a greaseless tap ampoule in order to isolate the product for infrared by pumping off the silyl halide and solvent.

(xi) 61.2 mg. B (0.2 m moles) and 0.45 m moles SiH_3PH_2 in benzene for two hours then 1.0 m moles GeH_3F added. The volatile materials were removed by pumping and fresh solvent (benzene) distilled into the ampoule for solution n.m.r. or i.r.

(xii) 240.0 mg. B (0.8 m moles) and 1.5 m moles PH_3 and 0.16 m moles SiH_3PH_2 in benzene for 3 hours then 0.2 m moles GeH_3F added. The product was handled as in (xi).

APPENDIX A

MOLECULAR STRUCTURE OF DIGERMYL SELENIDE IN THE GAS PHASE

References given in this Appendix refer to the list given at the end of Section I of the thesis.

The sample of digermyl selenide was prepared by Dr. D.W.H. Rankin, who also recorded the electron diffraction pattern using the same apparatus and methods as those described in Section 2.1 of this work. Data reduction was carried out by Dr. Rankin on the Cambridge University 'Titan' computer using an established program.[87] The least squares refinements were carried out as described in Section 2.1.

The weighting functions, correlation parameters and scale factors are given in table 1. The wavelength was evaluated by direct measurement of the accelerating voltage and from the diffraction pattern of powdered thallous chloride and was found to be 0.057913 $\pm$ 0.000030Å. The scattering factors used were those of Cox and Bonham.[39]

Molecular Model

Certain assumptions were made about the structure and these were imposed as restrictions in the least squares refinements:-

i) local C_{3v} symmetry is maintained in the germyl groups.

ii) their C_{3v} axes coincide with the (Ge-Se) bonds.

Variation of the angle between the C_3 axes and the (Ge-Se) bonds made no significant difference to the refinements.

Four geometrical parameters were chosen to define the major interatomic distances. These were the (Ge-Se) and (Ge-H) bonded and (Ge...Ge) non-bonded distances, and the (H-Ge-H) angle. These define all the interatomic distances except those that depend also on the conformation of the germyl groups. The

Height	Del S	S Min	S1	S2	S Max	P/H	Scale Factor
250mm	0.400	5.200	9.000	21.000	26.000	0.4281	0.780 ± 0.019
500mm	0.200	3.800	6.400	12.000	15.200	0.4987	0.718 ± 0.019
1000mm	0.100	1.000	2.500	6.000	7.200	0.4998	0.527 ± 0.039

TABLE 1 - Weighting Functions, Correlation Parameters and Scale Factors.

R 1	R 2	R 3	U 1	U 2	U 3	K 1	K 2	K 3
999	7	29	27	-56	29	27	1	-4
7	999	248	33	22	280	17	48	49
29	248	999	84	36	-38	78	116	28
27	33	84	999	204	116	814	365	49
-56	22	36	204	999	32	219	118	15
29	280	-38	116	32	999	124	140	83
27	17	78	814	219	124	1000	303	42
1	48	116	365	118	140	303	999	27
-4	49	28	49	15	83	42	27	999

TABLE 2 - Least Squares Correlation Matrix Multiplied by 1000.

other parameters used in the refinements were the vibrational amplitudes of all the interatomic distances and separate scale factors for the 250, 500 and 1000 mm. data sets.

As they were expected to be small, no shrinkage corrections were applied.

Results

Satisfactory refinements were carried out on (Ge-H), (Ge-Se) and (Ge...Ge) distances. In the radial distribution curve (Figure 1) the weak (Se...H) peak is very close to the much stronger (Ge...Ge) peak, and so the (Se...H) amplitude could not be refined. Its amplitude and other amplitudes were fixed at typical values.[85]

Allowing the three independent distances and their amplitudes to refine the $(H\text{-}\hat{G}e\text{-}H)$ angle would not refine satisfactorily. Thus refinements of these distances and amplitudes were carried out with the angle $(H\text{-}\hat{G}e\text{-}H)$ fixed at values in the range 106° to 114°. The R factor was found to be a minimum with the angle at 109°, with an estimated random error of 2°.[88]

A similar method was used to obtain information on the conformations of the two germyl groups. The $(H\text{-}\hat{G}e\text{-}H)$ angle was now fixed at 109°, and the germyl groups were rotated in opposite directions, retaining the C_{3v} symmetry of the H_3GeSe groups and overall C_2 symmetry. The R factor was found to be a minimum when each germyl group was staggered with respect to the further

Figure 1.

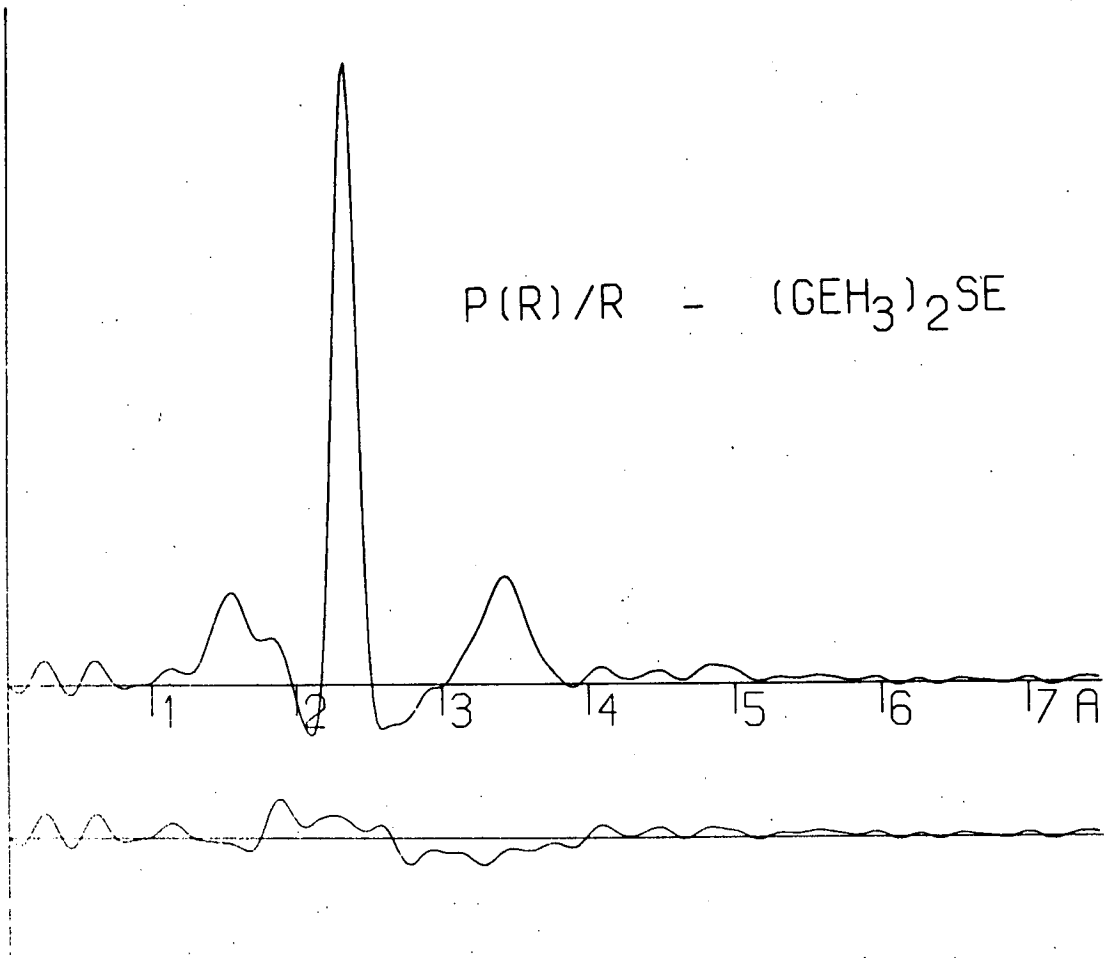

(Ge-Se) bond. In this conformation the molecule has overall C_{2v} symmetry with four (Ge...H) distances of 3.69Å and two of 4.89Å.

The least squares correlation matrix is presented in table 2 and the final molecular parameters are given in Table 3. Allowance has been made in the quoted uncertainties for possible systematic errors. These have been added to the random errors obtained by the least squares analysis.

The observed molecular intensities and weighted residuals are shown in Figure 2. The final R factor was:

$$R_G = (U'WU/I'WI)^{\frac{1}{2}} = 0.15$$

Discussion

From the studies of $(H_3M)_2E$ where M = Si. Ge and E = O, S it is evident that either the extent or the steric effects of multiple bonding between the atoms M and E decreases from silicon to germanium and decreases even more from oxygen to sulphur. This trend was confirmed by the study of $(H_3Si)_2Se$[84] in which the Si-Se bond length found was almost exactly the calculated value and the angle at selenium was almost identical to its value in dimethyl selenide. The experimental (M-E) bond length and (M-$\hat{E}$-M) angles for these molecules are given in Table 4, together with bond lengths predicted on the basis of tetrahedral covalent radii derived from bond lengths in C_2H_6[89], CH_3SiH_3[90], CH_3GeH_3[91], $(CH_3)_2O$[78], $(CH_3)_2S$[80] and $(CH_3)_2Se$[81].

(A) Independent Distances

		Distance	Amplitude	Anharmonic Constant
R 1	(Ge - Se)	2.344±0.003	0.053±0.003	2.0
R 2	(Ge - H)	1.563±0.015	0.093±0.024	2.0
R 3	(Ge...Ge)	3.445±0.010	0.137±0.009	0.0

(B) Dependent Distances

D 1	(Ge...H)	3.685±0.015	0.150 (fixed)
D 2	(Ge...H)	4.886±0.020	0.150 (fixed)
D 3	(Se...H)	3.230±0.013	0.100 (fixed)
D 4	(H...H)	3.232±0.016	0.200 (fixed)
D 5	(H...H)	4.114±0.022	0.200 (fixed)
D 6	(H...H)	5.156±0.026	0.200 (fixed)
D 7	(H...H)	6.221±0.031	0.200 (fixed)
D 8	(H...H)	2.545±0.024	0.120 (fixed)

(C) Angles

∠1	(H-Ge-H)	109 (see text)
∠2	(Twist)	60 (see text)
∠3	(Ge-Se-Ge)	94.6±0.5

TABLE 3 - Molecular Parameters.

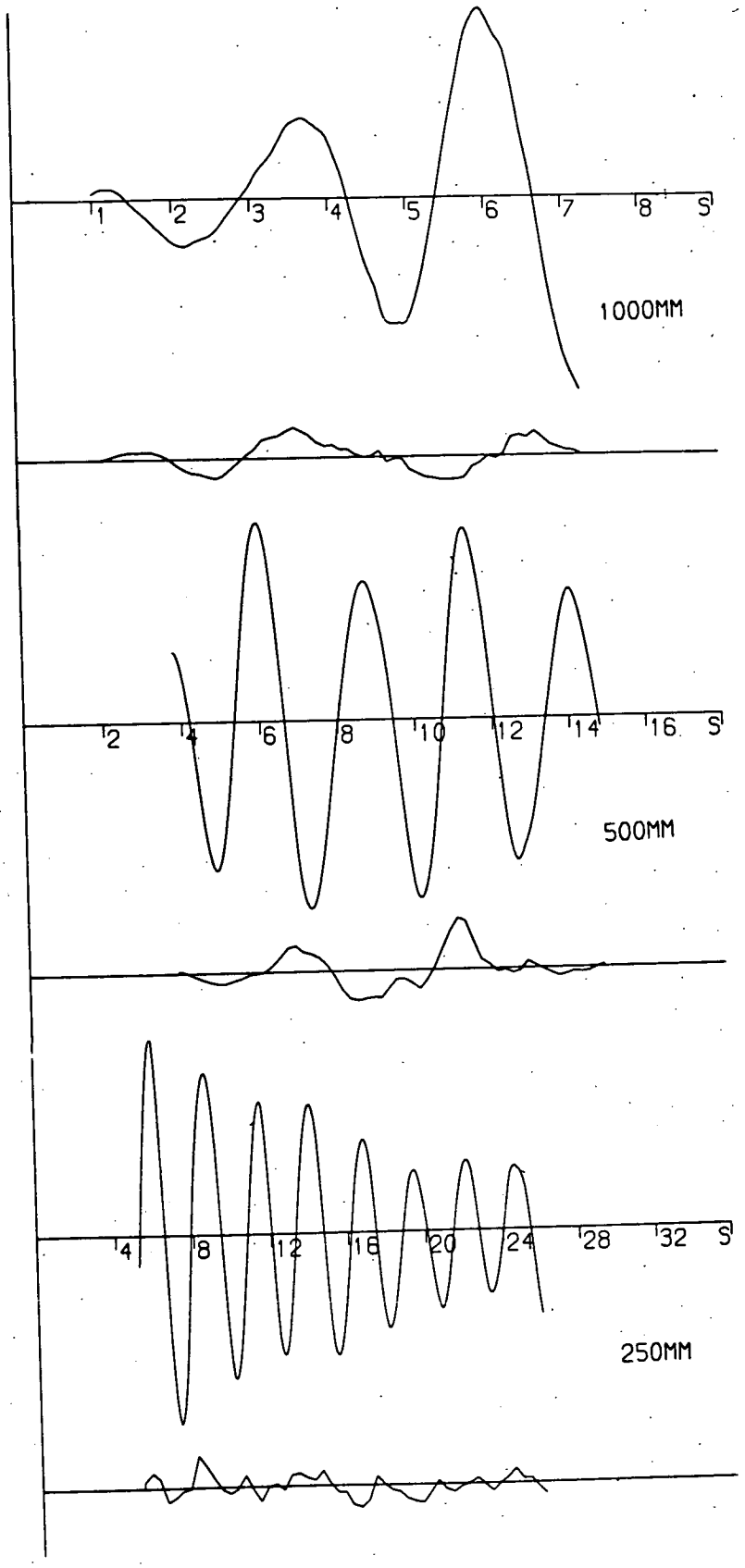

Figure 2 - INTENSITY DATA FOR $(GEH_3)_2SE$

E	M	r(M-E) experimental	r(M-E) calculated*	(M-$\hat{E}$-M)	refs. to Part I of this work.
O	C	1.416	-	111.5	78
	Si	1.634	1.749	144.1	82
	Ge	1.766	1.829	125.6	85
S	C	1.802	-	98.9	80
	Si	2.136	2.133	97.4	83
	Ge	2.209	2.211	98.9	85
Se	C	1.943	-	96.8	81
	Si	2.273	2.274	96.6	84
	Ge	2.344	2.352	94.6	86

*See text.

TABLE 4 - Bond Lengths and Angles in Molecules of Type $(MH_3)_2E$.

The results of this present study are consistent with the trends found previously and thus it seems tenable that multiple bonding if present has little stereochemical significance in compounds of selenium with the elements of group IV.

The conformation of the two germyl groups found for digermyl selenide is the same as that found for digermyl ether. This conformation has four short (Ge...H) distances and two longer ones. For digermyl ether these were 3.68Å and 4.43Å, and for digermyl selenide they are found to be 3.69Å and 4.89Å. As the sum of the van der Waal's radii for germanium and hydrogen is about 3.2Å it is clear that there can be no significant steric repulsion between the germyl groups in any of these compounds, and so it cannot account for the wide angle in the ether. The study of digermyl sulphide did not give any information on the conformation of the germyl groups but in view of the results from the ether and selenide it seems very likely that the germyl groups in digermyl sulphide will have the same staggered conformation.

APPENDIX B

SUBROUTINE HOBBIT

```
      SUBROUTINE HOBBIT(IT,IIR,MP)
C PIPPIN
C HOBBIT FOR SPIN SYSTEM (AM(N)X(MA))2
      DIMENSION GR(500),IMAT(500),AX(60),DM(6000),ZM(5000),BX(60),FR(500
     #),PM(42),NUM(42),HAM(6000),PAR(23),DN(2500),ZN(2500),EF(500),EI(50
     #0)
      COMMON/AREA1/GR,IMAT,AX,DM,ZM,BX,FR,PM,NUM,NT,JM,DN,ZN,NPTS,IP,NST
      COMMON/AREA3/HAM,PAR,EF,EI
      IIR=0
      IF(MP.EQ.1)GO TO 28
      C=PAR(5)
      P=PAR(6)
      Q=PAR(7)
      R=PAR(9)
      T=PAR(10)
      S=PAR(12)
      XM=PAR(13)
      N=IMAT(3)
      MA=IMAT(5)
      AXL=ABS(R-T)
      AXN=ABS(R+T)
      ZV=0
      ZT=0
      I=1
      II=1
      M=2*N+1
      DO 2 KB=1,M,2
      DO 2 KC=1,M,2
      K=KB-N-1
      L=KC-N-1
      DN(I)=AXN+K*S+L*XM
      AM=1
      MR=(N+K)/2
      IF(MR.EQ.0)GO TO 15
      IF(MR.LT.0)MR=-MR
      DO 3 JA=1,MR
    3 AM=AM*(N-JA+1)/JA
   15 AN=1
      NR=(N+L)/2
      IF(NR.EQ.0)GO TO 16
      IF(NR.LT.0)NR=-NR
      DO 4 JB=1,NR
    4 AN=AN*(N-JE+1)/JB
   16 ZN(I)=AM*AN
      ZV=ZV+ZN(I)
      I=I+1
      MB=2*MA
      DO 2 KA=1,MB
      KK=KA-MA
      RY=(K-L)*Q+(KK-1)*AXL
      RZ=(KK*AXL+(K-L)*Q)
      RA=SQRT(RZ**2+P**2)
      RB=SQRT(RY**2+P**2)
      RC=RY*RZ+P**2
      RD=SQRT(RZ**2+P**2)*SQRT(RY**2+P**2)
      DM(II)=K*S+L*XM+RA+RB
```

```
      ZM(II)=(1-RC/RD)*AM*AN
      ZT=ZT+ZM(II)
      II=II+1
      DM(II)=K*S+L*XM-RA-RB
      ZM(II)=ZM(II-1)
      ZT=ZT+ZM(II)
      II=II+1
      DM(II)=K*S+L*XM-RA+RB
      ZM(II)=(1+RC/RD)*AM*AN
      ZT=ZT+ZM(II)
      II=II+1
      DM(II)=K*S+L*XM+RA-RB
      ZM(II)=ZM(II-1)
      ZT=ZT+ZM(II)
    2 II=II+1
      IIM=II-1
      IM=I-1
      IT=I+II-2
      V=100/ZV
      TA=100/ZT
      DO 5 I=1,IM
    5 ZN(I)=ZN(I)*V
      DO 6 II=1,IIM
    6 ZM(II)=ZM(II)*TA
      II=1
      IM=IM+1
      DO 7 I=IM,IT
      DN(I)=DM(II)
    7 II=II+1
      II=1
      DO 8 I=IM,IT
      ZN(I)=ZM(II)
    8 II=II+1
      DO 10 I=1,IT
   10 DN(I)=C+ABS(DN(I)/2)
      DO 35 I=1,IT
      K=I+1
      DO 35 J=K,IT
      IF(DN(I).NE.DN(J))GO TO 35
      ZN(I)=ZN(I)+ZN(J)
      ZN(J)=0
   35 CONTINUE
      IR=IT
      DO 36 I=1,IT
      IF(I.GT.IR)GO TO 38
   39 IF(ZN(I).GT.0.01)GO TO 36
      IR=IR-1
      IF(I.GT.IR)GO TO 38
      DO 37 J=I,IR
      DN(J)=DN(J+1)
   37 ZN(J)=ZN(J+1)
      GO TO 39
   36 CONTINUE
   38 IT=IR
   28 IF(NPTS.EQ.0)GO TO 33
      W1=4/(PAR(2)*1.2)**2
      W2=4/(PAR(2)*0.8)**2
      DO 29 I=1,NPTS
      HAM(I)=0
      DO 29 J=1,IT
      W=W1
      D=DN(J)-EF(I)
      IF(D.LT.0)W=W2
   29 HAM(I)=HAM(I)+ZN(J)/((1+W*D*D)*PAR(2))
   33 IP=IT
      RETURN
      END
```

1. Gamble, Gilmont — J.A.C.S., 62,717(1940).
2. Rudolf, Parry, Farran — Inorg.Chem. 5,725(1966).
3. Martin, Dial — J.A.C.S., 72,852(1950).
4. Holtje, Meyer — Z.Anorg.Allgem.Chem., 197,93(1931).
5. Holtje — Z. Anorg.Allgem.Chem., 190,241(1930).
6. Scholder, Pattock — Z. Anorg.Allgem.Chem., 220,250(1934).
7. Hieber, Winter — Chem.Ber., 97,1037(1964).
8. Fischer, Louis, Scheider — Ang.Chem.Int., 7,137(1968).
9. Holywell — Ph.D. Thesis (Edinburgh).
10. Lauterburg, King — J.A.C.S. 81,3266(1965).
11. Dunitz, Pauling — Helv.Chem.Acta 43, 2188(1960).
12. Allen, Barrett — Canad.J.Chem. 46,1655(1968).
13. King — Inorg.Chem. 3,1039(1964).
14. Pidcock, Taylor — J.C.S.(A) 877(1967).
15. Lingales, Gioznam, Belmoo — J.A.C.S., 88,256(1966).
16. Fischer, Louis, Scheider — Ang.Chem.Int. 7,136(1968).
17. Fischer, Louis, Bathelt, Muller — Chem.Ber.102, 2547(1969).
18. Moser, Fischer — J.Organometal.Chem. 15, 151(1968).
19. Fischer, Louis, Bathelt — J.Organometal.Chem. 20,147(1969).
20. Holywell — Pers.Communication from Schunn.
21. Klanberg, Muetteries — J.A.C.S. 90, 3296(1968).
22. Fischer, Louis, Bathelt, Moser, Muller, — J.Organometal.Chem. 14,9(1968).
23. Emeleus, McDiarmid, Maddock — J.I.N.C., 1,195(1955).
24. Cradock, Whiteford — J.C.S. Farraday II, in press.
25. Murdoch, Rankin, Glidewell — J.M. Struc. 9, 17(1971). (and references therein).
26. Hedberg — J.A.C.S. 77, 6491(1955).
    and
    Beagley, Conrad — Trans.Farad.Soc. 66, 2740(1970).
27. Glidewell, Rankin,. Robiette — J.C.S.(A) 2935(1970).
28. Beagley, Robiette, Sheldrick — J.C.S.(A) (1968) 3002.
29. Rankin, Robiette, Sheldrick, Beagley, Hewitt — J.I.N.C., 31,2351(1969).
30. Cradock, Whiteford — J.C.S. Faraday II, in press.
31. Ebsworth, Glidewell, Sheldrick — J.C.S.(A) 352(1969).

32. McDiarmid	Ang.Chem.Int.Edn. 5, 418(1966).
33. Drake, Simpson	(Chem.Comm. 249(1967) (Inorg.Chem. 6,1984(1967).
34. Drake, Riddle	J.C.S.(A) 1675(1968).
Drake, Goddard, Simpson	J.I.N.C.Letts. 4,361(1968).
35. Cradock, Ebsworth, Davidson, Woodward.	J.C.S.(A) 1229, (1967).
36. Clark,Hoberman	Inorg.Chem. 4,1771(1965).
37. Abel, Stone	Quart.Rev. 23,361(1969).
38. Haigh reported by Bishop	Ann.Rev. N.M.R. Spec. I,91(1968).
39. Corio	Chem.Rev. 60,363(1960).
40. Pople, Schneider, Bernstein	High Resolution n.m.r., McGraw-Hill N.Y., 1959.
41. R.K.Harris	Personal communication from Naar-Colin, Bothner-By.
42. Anet	J.A.C.S. 84, 747(1962), and Proc.Chem.Soc. 327(1959).
43. Bothner-By, Naar-Colin	J.A.C.S., 84,743(1962).
44. Harris	Can. J.Chem. 42, 2275(1964).
45. Mann	J.C.S.(A) 3050(1970).
46. Mann	Personal communication.
47. Subroutine Hobbit	Appendix B of this work.
48. Glidewell, Rankin, G.M.Sheldrick	Trans.Farad.Soc. 65, 2801(1969).
49. Barlow, Holywell	J.Organometallic Chem.439(1969).
50. Fluck, Buerger, Goetze	Z.Naturforsch. 622(9),912-5(1967)
51. G.M.Sheldrick, Ebsworth	Trans.Farad.Soc. 63,1071(1967).
52. Mannatt, Juvinall, Wagner, Elkman	J.A.C.S., 88,2689(1966).
53. Drake Jolly	J.Chem.Phys. 38,1033(1963).
54. Glidewell, G.M.Sheldrick	J.C.S.(A) 350(1969).
55. Sudarshan, Gockhale, Jolly	Inorg.Chem. 3,1141(1964).
56. Drake, Riddle	J.C.S.(A) 2709(1968).